Analogue experiments for understanding of factors controlling morphological transition in columnar joints

濱田, 藍

https://doi.org/10.15017/1654659

出版情報：九州大学, 2015, 博士（理学）, 課程博士
バージョン：
権利関係：全文ファイル公表済

学位論文

Analogue experiments for understanding of factors controlling morphological transition in columnar joints

アナログ実験による柱状節理の形態的遷移についての研究

濱田 藍

九州大学大学院理学府

地球惑星科学専攻

平成 28 年 3 月

Abstract

Columnar joints in lava flows and welded tuffs have two different types of column structures adjacently within a single flow unit in terms of column width, column configurations and the directions of developed columns, which are called as Colonnade and Entablature. Colonnade consists of relatively large width, straight and ordered columns, while Entablature consists of relatively small width, curved and disordered columns. Columnar joints are formed due to volume contraction during cooling. The isotherms at a time are assumed to be perpendicular to the direction of columns if the directions of maximum tensile are parallel to the isotherms. The assumption, which is based on thermal diffusion process during cooling, has been applied to the formation of simple cases in the curved structures. However, it still has not been clearly solved how complex isotherms are formed for the formation of Entablature. In order to understand the formation process of Colonnade structure in columnar joints, analogue experiments using starch and water mixture as analogue materials have been conducted in terms of morphology, theory and crack formation. However, attempts to reproduce morphological transition from Colonnade to Entablature have not been conducted yet. This thesis aims at understanding the factors to control the transition between Colonnade and

Entablature by means of drying experiments as well as reproducing curved structures which are seen in Entablature. I investigated the process of crack propagations and the relations between the water distribution and crack developments in mixture by observing X-Ray CT images with changing time. In addition, morphological analysis for experimental products for reproducing columns width change was conducted.

Three sets of experiments conducted focus on: (1) Transfer processes in drying and cracking samples, (2) Water concentration and the direction of cracks with time and (3) Effects of sudden increase in desiccation rate on drying and cracking processes. The samples after all experiments are observed by using X-ray CT and compared with the models based on a diffusion equation in Experiment 1 and 2. Further morphological analysis is developed for images taken in Experiment 3 in the master thesis [Hamada, 2012]. Results suggest: 1. Water transportation within the mixture can be explained by the diffusion process, 2. Crack development occurs perpendicular to the iso-water concentration surface in the mixture and 3. Instantaneous increase in desiccation rate causes column nucleation.

I propose a scenario of morphological transition from Colonnade to Entablature at Shakushiiwa in Oita prefecture, Japan, on the basis of above suggestions by introducing two heat transports: vertical heat transport Q_1 within rocks by thermal diffusion to the uppermost of the rock and horizontal heat transport Q_2 through the cracks.

Shakushiiwa which consists of Aso-4 welded tuffs, shows a threefold structure; Upper Colonnade – Entablature – Lower Colonnade. Central Entablature has radial structures by the columns originated from the tips of cracks in Upper Colonnade. These radial structures are horizontally aligned repeatedly. As the cooling process proceeds in Upper Colonnade by thermal diffusion Q_1 from hotter interior of the rock to the cooling surface at the top of the rock, cracks develop perpendicular to the isotherm of T_c, which is the temperature when cracks restart to propagate to form Upper Colonnade. When cracks developed from Upper Colonnade part to the boundary to Entablature, cracks themselves become the cooling surface and the heat transport Q_2 proceeds. This cooling process makes the configuration of the T_c isotherm to be convex downward around the tips of cracks. The heat transport transition from Q_1 to Q_1 and Q_2 causes the abrupt increase in cooling rate and form smaller widths of columns than those in Upper Colonnade by

column nucleation. Such morphological change of columns is consistent with the field observation. Simultaneously, the cooling process at Lower Colonnade advances and cracks develop vertically upward. The upper part of Lower Colonnade meets at the lowermost part of Entablature.

Acknowledgement

I would like to express my best gratitude to my supervisor, Prof. Atsushi Toramaru for his supporting my research in all aspects at Kyushu University. His bunch of ideas always gives me stimulative perspectives and the ways how to approach the problems with many complexities of nature. I also appreciate his earnestly teaching me many times the points of modelling and the skills of Matlab until I could understand. I want to thank the technical engineers, Mr. Kei Itohira and Mr. Yoshihiro Takamiya of Fukuoka Industrial Technology Center for teaching me how to use Micro-focus X-ray CT system. Special thanks to Mr. Itohira for advising me on not only operating the X-ray CT system but also processing and analyzing CT images with VGL software. I want to thank Dr. Tsukasa Nakano of National Institute of Advanced Industrial Science and Technology, who advised me on how to eliminate the noise from the CT images technically. I thank the technical engineer Mr. Shinji Yamanouchi of Factory of Faculty of Science, who made many apparatus for my experiments. I also want to thank Prof. Yasuhiro Fujimitsu of Department of Earth Resources Engineering, Faculty of Engineering at Kyushu University, who rented an infrared camera to me. I appreciate Prof. Akio Nakahara of Nihon

University, Associate Prof. Takeshi Ikeda and Associate Prof. Shigeo Yoshida of Kyushu University for their judges my Ph-D thesis. A lot of advices and comments given by the members of my laboratory at Kyushu University have been a great help in constituting my research scenario and improving its quality.

This work was supported by The Late Professor Tatsuro Matsumoto Scholarship and The Sasakawa Scientific Research Grant from The Japan Science Society.

Finally I would like to thank my family and my dear friends for their all supporting in any time.

At the end I want to express my 'guilty' of throwing away tons of potato and kuzuko starch for my experiments instead of using their original purpose as foodstuff.

Contents

List of Tables

List of Figures

Chapter 1

Introduction

Various pattern formations can be seen in nature. For example, manganese dendrite on the surface of limestone at Gerlingen in Germany is crystalized from supersaturated solution and varies the dendritic patterns depending on the basic crystal structure and the degree of supersaturation of liquid. Snowflakes patterns vary from surrounding temperature and amount of water vapor in the air after nucleation. Striped patterns on fish are the pattern formation by following reaction-diffusion equations proposed by Alan Turing. To understand how these characteristic patterns are formed under a regulation is surely interesting. Some pattern formations can be changed their regularities by some reasons and form new different patterns. Columnar joints, which are the crack pattern in cooling rock, have mainly two different types of structures in a series of structure formation. There are many columnar joints in a volcanic island, Japan, especially the columnar joints at Takachiho Gorge in Miyazaki prefecture, which is consisted of welded tuffs originated from Aso-3 and 4 pyroclastic flow deposits, have two distinct morphological features within one flow unit as shown in Figure 1.4. It is still not clear how two different structures were formed during one cooling process. This thesis will focus on such a morphological transition in columnar joints.

1.1 A history of previous studies on columnar jointing

The oldest sketch of columnar joints was drawn by Kentmann in 1565 [Schmincke, 2004 and references therein] (Fig. 1.1). It is surprising that it had already been expressed well that prismatic columns with various number of sides and successive horizontal banding structures perpendicular to the column axes. The first scientific paper on columnar joints was reported by on the Giant's Causeway in Ireland. The spectacular columnar structures along the Causeway Coast subsequently stimulated researchers' imaginations and many descriptive studies with detailed drawings were recorded [e.g., Foley and Molyneux, 1694; Molyneux, 1698]. Molyneux, 1698 mentioned the first petrological identification of the columnar rocks at Causeway as basalt. In the middle of 18th century, which was the era of a controversy between Neptunist and Vulcanist, Desmarest in 1763 concluded that the origin of the columnar joints at Giant's Causeway was cooled basaltic lava, after his discovery of columnar joints composed by lavas from a volcanic crater at Auvergne in France (Tomkeieff, 1940). Scrope in 1825 noticed that the direction of developed columns is perpendicular to the cooling surface when he explained the

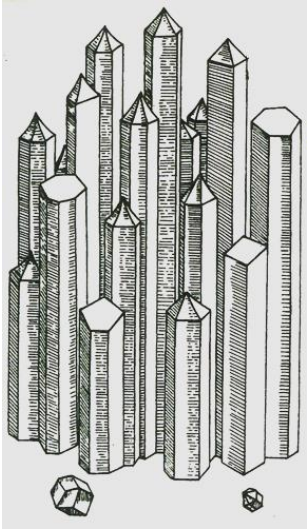

Figure 1.1: The illustration of basaltic columns at Stolpen castle in Dresden drawn by Kentmann in 1565 [Schmincke, 2004 and references therein]. Prism structures consist of not only hexagons but also pentagons and squares, and successive banding structures along the lateral surface can be seen. Triangular parts at the top of columns were put afterwards to express the idea of Neptunism that these columns are formed by crystallization from water.

formation of inclined columns (Schmincke, 2004 and references therein). Mallet (1874) first mentioned that the fundamental cause of formation of columnar joints is the tension stress driven by thermal contraction during cooling of rock and the direction is perpendicular to the cooling surface (Sosman, 1916). The contraction hypothesis suggested by Mallet (1874) subsequently became a common interpretation as the principle of formation of columnar joints and many researchers applied his idea to determine the past isothermal surfaces by observing the column directions [e.g., James, 1920; Jaeger, 1961; Spry, 1962].

Multi-tiered structures with columnar joints caused by multi-lava emplacements and cooling are recognized at the places where a large amount of emplacements of lavas, for example, Giant's Causeway, Fingal's Cave in Scotland, Columbia River Basalt Flows in USA and Hjárparfoss in Iceland. In such thick lava flows, twofold or threefold arrangements are common to observe within one flow unit. Tomkeieff (1940) started using 'Colonnade' and 'Entablature' for the upper part of Colonnade to specify their positions of twofold arrangement within one flow unit and subsequent researchers modified his terminology to add morphological features in terms of width, configuration and regularity of column directions [Spry, 1962; Long and Wood, 1986; Swanson, 1967; Long & Davidson, 1981]. The formation of

Entablature is a long-standing problem to be discussed. Rock textures in Colonnade and Entablature each indicated the evidence that the part of Entablature was suffered from rapid cooling compared to that of Colonnade [Long and Wood, 1986; DeGraff et al., 1989; Forbes et al., 2014].

Although the proposals were on some papers in older times, incremental growth of columnar joints has not been studied in detail until the following papers were published; DeGraff and Aydin (1987), Aydin and DeGraff (1988) and DeGraff et al. (1989). DeGraff and Aydin (1987) sketched the band structures in details, which are called 'stria'. Successive stria are the evidences of incremental growth of columnar joints and individual striae has plumose structures on which indicate the origin of cracks and the direction of crack propagation. Striae is composed of smooth parts that are caused by brittle lava which is relatively cooler at crack initiation and and rough parts produced by ductile lava, which is hotter. These two results determined that columnar joints were formed from outside to inside of cooling rock.

Calculations for cooling process of rock have been attempted by solving heat conduction equations [e.g., Lovering, 1935; Jaeger, 1957; 1959; 1961]. Jaeger (1961) made an assumption that if a temperature T_c which cracking occurs exists, cracks perpendicular to the direction of the maximum tensile stresses on the same surface

of isotherm of T_c. He drew the isotherm distribution by applying the solutions of a heat conduction equation to various types of boundary conditions associated intrusive and extrusive rocks in many situations, as it will be described in Section 1.3.

In the end of 1990's analogue experiments by drying starch-water mixture as analogue materials were well conducted [e.g., Muller, 1998a, 1998b; Toramaru and Matsumoto, 2004; Mizuguchi et al., 2005; Goehring et al., 2006; Goehring and Morris, 2008]. The hydraulic diffusion process has been assumed for drying specimen as analogue theory to heat conduction process on cooling rock and its details are given in Section 1.4.

So, the researches on columnar jointing systems have been studied from descriptive, petrographic, calculative and experimental ways. However, there are two questions are still unclear; 1) the directional relationship between the isotherm and maximum tensile stresses when the cracks occur and 2) how and why morphological transition happens from Colonnade to Entablature?

1.2 Field observations

1.2.1 Surface morphology of column side

Columnar joints are caused by volume contraction during cooling of rock. As emplaced magma bodies start cooling down, thermally induced tensile stresses in all directions act on the cooling surface and gradually concentrate at some points. When the concentrated tensile stresses become above the strength of the rock, mode-I cracks generate at a point of the cooling surface. According to the observation of cooling Hawaiian lava lakes by Peck and Minakami (1968), the crack propagation advanced from the top of lava lakes into hotter inside and then a set of columnar joints were formed at upper part of the solidified lava lakes. They also discovered on the side of columns that the successive band structures, which are called 'stria', normal oriented to the column axes. These observations indicate that columnar joints at Hawaiian lava lakes developed incrementally downwards from the cooling surface. DeGraff and Aydin (1987) investigated the surface morphology on column sides at the sites of Columbia River Basalt in USA. There were distinct stria with plumose structures which can be traced their pattern without weathering. By analyzing the plumose structures on individual stria, they got new observations

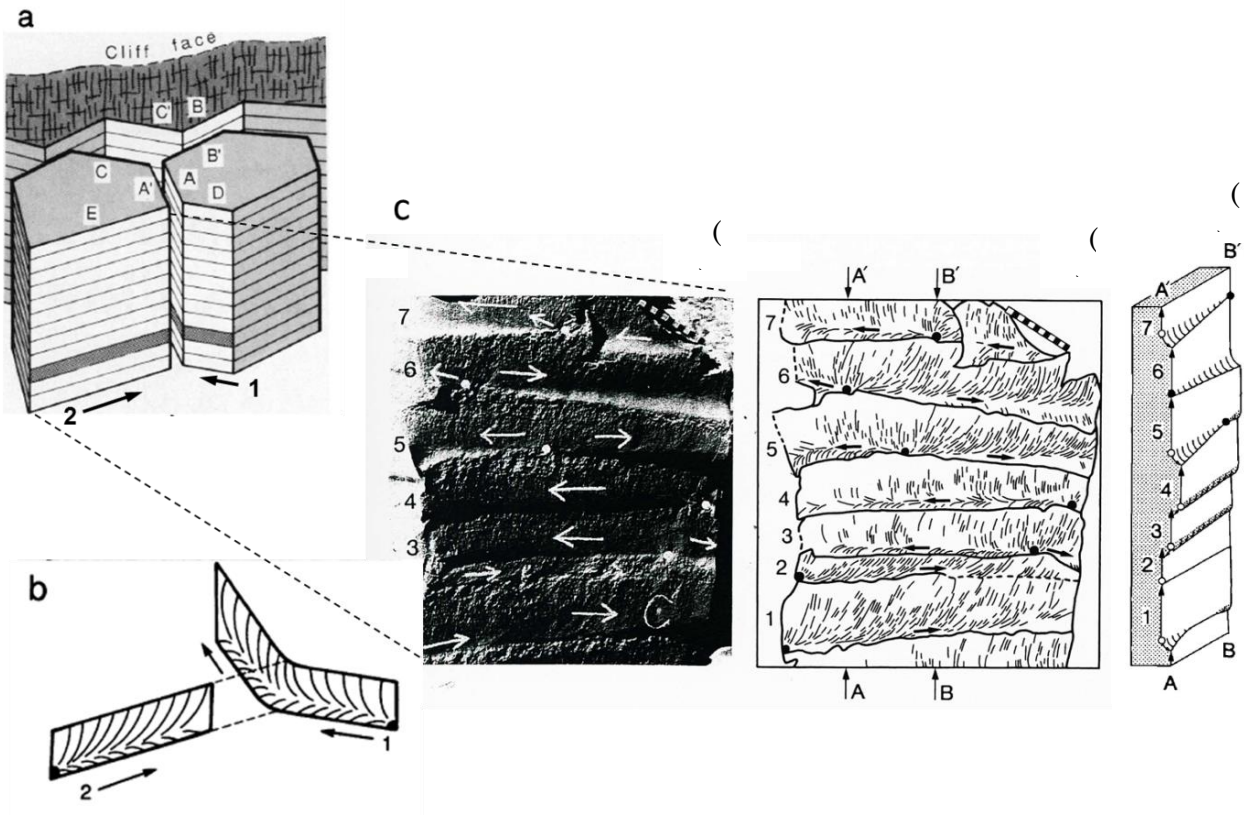

Figure 1.2: Interpretation of surface morphology of a column side near a flow base from Snake River Basalt flow [modified from DeGraff and Aydin (1987) Figure 5 and Aydin and DeGraff (1988) Figure 3]. a. Schematic drawing of an exposure normal to column axes. Letters indicate the eight joint surfaces. b. Schematic surface morphology of a set of stria which is indicated as dark band in a above. Plumose structure shows on each striae with the arrows which indicates the direction of propagation. c. (1). Band structures (stria) of the column surface. Each band has one plumose structure and its origin shown as white dots. (2). Sketch of the column face. Black dots are crack origins in each striae and black arrows are the direction of crack propagation along the plume axis. The numbers along the column indicate the order of crack propagation from the bottom up. (3).Cross section view A-A'-B'-B. Overhangs and ledges of column face are shown by parallel curved lines.

that one asymmetric plume-like fracture pattern on one striae. It fans away from the crack origin generating on the edge of older striae (Fig. 1.2). Columnar joints are gradually formed by such an incremental propagation process into the inside of cooling of rock.

1.2.2 Morphological transition between Colonnade and Entablature

When a lava flow emplaces at a place, it is cooled down from the surfaces contacting on the ground and on the air. Columnar joints can be found in multiple-tiered structures caused by multiple emplacements of lava flows at different times. Richardson (1808) made a detailed sketch of basaltic lava flows in Causeway Coast and noted the two-fold division in each lava flow with columnar structure (Fig. 1.3). He mentioned the two different structures in terms of their morphology as 'the upper irregular prismatic' and 'the lower regular columnar' in his letter. Although subsequent researchers described their morphological features using various expressions [e.g., Iddings, 1886; Sosman, 1916; James, 1920]. Tomkeieff (1940) cited from the architectural words and assorted mainly two structures in columnar joints in terms of their positions; the lower columns are *Colonnade* and the upper columns

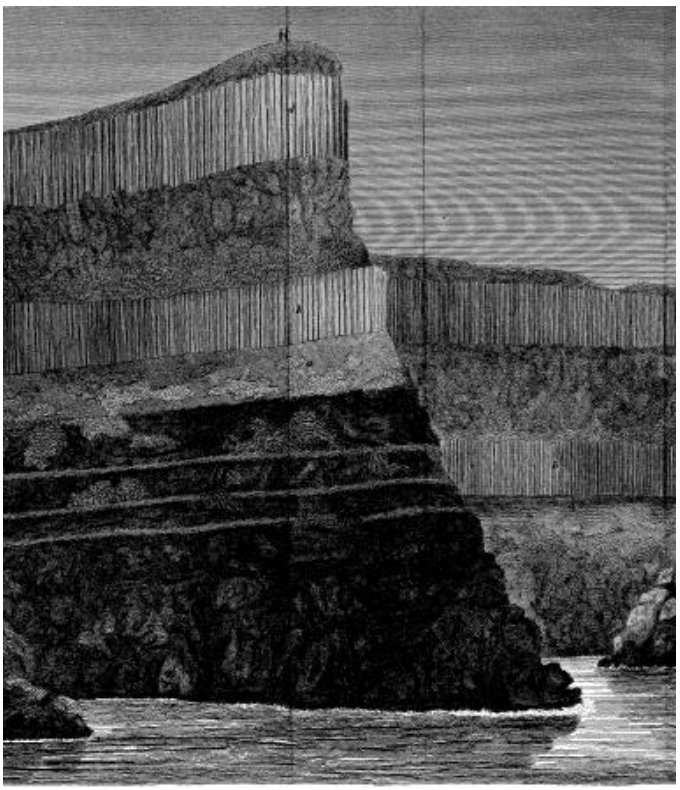

Figure 1.3: The sketch of columnar joints along Causeway Coast by Richardson (1808). Two-fold structures are drawn clearly as he recognized within one flow unit. The top of the basaltic flows are illustrated irregular columns, while the lower of it are regular columns.

are *Entablature*. Some both structures are seen within one flow unit and the difference of them are clear as shown in Figure 1.4. Spry (1962) summarized that morphological variations in Entablature itself formed by curved columns (Fig. 1.5). He mentioned that the isotherm patterns to form curved columns can be described reasonably under the assumption that the directions of columns are perpendicular rock, however, the directions of columns more likely to the distribution of tensile stresses rather isotherms.to the isotherms of cooling

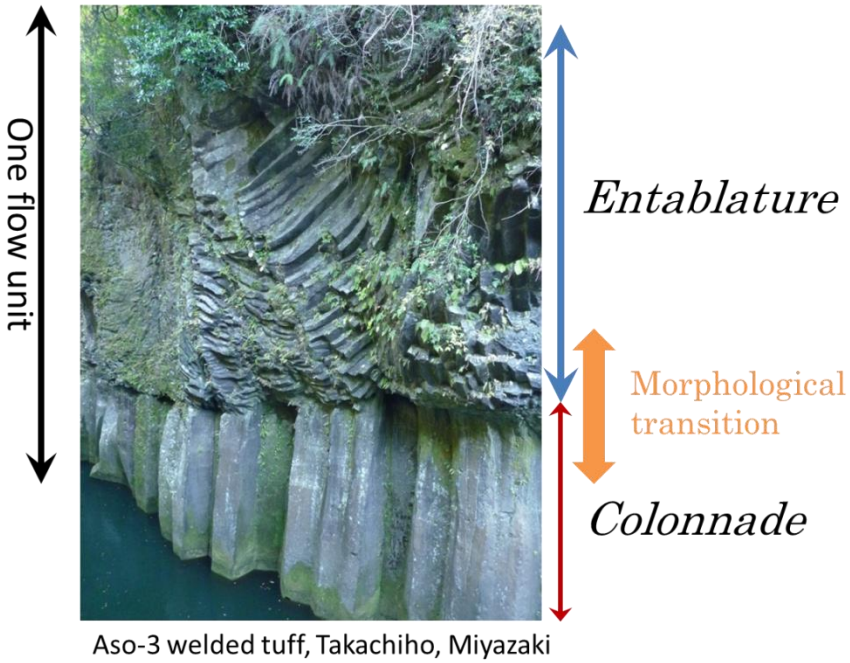

Figure 1.4: Morphological transition between Colonnade and Entablature within one flow unit. This is one of the examples of columns joints at Takachiho in Miyazaki, which is composed of Aso-3 welded tuff. The upper part is Entablature with relatively smaller width, curved and irregular columns, while the lower part with relatively larger width, straight and regular columns.

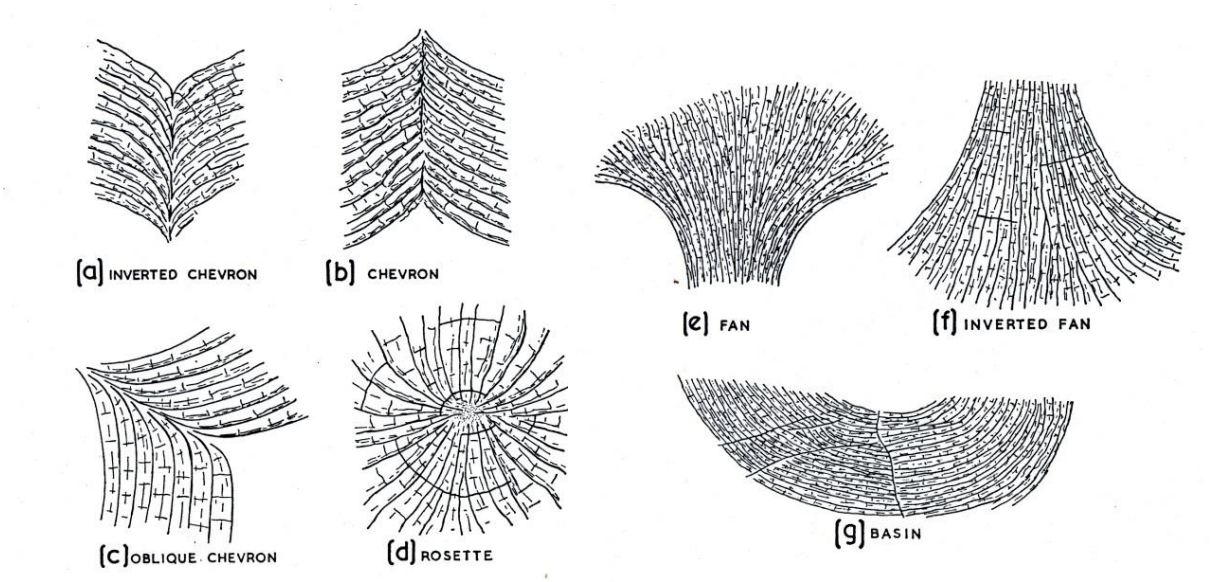

Figure 1.5: Various structures of Entablature formed by curved columns [Spry, 1962]. [a], [b] and [c] are called 'chevron' depending on which the direction of tapered columns are. The columns extended out from a plane. [d] is called 'rosette', which has the radial pattern. [e] and [f] are called 'fan' structures, which radiated from a point. [g] is called 'basin', which has horizontal columns in the center and curved up at the ends.

1.2.3 Cooling rate between two structures from texture analysis

The size of columns is related to cooling rate and temperature of rock. Rapid cooling rate causes small size of columns from field observation. As the evidence of rapid cooling in rock texture, Fe-Ti oxide in Entablature includes dendritic shapes, not including in colonnade [Long and Wood, 1986]. In addition, glassy mesostasis, which is formed by fast cooling of the rock, is included higher percentage in Entablature part than in Colonnade part. Both characteristics indicate that the part of Entablature was suffered from more rapid cooling than that of Colonnade. They suggest that extremely heavy rainfall (>>250 cm/yr) and extensive flooding caused enhanced cooling at the level that cracks propagated just around the morphological transition between Colonnade and Entablature. Forbes et al. (2014) investigated fracture and texture observations of Entablature part in Iceland and suggested that the coolant such as water and/or steam entered through master joints and caused most rapid cooling around master joints.

1.3 Calculation analysis for cooling process

The cooling process of igneous rock has been discussed based on heat conduction for many years [e.g., Ingersoll and Zobel, 1913; Lovering, 1935; Jaeger, 1961; 1959; 1957]. Ingersoll and Zobel (1913) summarized the principle of heat conduction for applying to geological and engineering subjects. In geological part, they gave the formulae for extrusive sheet. Lovering (1935) suggested the formulae for various form of intrusions. These works gave the assumptions that the country rock was zero temperature at initial and the magma was initially at a homogeneous temperature T_0 . Jaeger (1957, 1959, 1961) considered the temperature distributions in the cases of intrusive sheet as shown in Figure 1.6. As it mentioned in the former section, Entablature has various structures, which are described as chevron, fan and basin type in Spry (1962). The assumptions that thermal diffusion process during cooling and cracks develop perpendicular to the isotherms of T_c have been applied to consider relatively simple cases of curved structures.

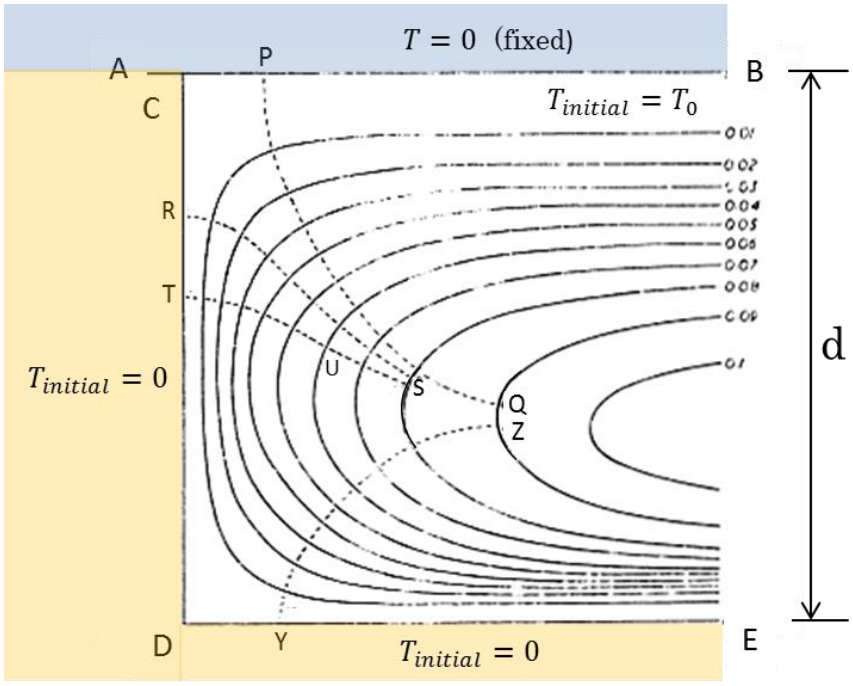

Figure 1.6: The progress of the 0.6 T_0 for an extrusive sheet initially temperature T_0 occupying the region BCDE of thickness d (modified from Jaeger (1961) Figure 2). The surface BC is maintained at zero temperature and the region below the surface ACDE contains country rock initially at zero temperature. The dashed lines are drawn under the assumption that if the maximum tensile stresses are parallel to the isotherms, the temperature T_c at which cracks generate exists and cracks can be extended from the cooling surface to the T_c isotherms. The set of dashed line PQ, RS, TU are expected as 'fan' structures in Figure 1.5.

1.4 Analogue experiments of columnar jointing

Analogue experiments help us understand the physical phenomena by using daily-use materials which have the same physical characteristics as those in nature. In fluid dynamics, for example, some reproductive experiments have been known; Karman vortex by moving a stick straight in black ink poured into milk and Benard-Rayleigh convection by heating silicon oil in a container. It is quite interesting to see the same morphological change just in front of us as those at troposphere although they are much smaller size and time scale. In the case of columnar jointing, starch and water mixture has been used as an analogue material of lava flows or welded tuff during cooling. Morphological structure and crack developments by volume contraction of mixture are well reproduced as columnar joints in rock. Such a characteristic of dried starch slurry has been found by French (1925) [Müller, 1998a and references therein]. Müller (1998a) conducted the first systematic study on laboratory experiments of columnar joints. He used corn starch (in his paper 1998a, while he used rice starch later in 1998b for getting more similar morphological features of basalt columns) mixture and dried a specimen under a lamp, which was supposed to be a parameter of the evaporation rate. He described

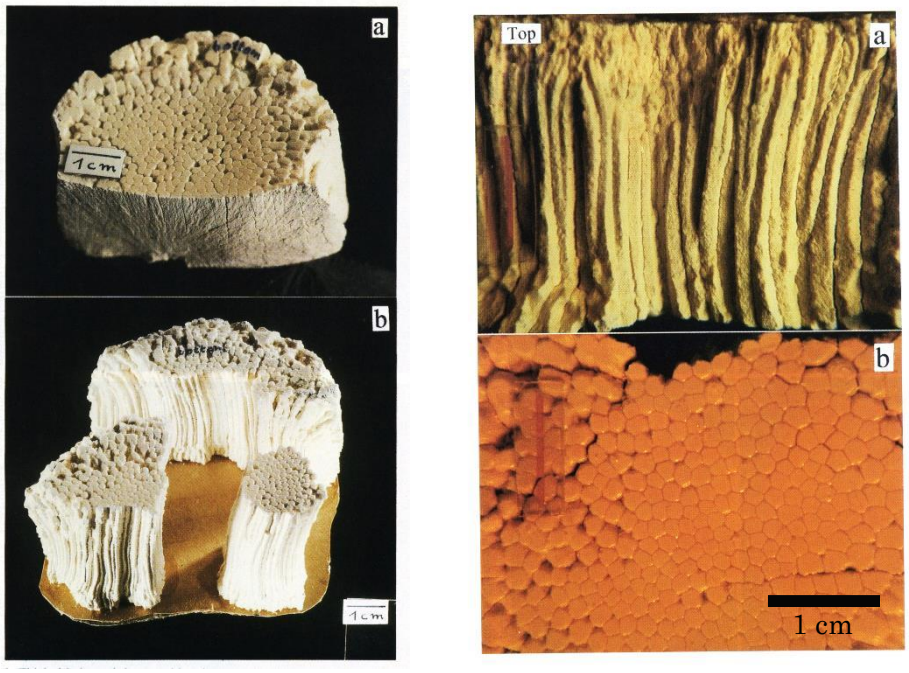

Figure 1.7: Thick dried starch specimen with columns from Müller (1998a). Left: The top view is the bottomside of the specimen. (a) The front side is the surface of first-generation crack showing plumose structure radiating into pieces. (b) The columns develop about 5-10mm from the top of the specimen. Right: Detailed side view and bottomside of the same specimen of Left (a) and (b). Polygonal cross-sectional surface can be recognized at the bottomside of the specimen.

mainly two crack propagation process: first-generation cracks, which penetrated to the bottom of the specimen at a point at the beginning with large thickness loss, and second-generation cracks, which propagated all over the surface with irregular, small-scale cracks at first and then grew downward. He assumed that the hydraulic diffusion process for drying starch-water mixture as an analogue theory of heat conduction for cooling basalt. He concluded that the diffusivity in starch is 2 order of magnitude smaller than that in basalt. Toramaru and Matsumoto (2004) focused on the relation between column size and desiccation rate and the dominance of polygonal shape. They used potato starch and changed the distance between lamp and starch surface as a parameter. As a result, the inverse relationship between the averaged cross-sectional area and desiccation rate was experimentally-verified and the higher cooling rate provides pentagon dominance, on the other hand the lower cooling rate provides hexagon dominance. Advanced diffusion equations as water transportation in drying starch mixture were suggested [Mizuguchi et al., 2005; Goehring et al., 2006]. Mizuguchi et al. (2005) introduced the term of drainage through cracks into the hydraulic diffusion equation and suggested that the evaporation through cracks become to dominate when the hydraulic diffusivity is much smaller than the coefficient which is the multiplicative value of an

evaporation resistance and air density. Goehring et al. (2006) used advection-diffusion equation for assuming that the convective cooling regime at the far from the cooling surface. In time-independent case, they simplified the advection-diffusion equation by introducing the Peclet number, Pe and they got Pe = 0.15 ± 0.05 from starch specimen of analogue experiments, while Pe = 0.3 ± 0.2 from basalt columns to control crack spacing. All experiments are conducted for reproducing Colonnade structures.

1.5 Aims and Outlines of this thesis

There are some problems that still remain to be solved:

- Do the maximum tensile stresses work on parallel to the isotherms when cracks generate?

- Are the crack direction is perpendicular to the isotherms T_c, which is the temperature to generate cracks?

- Is it possible to form such a complex isotherms in Entablature part?

- What is the factor of controlling the morphological transition from Colonnade to Entablature in a single flow unit during cooling?

In this thesis, I conducted three experiments to examine: (Experiment 1) Transfer processes in drying and cracking samples under simple experimental condition of the drying process from one direction in Chapter 3, (Experiment 2) Water concentration and the direction of cracks with time under experimental condition of the drying process from two directions in Chapter 4 and (Experiment 3) Effects of sudden increase in desiccation rate on drying and cracking processes in Chapter 5. Finally, I give an implication for the morphological transition from Colonnade to Entablature taking up one example at Shakushiiwa in Oita in Chapter 6.

Chapter 2

Analogue materials and X-Ray CT systems

I conducted three experiments as following analogue materials and X-Ray CT systems. Section 2.1 will describe analogue materials and Section 2.2 will describe X-Ray CT systems in all experiments.

2.1 Starch types

I used starch and water mixture as analogue material following previous studies. Two types of starch are used as shown in Table 1. Potato starch is used in Experiment 1 and 3, while kuzuko starch is used in Experiment 2 because of the stiffness of kuzuko starch mixture compared to potato starch mixture. A small amount of starches, which was mixed with a little of distilled water and put on a plate each, was observed through one nicol under a polarizing microscope as shown in Fig. 2.1. The grain sizes were measured on a photograph by the image processing software, Image J. The measurements were conducted along long axis and short axis to a grain. Potato starch (Fig. 2.1 (a)) is shaped an ellipse with broad distribution of grain size shown as Fig. 2.2 (a). Averaged grain size is 29.1±15.1 μm, which is calculated by (w+ℓ)/2: w is long axis and ℓ is short axis in one grain. The distribution of aspect ratio of potato starch grains is shown in Fig. 2.3 (a) calculated by ℓ/w (short axis / long axis). The highest frequency of aspect ratio of potato starch

is between 0.7 and 0.8, which shape parts from sphere. It corresponds with the observation under a polarizing microscope that elliptical shapes of potato starch grain can be seen a lot. The distribution tends to Gaussian profile. Kuzuko starch (Fig. 2.1 (b)) is shaped sphere with narrow distribution of grain size shown in Fig. 2.2 (b). Averaged grain size is 7.9±2.7 μm. Some grains with angular shapes are seen in a photograph. The distribution of aspect ratio of kuzuko starch grains is shown in Fig. 2.3 (b). The highest frequency is around 1.0 prominently with Gaussian profile in base. It is consistent that spherical shape of kuzuko starch grains can be seen a lot in Fig. 2.1 (b).

Table 1 Starch types in each experiment

Experiment No.	Starch type (brand name)	Averaged grain size [μm]
Experiment 1 and 3	Potato starch (Hinokuni)	29.1 ± 15.1*
Experiment 2	Kuzuko starch (Muso)	7.9 ± 2.7*

※Averaged grain size was calculated by (w+ℓ)/2: w is long axis and ℓ is short axis of one grain.

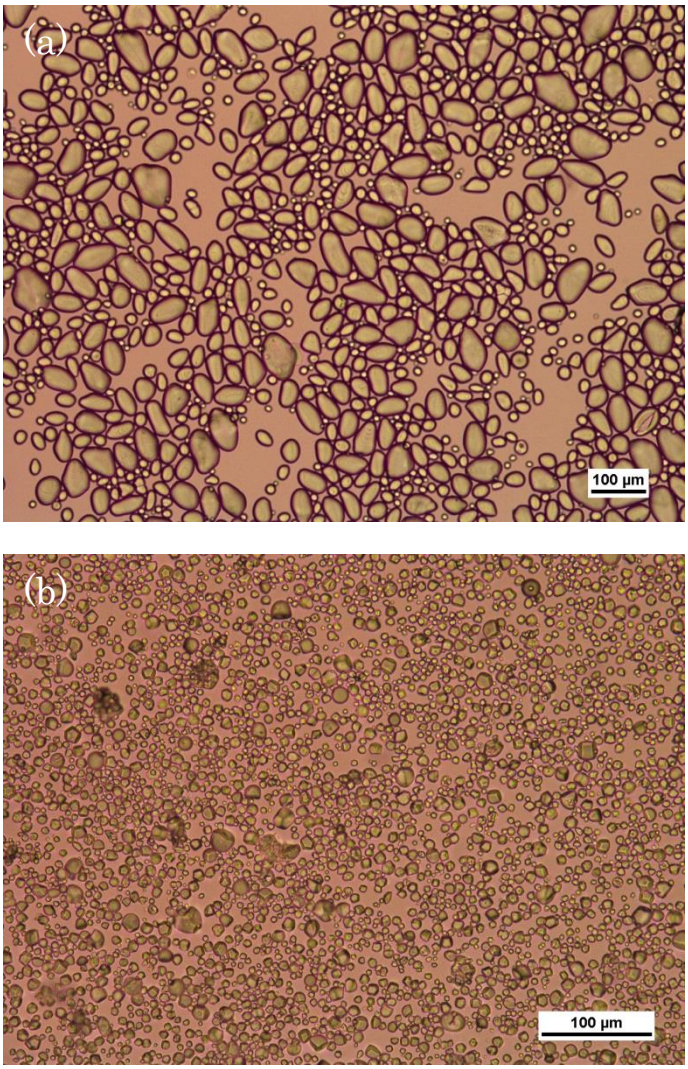

Figure 2.1: Starch grain of two types of starches. The scale in both pictures are shown 100 µm. (a) Potato starch. Grains are ellipsoidal shape or very smaller grains (the diameter is around 10µm) are almost sphere. The image is taken under using magnified a 10 times objective lens. (b) Kuzuko starch. Almost all grains are spherical or a little angular shaped particles. The image is taken under using magnified a 20 times objective lens.

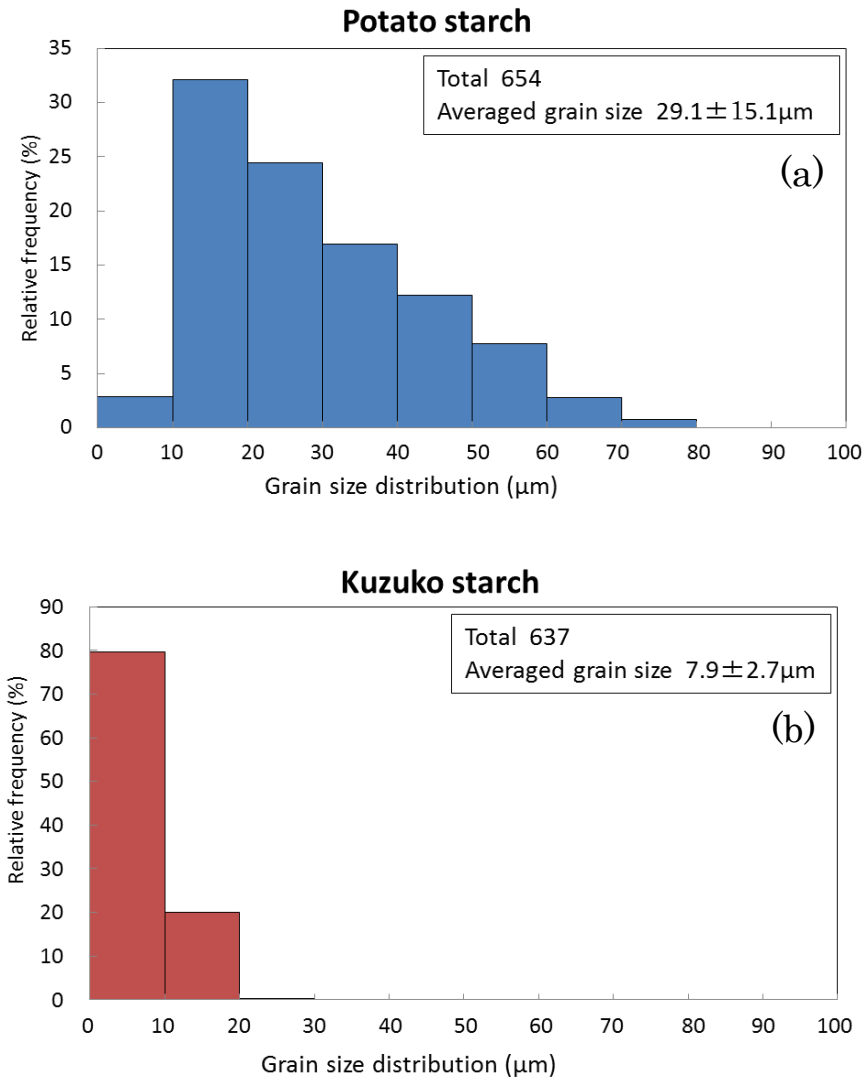

Figure 2.2: Relative frequency of grain size distribution of both potato and kuzuko starches. Grain size is calculated by (w+ℓ)/2, which w is long axis and ℓ is short axis of one starch grain. (a) Potato starch. The distribution of grain size of potato starch is wide range and the highest range is between 10 and 20 μm. The distribution of larger grain size decreases in a staircase pattern. Averaged grainsize distribution is 29.1±15.1μm. (b) Kuzuko starch. The distribution of kuzuko starch is in contrast is narrowly distributed between 0 and 30 μm. Averaged grainsize distribution is 7.9±2.7μm.

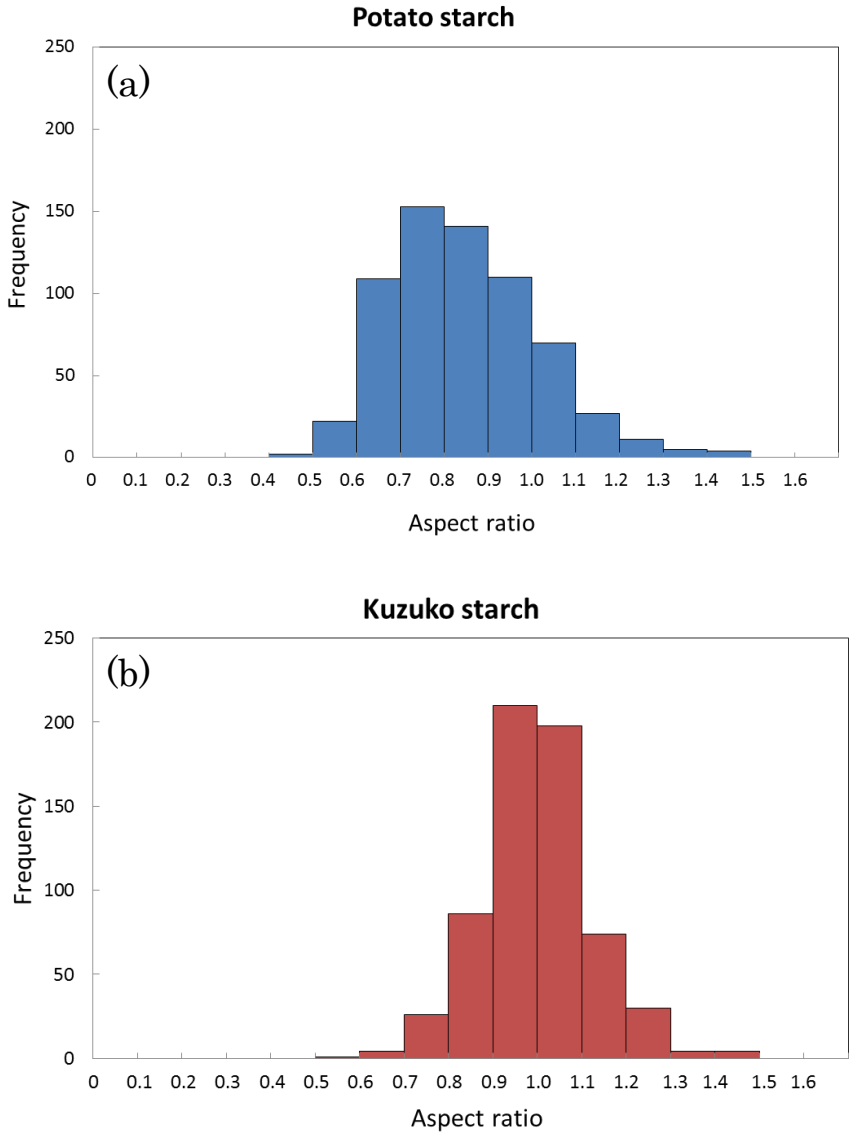

Figure 2.3: Aspect ratio of both potato and kuzuko starch grain. (a) Potato starch. The distribution has broad base with the highest frequency between 0.7 and 0.8 in the center. (b) Kuzuko starch. The highest frequency is distributed around 1.0 prominently with broad base. It means that spherical shape of kuzuko starch grains are in major.

2.2 X-ray CT systems and photographing conditions

X-ray CT system has been used to observe inside of starch structures without any destruction [Müller, 1998a; Goehring, 2008 PhD thesis]. X-ray CT system produces multiple sectional images, which are called CT images, by reconstructing transmission images from detected transmitted X-ray intensity (Fig. 2.4 (d)). I used a micro focus X-ray CT system for all experiments as shown in Table 2. The systems are owned by Fukuoka Industrial Technology Center (Fig. 2.4 (a)). The sample is fixed on a rotating table in front of X-Ray source assembly (Fig. 2.4 (b)) and rotated 360 degrees during X-radiating. It takes about 15 – 20 minutes for getting transmitted images for one time and transmitted X-Ray intensity is detected by the detector as shown in Fig. 2.4 (c).

Table 2 The condition of X-Ray CT system

Experiment No.	Micro-focus X-ray CT system	Matrix size	Resolution [mm]	Slice width [mm]	Number of images
Experiment 1	MCT225K (Nikon Instech Co., Ltd.)	2000 × 2000 × 2000	0.06 (voxel)	0.06	2000
Experiment 2		2000 × 2000 × 2000	0.03 (voxel)	0.03	2000
Experiment 3	HMX225-ACTIS+3 (Tesco Co.)	512 × 512	0.12 (pixel)	0.2	330

Figure 2.4: X-ray CT system, MCT225K (Nikon Instech Co.) owned by Fukuoka Industrial Technology Center. (a) MCT225K and PC for reconstructing CT images and analyzing data. (b) X-ray tube and the sample, which is fixed on the table. (c) The detector of transmission X-ray.

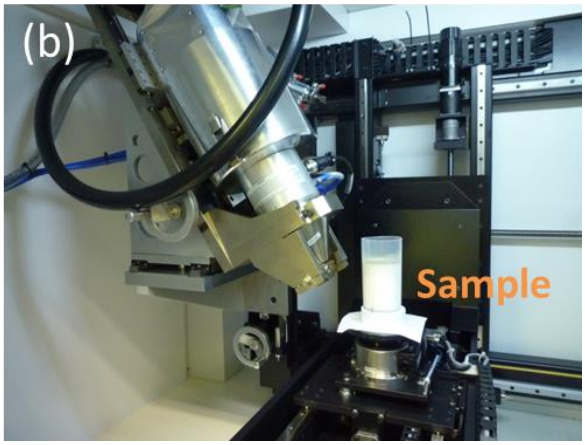

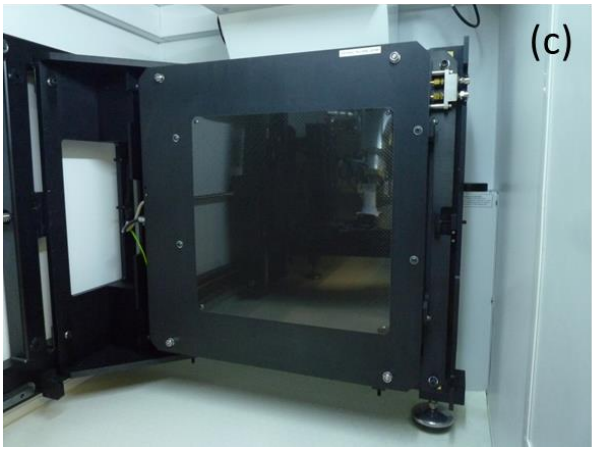

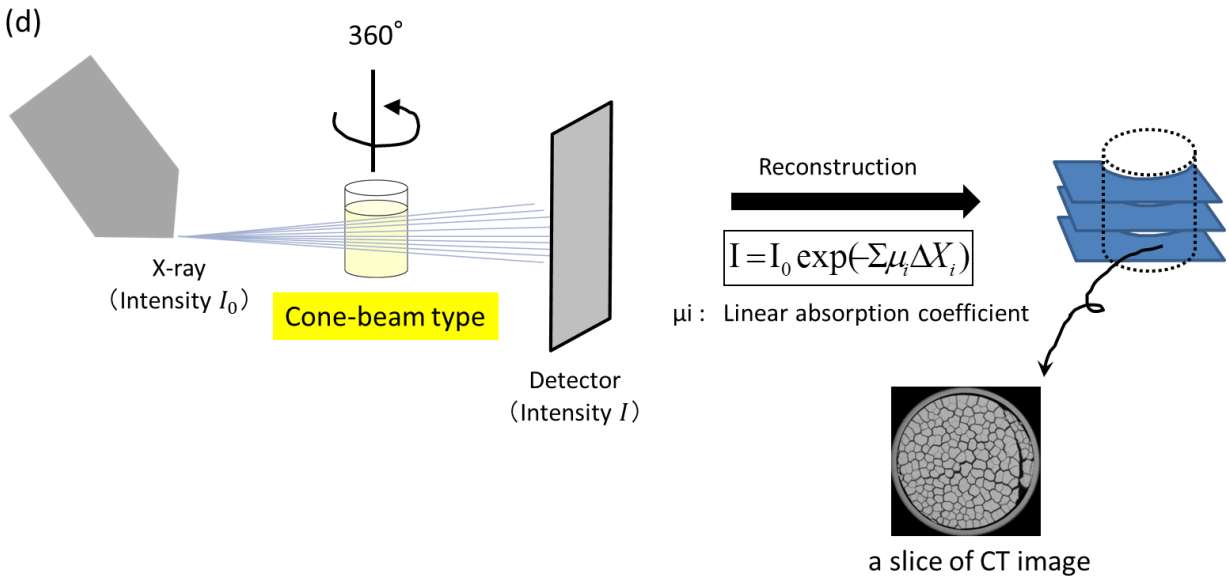

(d) The principle of X-ray CT photographing. The X-Ray is radiated with cone-beam type. The reconstruction of CT images is conducted on a computer using detected transmitted X-Ray on the detector.

Chapter 3

Experiment 1: Drying process from one direction

Experiment 1 is the case that mixture is dried from one direction, simulates that one flow unit is cooled from one surface homogenously. The purpose of this section is to describe a drying process from one drying surface in detail. Crack propagation process in the mixture and the relationship between water distribution and cracks with time are also described.

3.1 Experimental setup

Mixture by mixing 150 g potato starch (Hinokuni) and 150 g distilled water each is put into an acrylic cylindrical container (6 cm in diameter and 11 cm in height) and lit by a 60 W light bulb. The distance between mixture surface and the bottom of the light bulb is set 1.5 cm in the early stages. The position of the lamp is fixed from beginning to end of the experiment. All experimental apparatuses except a PC are put into the desiccator (Fig. 3.1). Temperature and relative humidity within the desiccator are monitored by a sensor in the defumidifier (Thermoelectric defumidifier BOXDRY, OHM Electric Co., LTD.) every 10 minutes. The relative humidity is set 30%RH (RH = Relative Humidity) at a given temperature in the desiccator. The container with mixture is put on the electric balance (Compact balance EK-610i, A&D Co.) and the weight of mixture is monitored by PC every 5

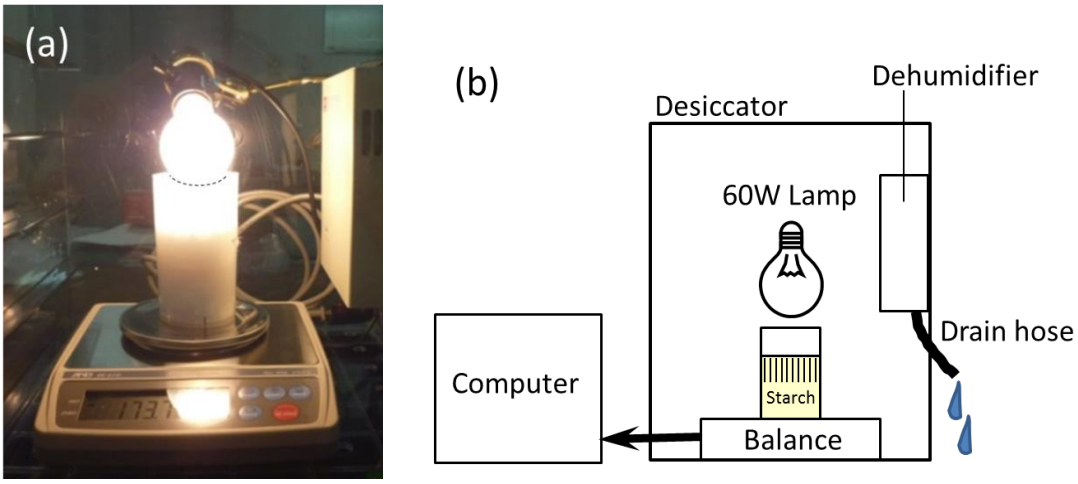

Figure 3.1: Experimental setting of Experiment 1. (a) Starch and water mixture in a cylindrical container is put on electric balance to record the weight automatically every 5 mins. A lamp is set above the container and it makes the mixture to dry faster than natural drying. (b) Temperature and humidity on the substrate in the dehumidifier are recorded every 10 mins. The dehumidifier has peltier cooling system, which condenses the humidity within the desiccator and emits the water through a drain hose.

minutes. The weight change is shown in Fig. 3.2. Since the container and the desiccator are transparent, the depth of developed crack fronts with time are visible thorough the wall of container.

Figure 3.2 shows weight and desiccation rate change of Experiment 1 as (a) and (b) respectively. In both figures red dots are interrupted by gaps during which samples were removed from electric balance to take CT images, while blue dots depict for the preliminary experiment to show the case without taking CT images during the experiment.

In the preliminary experiment, the weight of mixture monotonically decreases and the slope changes at around 24 hours from the beginning. Weight change in the case of taking CT images shows the same trend, though there is a time lag of slope change due to the period of inactive drying process during taking CT images. The desiccation rate change in Figure3.2 (b) is calculated by the differentiation from the weight loss per 5 minutes by the period. In both figures solid and dashed arrows indicate the time when the first cracks occur on the surface of mixture ; solid arrow is the case of preliminary experiment, while dashed arrow is the experiment taken by X-ray CT system.

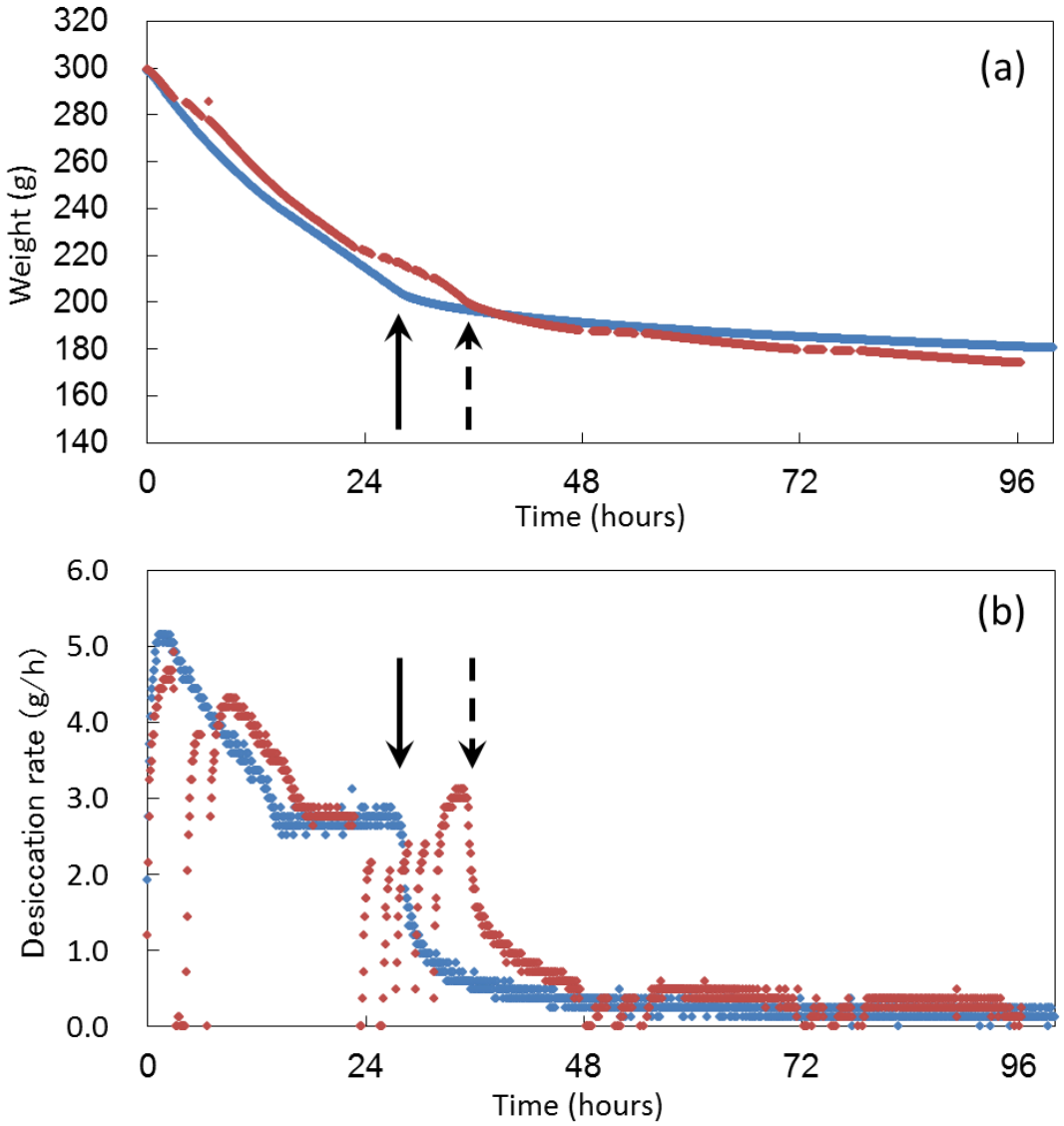

Figure 3.2: Weight and desiccation rate change of Experiment 1. Red dots are data of the experiment in which the sample was removed for X-ray CT operation. Blue dots are data without picturing by X-ray CT. Discontinuous gaps in red dots correspond to the period when the sample was removed from the electric balance. (a) Weight change recorded automatically by electric balance every 5 mins. (b) Desiccation rate change. The values are calculated by the differentiation from the weight loss per 5 minutes by the period. In both figures the time when first cracks occur on the surface of mixture is shown as solid arrows in the preliminary experiment and dashed arrows in the experiment with CT operation each.

3.2 Description of desiccation process from external observations

The behavior of the desiccation rate change in the result of taking CT images is basically the same as that of preliminary experiment (the result without taking CT images) except time delay caused by removing the sample. Figure 3.3 shows the desiccation rate change of preliminary experiment, which is the same as blue dots cited from Figure 3.2, and the illustrations of desiccation process with time, which is based on direct observation of mixture during the experiment. It is found that there are three phases shown as different colors, numbers and illustrations; （Ⅰ） Monotonic decrease of desiccation rate with decrease of supernatant liquid (t = 0 ~ 14.25 [hours]), （Ⅱ） Constant desiccation rate under no supernatant liquid phase (t = 14.25 ~ 28.5 [hours]) and （Ⅲ） Abruptly decrease of desiccation rate at the beginning of horizontal crack propagation on the surface and small decrease of desiccation rate with vertical crack propagation phase (t = 28.5 ~ end of experiment). The detailed observations are following below. The time lag between preliminary experiments and CT operation is shown in Table 3.

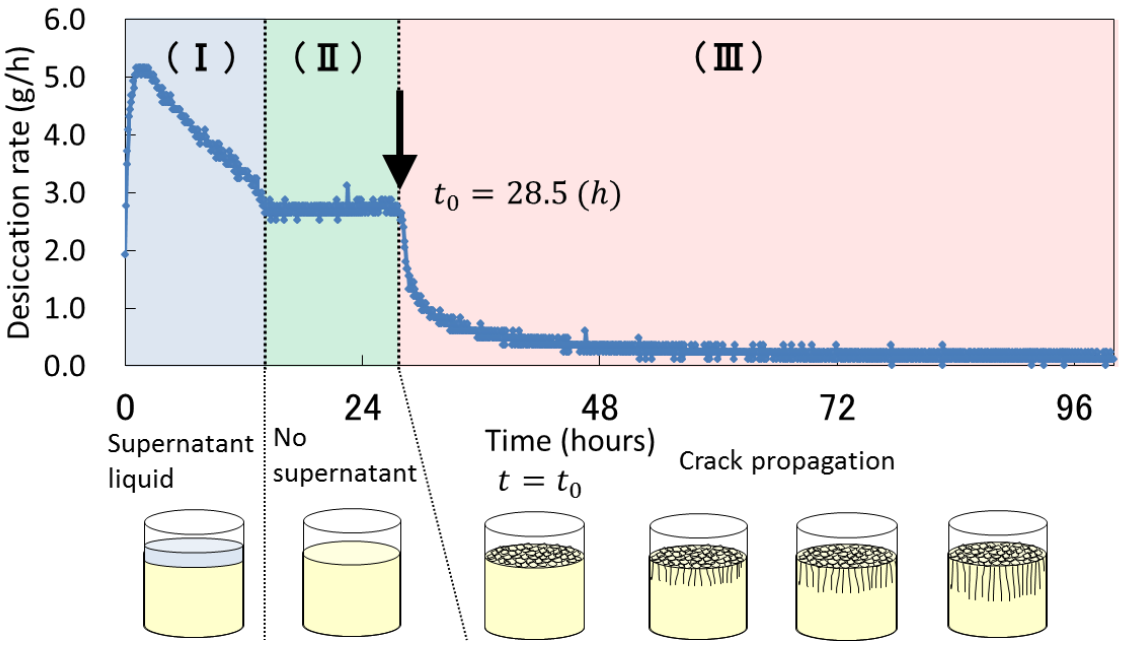

Figure 3.3: Desiccation rate change in the case of preliminary experiment. The periods shown by（Ⅰ）Supernatant phase,（Ⅱ）No supernatant phase and (Ⅲ) Vertical crack propagation phase, which are colored according to Table 3. The illustrations below the graph were based on the direct observation through the Experiment 1.

Table 3: The period of three phases of desiccation rate change and time lag between preliminary experiment and CT operation.

Three Phases	Preliminary experiment (hours)	CT operation (hours)	Time lag (hours)
（Ⅰ）Supernatant phase	0 - 14.25	0 - 17	2.75
（Ⅱ）No supernatant phase	14.25 - 28.5	17 - 35.25	6.75
（Ⅲ）Vertical crack propagation phase	28.5 - end	35.25 - end	—

（Ⅰ）Monotonic decrease of desiccation rate with decrease of supernatant liquid phase (t = 0 ~ 14.25 [hours])

Desiccation rate monotonically decreases from the maximum value 5.2 g/h to 2.8 g/h at the end of this phase. There is a supernatant liquid on the surface of mixture as described in Figure 3.4. The distance between the bottom of lamp and the surface of mixture, ℓ is initially 1.5 cm. The surface of mixture in this phase must be considered as the distance between the bottom of lamp and the surface of 'supernatant'. As the evaporation of supernatant liquid advances, ℓ increases and at the end of this phase it becomes 3.0 cm, which equals to just on the surface of mixture.

（Ⅱ）Constant desiccation rate under no supernatant liquid phase (t = 14.25 ~ 28.5 [hours])

In this phase, the desiccation rate is nearly constant at 2.8 g/h. This phase is coincided with the period when no supernatant liquid exists on the mixture surface and no cracks form in the mixture.

（Ⅲ） Crack propagation phase (t = 28.5 ~ end of experiment [hours])

At t = 28.5 hours, first cracks on the surface were found to occur by the observation. They are uniformly distributed on the surface. Soon after first cracking, the desiccation rate falls abruptly as shown in Figure 3.3 and it becomes slightly above 0 g/h to the end of the experiment.

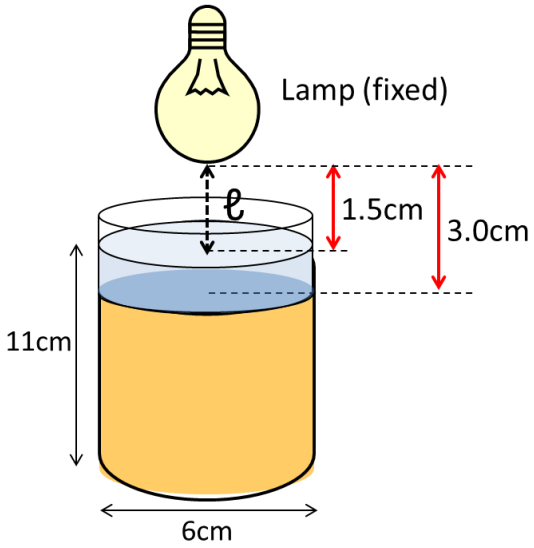

Figure 3.4: Schematic diagram of Experiment 1. The distance between the bottom of the lamp and supernatant liquid will be set 1.5 cm as an initial condition. As supernatant liquid evaporates, it decreases and becomes 3.0 cm when supernatant liquid completely vanishes away.

3.3 CT image observations in each phase

CT photographing were operated 14 times through the experiment; t = 3, 6, 23, 25, 27, 29, 31, 48, 51, 54, 72, 75, 78, 101 (hours). These timing taken CT images are corresponds with discontinuous gaps in red dots as denoted by number in Figure 3.5. CT images through the experiment are shown in Figure 3.6 by grayscale image. The elapsed time from the beginning of the experiment is indicated below each image. The color gradation from white to black by grayscale image in Figure 3.6 is basically equal to the density of the object. In the case of the mixture, the lighter color corresponds with the part of higher density, which indicates the lower water distribution in the mixture. On the other hand, the darker color corresponds with the part of lower density, which indicates the higher water distribution in the mixture. The darkest part coincides with the air (no object) or cracks in the mixture. Due to have more clear contrast in the internal mixture, the colored images depending on the brightness of Figure 3.6 are shown in Figure 3.7. The colored image processing was conducted by using XMapTools. Here, I will describe the observations of colored images in Figure 3.7 on (Ⅰ), (Ⅱ) and (Ⅲ) each.

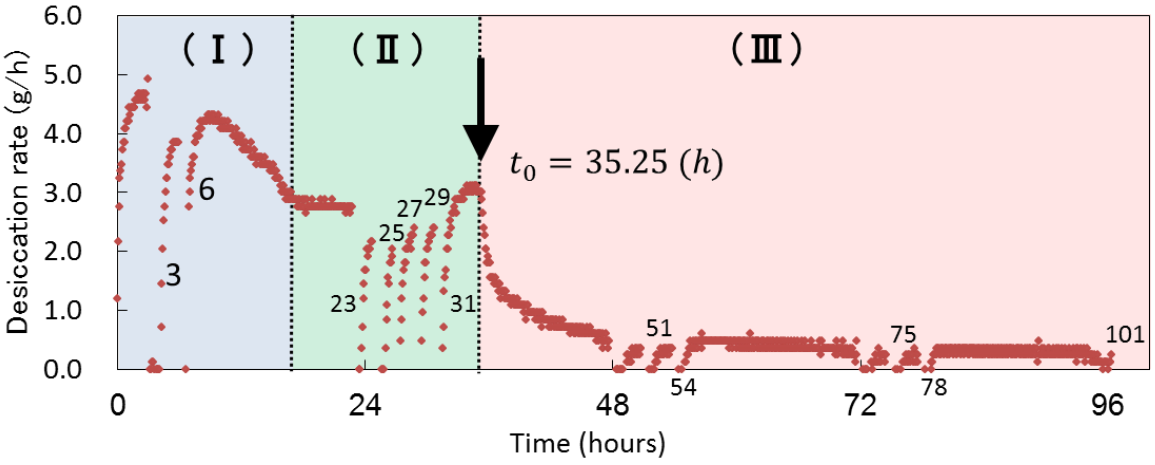

Figure 3.5: Desiccation rate change in the case of taking CT images. The numbers by the time gap of desiccation rate indicate the elapsed time when CT operations were conducted. t_0 is the time when the first crack propagated on the surface of mixture. The periods shown by (Ⅰ), (Ⅱ) and (Ⅲ) are colored according to Table 3.

（Ⅰ） t = 0 ~ 17 [hours]

The CT images at t = 3, 6 hours shows clear boundary between supernatant liquid and mixture in the internal structure. The part corresponding to supernatant liquid is darker, while the part below, which corresponds to the mixture, is lighter. The brightness of mixture part is uniform and there is no vertical volume change.

（Ⅱ） t = 17 ~ 35.25 [hours]

CT image of this phase can be seen in the images denoted that t = 23, 25, 27, 29, 31 hours, which shows the higher brightness part like crescentic shape at upper surface of the mixture. This crescentic part gradually decreases the area with time. Volume change of mixture and cracks on the surface were not observed during this phase from the CT images.

（Ⅲ） t = 35.25 ~ end of experiment [hours]

Cracks are seen at the upper part of mixture denoted that t = 48, 51, 54, 72, 75, 78, 101 (hours). Cracks develop vertically into the depth with time. The tips of cracks, which is called ‘crack front’, has the crescentic shape and keeps its shape during cracking into the depth.

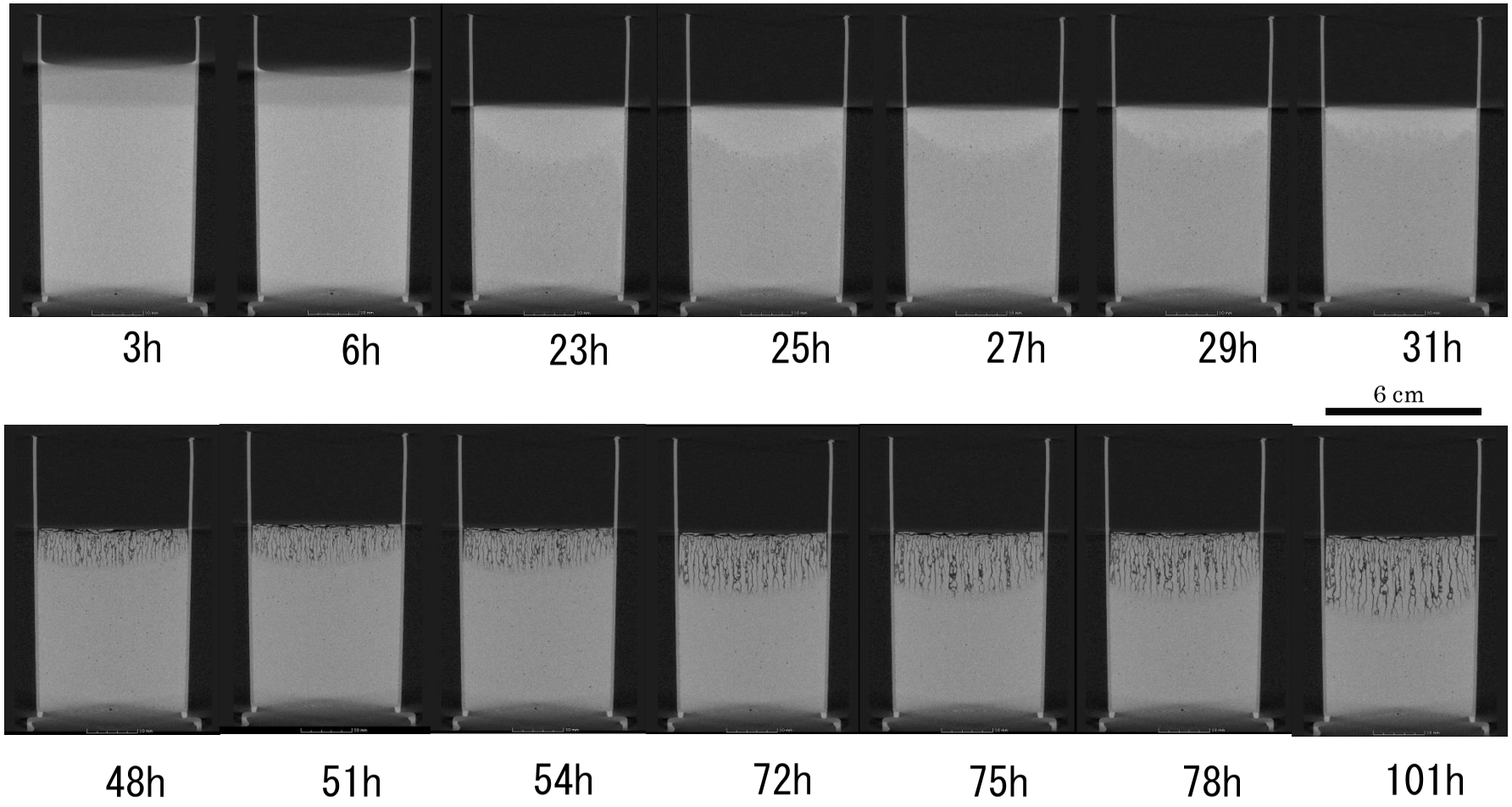

Figure 3.6: Gray scale CT images of Experiment 1. Times below each picture show elapsed time from the beginning of the weigh record. Brightness of images corresponds to the density of mixture. Black parts: Outside of container is air and lines in mixture are cracks. The gradation between white to gray in mixture depends on the density of mixture. More white indicates high density, while more gray (lower brightness) indicates low density.

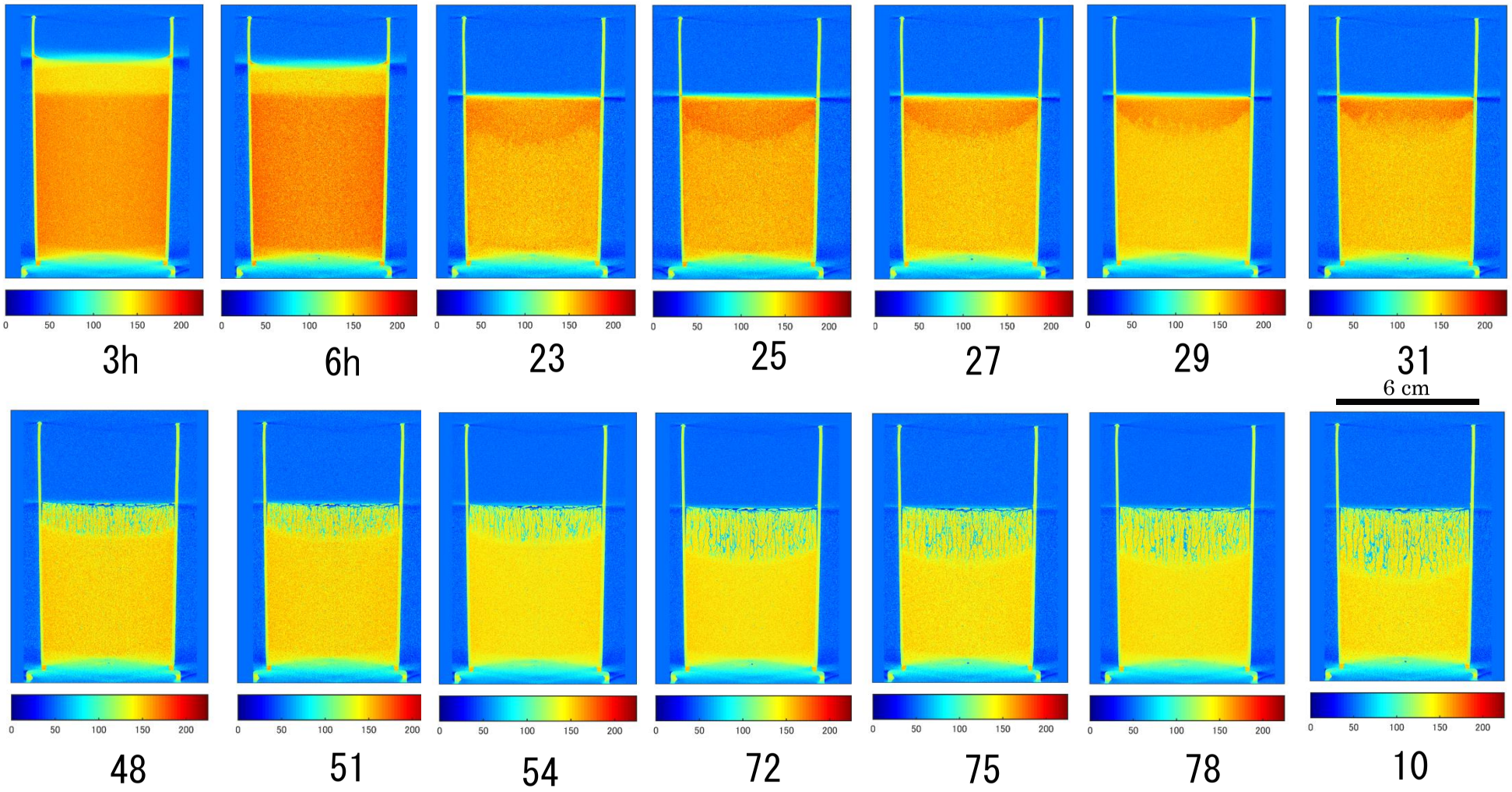

Figure 3.7: Colored CT images of Experiment 1 using XMapTools. Color range is 0 – 255 corresponding with the value of the brightness in grayscale. Time below each image indicate the elapsed time from the beginning of weigh record. The light blue parts at the boundary between the surface of mixture and the air, which become clear color difference compared to grayscale images, are the artifacts caused by between different materials (in this case mixture and the air).

3.4 Discussions

3.4.1 Summary of desiccation processes in three phases

Here I summarize three drying phases in Experiment 1 with some interpretations.

（Ⅰ）Supernatant liquid phase (t = 0 ~ 17 [hours])

Desiccation rate, $\dot{M}$ in this phase decreases linearly with time. When supernatant liquid evaporates with time, the distance ℓ between the lamp and the surface of mixture increases from 1.5 cm to 3.0cm. Desiccation rate of supernatant liquid (probably water) can be controlled by the temperature of the surface layer, T_s of it (Jones, 1992). Therefore $\dot{M}$ can be interpreted by the decrease of T_s of evaporating supernatant because T_s is proportional to $\ell^{-\frac{1}{2}}$ (Toramaru and Matsumoto, 2004). Because there is no volume and brightness change of mixture with time from the result of observing CT images, the water concentration within the mixture doesn't change. That is, weight change during this phase can be considered only by the evaporation from the surface of supernatant. If the total energy flux at the lamp, Q_L is constant through the experiment, the energy from the lamp, q_L can be expressed $q_L = Q_L/4\pi\ell^2$ in simple case (Toramaru and Matsumoto, 2004). So, it is assumed that the increase of ℓ during this phase makes q_L to decrease to the mixture and

decelerates $\dot{M}$ with time.

（Ⅱ） No supernatant phase (t = 17 ~ 35.25 [hours])

This desiccation phase corresponds to the period after all supernatant liquid evaporates until the first cracks occur on the surface of mixture. From the desiccation rate change in Figure 3.2 (b), the desiccation rate $\dot{M}$ is constant in this phase. Since the surface of mixture faces to the air, the water concentration of the surface layer of mixture, C_{sur} will decrease in the mixture at first and gradually decrease its value with time. To provide a certain amount of $\dot{M}$, however, it must be necessary for C_s to be constant through this phase. According to the CT images from 23 to 31 hours in Figure 3.7, in fact, the color at the surface of mixture keeps orange (the brightness is about 170 in the color bar). The uppermost parts of mixture show yellow which means lower density below them. In addition, as described in Section 3.3 (Ⅱ), there is a crescentic shaped higher density area at the upper part of mixture through this phase and the area gradually decreases from the bottom of it with time. Simultaneously, the total brightness of mixture under the crescentic area slightly changes lower with time. This can be considered that a constant supply of water comes from bottom up in the mixture.

Originally why such a higher brightness area appeared at upper part of the mixture? It is inferred that the lower bounding of a higher brightness area is convex downward and was caused by the different distance from the bottom of the lamp to the flat surface of mixture. As shown in Figure 3.8 (a), the closer the distance from the bottom of the lamp to the flat surface of mixture, the more noticeable the difference of ℓ_1 and ℓ_2 is. The temperature in the surface layer, T_s is proportional to $\ell^{-\frac{1}{2}}$ (Toramaru and Matsumoto, 2004) and it is confirmed by the infrared image shown as Figure 3.8 (b) that the larger central temperature on the surface is. Because the energy from the lamp, q is given by $q = Q/4\pi\ell^2$ (Toramaru and Matsumoto, 2004), the smaller ℓ has an influence in the mixture as higher brightness area.

Even though the upper part of mixture can be dried faster than the inside of mixture, why the brightness at the upper part of mixture shows higher? It can be considered that it causes fine cracks as gaps between starch particles to occur with little volume change, which is called dilatancy [狩野ほか. 1998]. Water in the mixture flows into the gaps and it causes the decrease of higher brightness area with time. Such water supplied from within mixture gives constant desiccation rate during this phase.

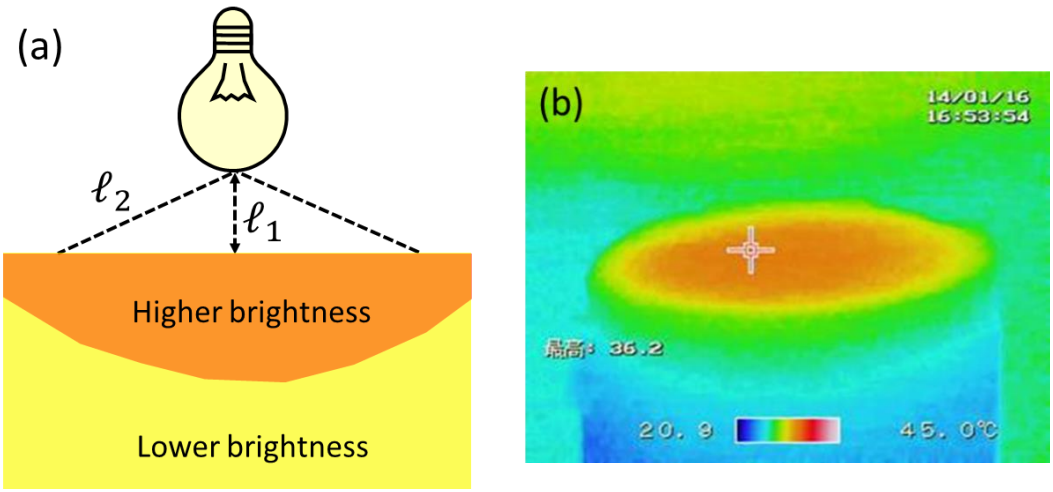

Figure 3.8: The difference of heat effect from the lamp depending the location on the flat surface. (a) The different distances ℓ_1 and ℓ_2 ($\ell_1 < \ell_2$) from the bottom of the lamp to the flat surface of mixture. The closer the distance from the bottom of the lamp, the larger the effect of input energy in the mixture because the difference of ℓ_1 and ℓ_2 becomes noticeable. (b) The image of the surface of mixture by infrared camera when ℓ = 1.5 cm. The color range indicates from 20.9 to 45.0 degrees C. The surface of mixture indicates a concentric color difference shown as the larger temperature is outside-in.

（Ⅲ） Crack propagation phase (t = 35.25 ~ end of experiment [hours])

Figure 3.9 is the log-log plot of Figure 3.3 (preliminary experiment) with the origin t_0 = 28.5 hours which corresponds to the initiation of the crack formation on the surface. The plots indicate along a straight line with the slope of $-1/2$.

Figure 3.10 shows the average lengths of cracks from the surface, L, with time, t', which is $t' = t - t_0$. Crack lengths measured on the CT images with Image J. The blue dots are the measurements in the case of the preliminary experiments after crack formation, while a red dot is the result of other experiments which was conducted for getting CT image soon after crack formation started. The CT image which indicates the red dot is shown in Appendix 2-B. The plots indicate almost straightly plots and the slope of plots shows 1/2.

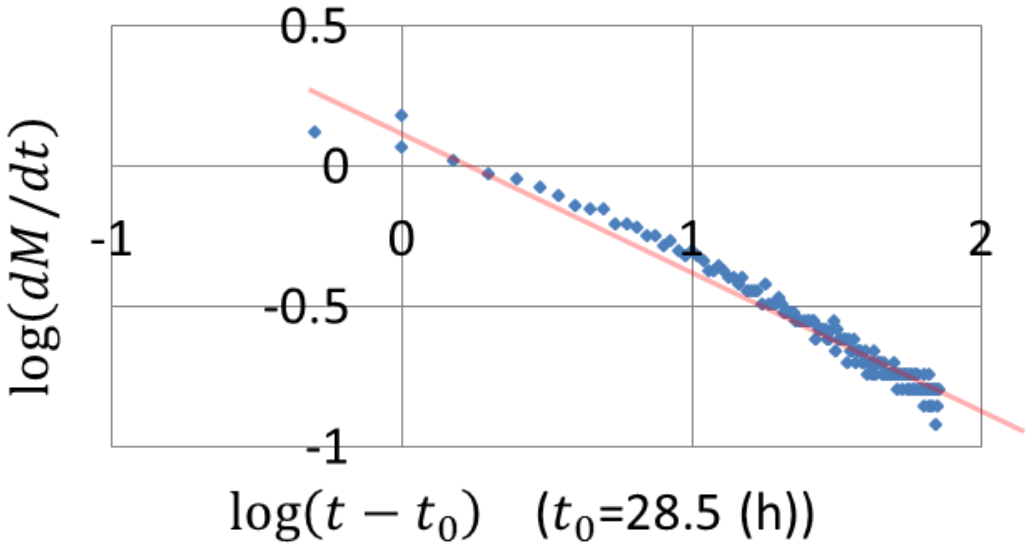

Figure 3.9: Desiccation rate change in the case of the preliminary experiment with log-log plot. The origin time t_0= 28.5 hours corresponds to the initial time of the crack generation on the surface of mixture. The slope of the red straight line indicates -1/2.

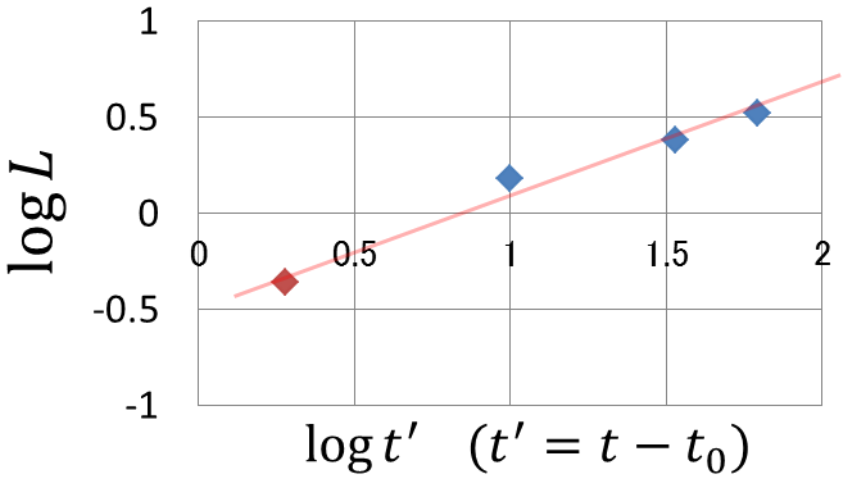

Figure 3.10: The length of crack from the surface with time. The origin time t_0 = 28.5 hours corresponds to the initial time of the crack generation on the surface of mixture. Blue dots were measured by CT images by using Image J. Red dot is the additional data from other experiment with CT operation which was taken just after crack generation as shown in Appendix 2-B.

3.4.2 Diffusion hypothesis for an interpretation of phase (Ⅲ)

3.4.2.1 Diffusion model

Here I introduce the diffusion hypothesis for explaining of the drying process in mixture during phrase (Ⅲ).

The diffusion equation is assumed from e.g., Jaeger, 1961,

$$\frac{\partial C}{\partial t} = D\frac{\partial^2 C}{\partial x^2} \qquad (1)$$

At the surface of mixture is x = 0 and now I think $x \geq 0$ as inside the mixture. The initial condition at t = 28.5 hours is defined as t_0.

$$C(x,0) = C_0\left(x > 0,\ t_0 = 0\right) \qquad (2)$$

the boundary condition is,

$$C(0,t) = C_{sur}\ (x = 0) \qquad (3)$$

The solution to the above problem is given in Caslaw and Jaeger (1959) which is the case $x \geq 0$ as,

$$C(x,t) = C_0 + (C_{sur} - C_0)erf\left(\frac{x}{2\sqrt{Dt}}\right) \qquad (4)$$

The solution as function of distance x for different time are shown in Figure 3.10.

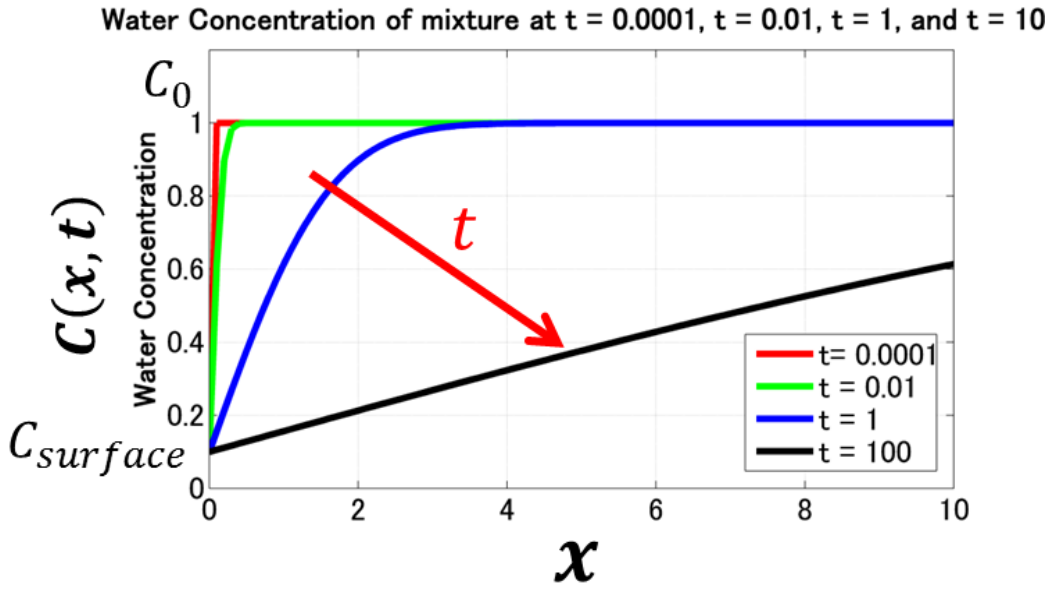

Figure 3.11: Water concentration change with time under diffusion process in condition that the initial water concentration at the surface of mixture is C_0 and the final water concentration at the end of the diffusion process becomes $C_{surface}$. The water concentration at a depth, C(x,t) decreases from the surface.

3.4.2.2 Drying process model

The amount of evaporation of water from the mixture W_q is expressed as

$$W_q = \int_0^{\infty} \big(C_0 - C(x,t)\big) dx \times S \qquad (5)$$

S is the cross area of the container. Differentiating W_q by t gives,

$$\frac{dWq}{dt} = \frac{S\sqrt{D}}{\pi}(C_0 - C_{sur}) t^{-\frac{1}{2}} \qquad (6)$$

It is obvious that $\frac{dWq}{dt}$ equals to the desiccation rate $\frac{dM}{dt}$. Now it is rewritten that the drying process after cracking on the surface of mixture is the diffusion process.

3.4.2.3 Crack propagation and its direction

The brightness at crack front shows relatively lower value than below mixture area. When the concentration at crack front is considered constant value of C_c, that is,

$$C_0 + (C_{sur} - C_0) erf\left(\frac{x}{2\sqrt{Dt}}\right) = C_c \qquad (7)$$

This equation requires the unique relationship between distance x and time t, which defines the crack front.

$$x = A\sqrt{t} \qquad (8)$$

A is an arbitrary constant which is determined by C_0, C_{sur} and D. As shown in Figure 3.10, plots of the depth of crack front with time is along the slope $\frac{1}{2}$. Thus, it is concluded that the crack front propagation can be explained by the diffusion

process.

3.5 Summary of Experiment 1

Experiment 1 is the experimental case that the mixture is dried from one direction homogeneously. This experiment simulates that one flow unit is cooled from one surface homogeneously. There are three phases in the desiccation rate: (Ⅰ) Monotonically decreases phase of drying supernatant liquid, (Ⅱ) Constant phase by water supply from inside of the mixture and (Ⅲ) Diffusion phase during crack propagation. The depth of crack front, which waster concentration is defined C_c, can be explained by diffusion process.

Chapter 4

Experiment 2: Drying process from two directions

Chapter 4 describes the experiment under the conditions that starch-water mixture is dried from two surfaces homogenously. The angle between two desiccation surfaces is arranged 90 degrees. X-ray CT photographing was periodically conducted to observe both crack development and water concentration change inside the mixture.

4.1 Experimental setup

I used kuzuko starch (Muso) in this experiment because of the stiffness to keep the shape of specimen even when the container is removed for X-ray CT execution. 290 g kuzuko starch and 290 g distilled water each were well mixed and put into a stainless triangular prism container, which has the right angle as one inner angle (Fig. 4.1 (a)). The container with mixture is put on the electric balance (Compact balance EK-610i, A&D Co.) and the weight of mixture is monitored by PC every 5 minutes. I put a little bleach into the mixture to prevent it from fermenting. There is supernatant liquid on the surface of the mixture at first. Soon after supernatant liquid evaporates, I poured the resin (Tomack NS-10, Sanko-Shoji Co., LTD.) on one surface from which the evaporation doesn't proceed (Fig. 4.1 (b)). After the resin

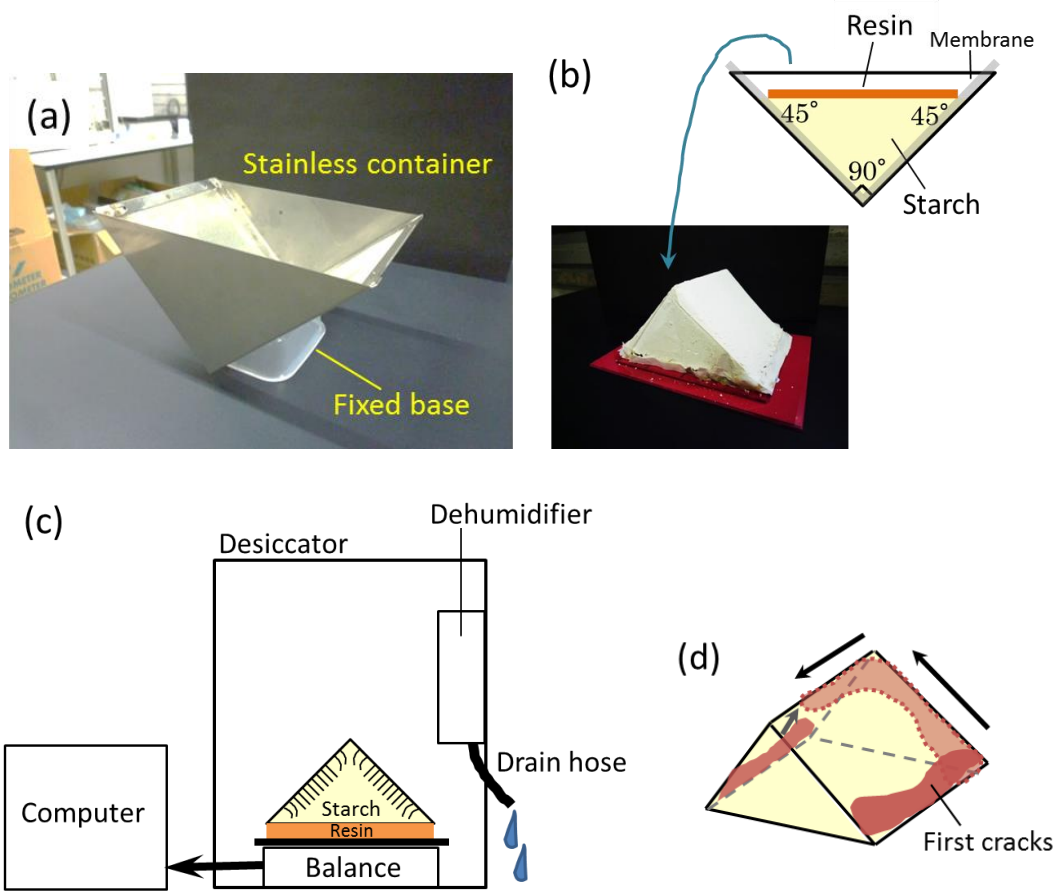

Figure 4.1: Experimental setup of Experiment 2. (a) The stainless prism container. The membrane is put between the mixture and the container to remove the mixture easily afterwards. The container with mixture is fixed on the base to maintain the right angle corner down and the mixture surface horizontal. (b) A schematic figure of cross section of the mixture, which is put the right angle side down. After supernatant liquid evaporates on the surface of mixture, resin is spread on it to prohibit the evaporation. After the resin is solidified, the resin side is put on a board upside down and membrane is removed from the surface of mixture in order to dry naturally. (c) All instruments are put into a desiccator except a PC. Temperature and relative humidity on the substrate in the dehumidifier are automatically monitored. The relative humidity is set 30%RH (RH = Relative Humidity) at a given temperature in the desiccator. (d) The propagation of first cracks on the surface of mixture. First cracks generate at the lower corners of each surface (darker red) and propagate along other corners within the same surface in order shown as black arrows (lighter red). Cracks propagate all over the surface for around 12 hours.

solidified, I removed the mixture from the container and turned it upside down as the resin side becomes the bottom on the electric balance. The membrane was removed from the surface of mixture and the mixture was dried under natural drying (no lamp). All experimental apparatuses except a PC are put into the desiccator (Fig.4.1 (c)). Temperature and relative humidity within the desiccator are monitored by a sensor in the defumidifier (Thermoelectric defumidifier BOXDRY, OHM Electric Co., LTD.) every 10 minutes. The relative humidity is set 30%RH (RH = Relative Humidity) at a given temperature in the desiccator. The weight of mixture is automatically recorded by the PC as shown in Figure 4.2.

Figure 4.2 shows weight and desiccation rate changes. Weight change is only the weight of mixture without showing any changes by the resin application and the removals of stainless container and membrane during this experiment. The calculation of desiccation rate is the same way as that in Experiment 1. Red dots express the results in the case that X-ray CT images were taken periodically interval, while blue dots are a preliminary experiment under the same condition except X-ray CT imaging due to know the time when first cracks occur on the surface of mixture (that's why the blue dots stop around at 118 hours after a while the first cracks occur). The gray bars in both Figure 4.2 (a) and (b) show the period

of the solidification process of resin on the mixture after the resin was poured on the mixture. The time when the slopes of decreasing mass changes in Figure 4.2 (a) shown as black arrow corresponds to the first cracks occur on the surface of mixture by the direct observation from the outside of the desiccator. There was no time lag of slope change between red and blue dots because CT operations were started after first cracks occurred. Figure 4.2 (b) shows the desiccation rate changes. Light orange bars shows the time when CT images were taken in red dots. Desiccation rates in both cases are constant before first cracks generate and decrease abruptly after first cracking around in 77 hours from the begging of the experiment. Blue dots have the variability throughout the record because the electric balance was unregulated well in preliminary experiment. But it was no problem because the time when first cracks occur in the experiment with CT operation corresponds with that in the preliminary experiment. The first cracking generates at the lower corners of each surface in 77 hours after the mixture was put into the container (Fig. 4.1 (d)). Cracks propagate along other corners within the same surface in order shown as black arrows. Cracks gradually propagate along all over the surface for around 12 hours. Crack propagation into the mixture can't be observed from outside in contrast with Experiment 1.

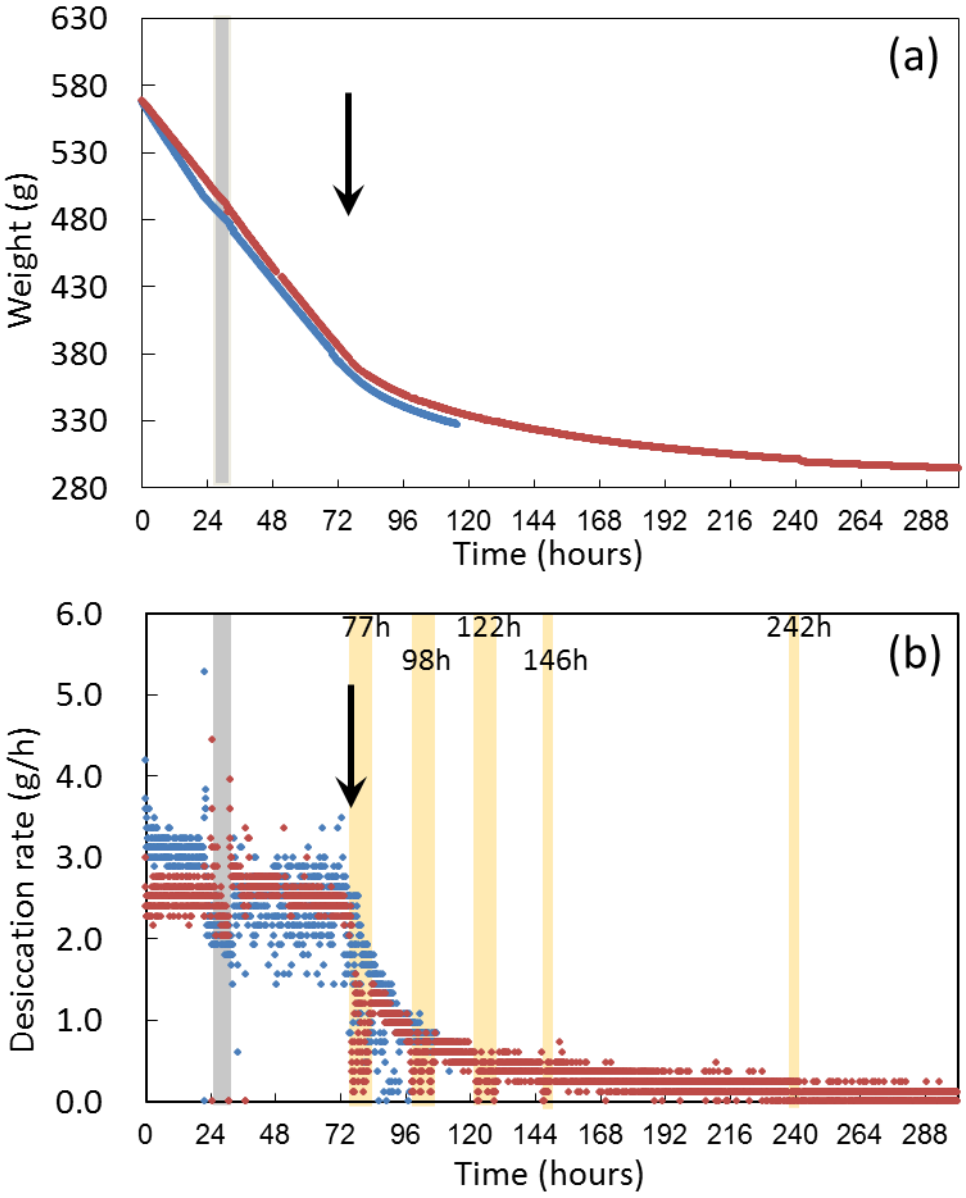

Figure 4.2: Weight and desiccation rate change of Experiment 2. Red dots are data of the experiment in which the sample was removed for X-ray CT operation. Blue dots are data without picturing by X-ray CT. In both figures the gray bars show the period of the solidification process of resin on the mixture after the resin was poured on the mixture and the time when first cracks occur on the surface of mixture is shown as solid black arrows. (a) Weight change recorded automatically by electric balance every 5 mins. (b) Desiccation rate change. The values are calculated by differential weight change per 5 mins. Discontinuous gaps in red dots correspond to the period when the sample was removed from the electric balance as shown light orange bars.

4.2 X-ray CT observations

X-ray CT images are taken periodically interval from when cracks on the surface appear near the right angle corner of the mixture. Figure 4.3 shows CT images of two magnifications (a) 2.68 times and (b) 6.68 times each. (b) was focused at the right angle of the mixture.

Figure 4.4 shows the time series of CT images focusing at the right angle of mixture. The time indicates the elapsed time from the beginning of the experiment. I converted the grayscale image to colored image with XMapTools corresponding with the brightness from 0 to 255 shows as Figure 4.5. All images in Figure 4.4 and Figure 4.5 have commonly a color shading at the lower part of images which is an artifact caused by only a right angle part of whole object is within the cone-beam X-ray area being irradiated. I ignore this uneven color effect when I observe changes in images with time.

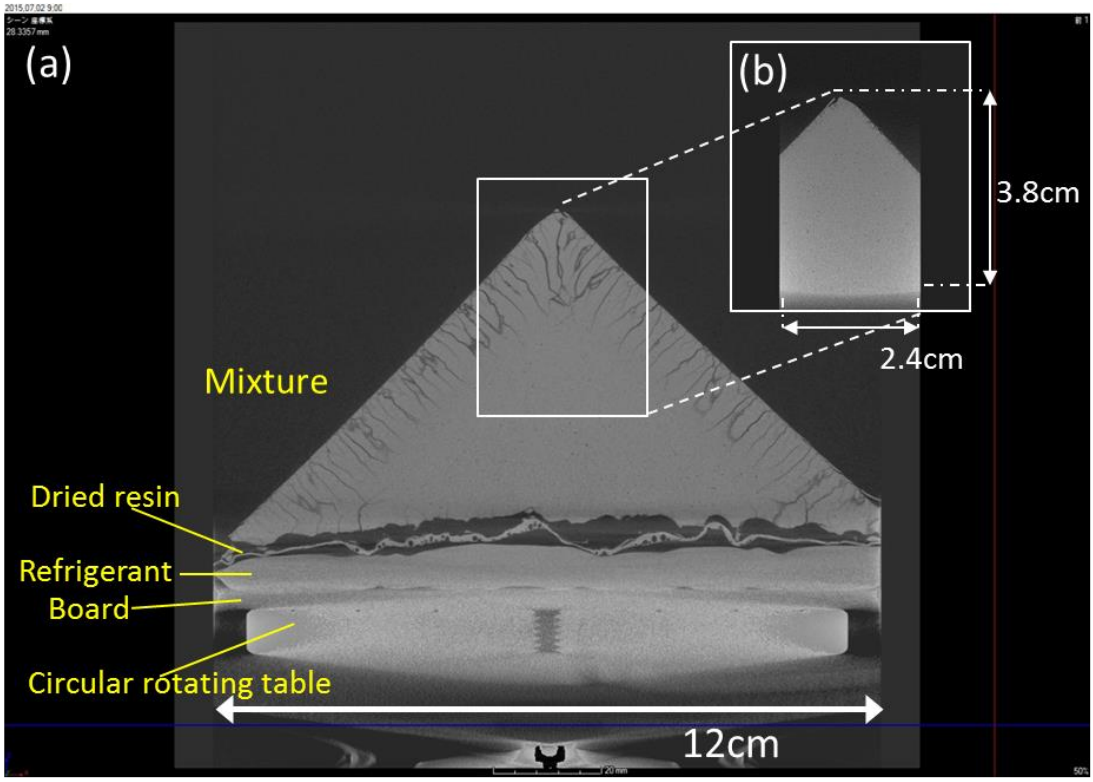

Figure 4.3: The grayscale CT image. (a) The CT image in the direction perpendicular to the prism axis. Refrigerant under the dried resin is used as a cushion to keep the mixture from deforming under its own weight. (b) The focused area around the right angle part.

In CT images from 77 to 82 hours, first cracks propagated to a depth of less than 1 mm. The color along the drying surface is relatively light blue in Figure 4.5, which indicates lower water concentration than inside. In the image from 98 to 104 hours, cracks develop inward from both drying surfaces to a depth of about 2 - 3 mm. All cracks propagate perpendicular to the drying surface and cracks just under the corner of the right angle propagate curved inward. The area which cracks propagated from 98 to 104 hours becomes lower water concentration. Crack propagation inward continues from 122 to 146 hours to a depth of about 4 - 8 mm and cracks propagated from two drying surfaces under the corner at the right angle curve without intersecting. The area which cracks propagated from 122 to 146 hours becomes lower water concentration.

Figure 4.6 shows crack propagation from two drying surfaces of one cross sectional area from 104 to 146 hours. There is no crack propagation from the opposite side of the right angle due to be covered by the resin to prevent from drying. The image in 242 hours that mixture is completely dried shows that almost all tips of cracks developing from both surfaces are curved to the center of mixture.

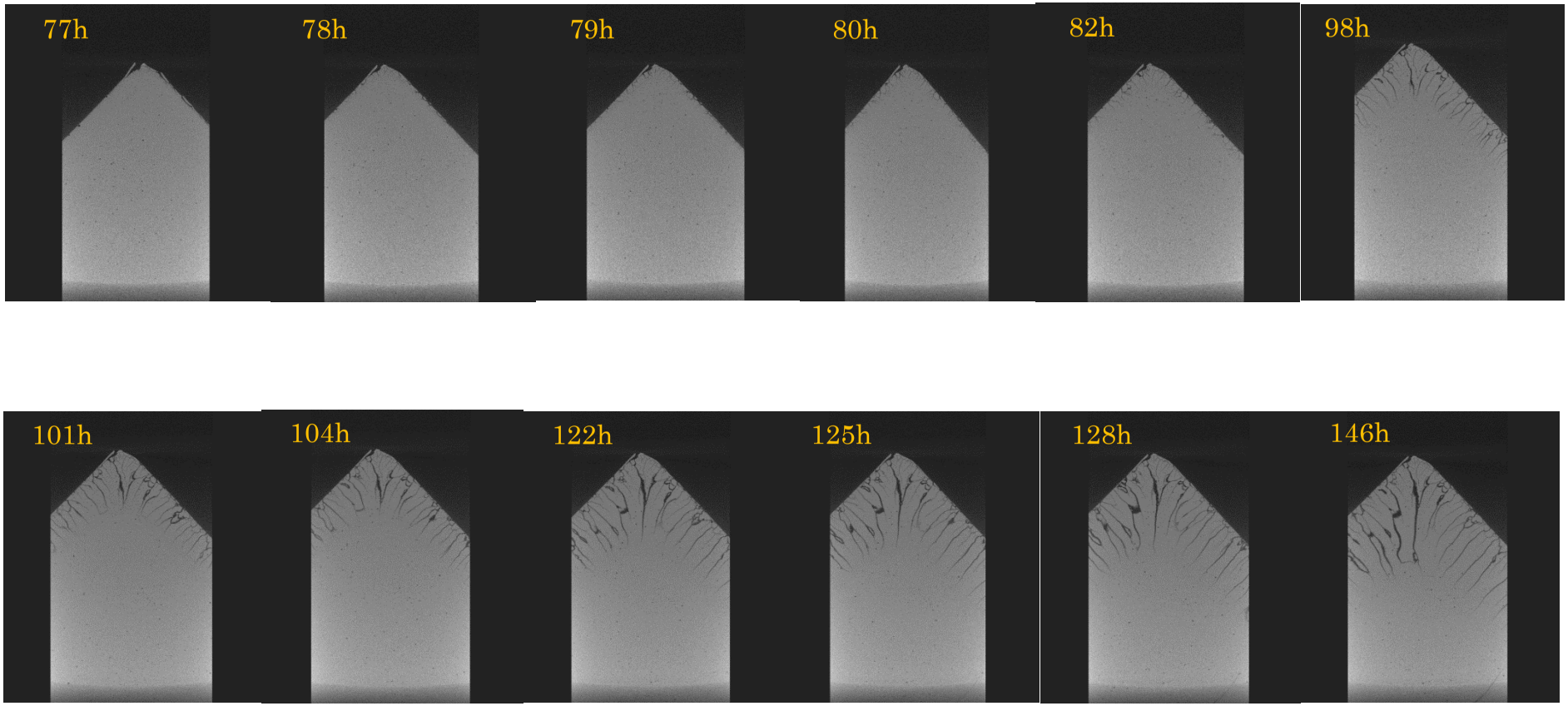

Figure 4.4: Grayscale CT images on focused area at the right angle of mixture. Times left upper each picture show elapsed time from the beginning of the weigh record. Brightness of images corresponds to the density of mixture. Black parts: Outside of container (air) and cracks in the mixture. The gradation between white to gray in the mixture depends on the density of mixture. More white indicates higher density, while more gray (lower brightness) indicates lower density. Lower part of the mixture in all images has the artifact which was caused by the corn beam shaped X-ray.

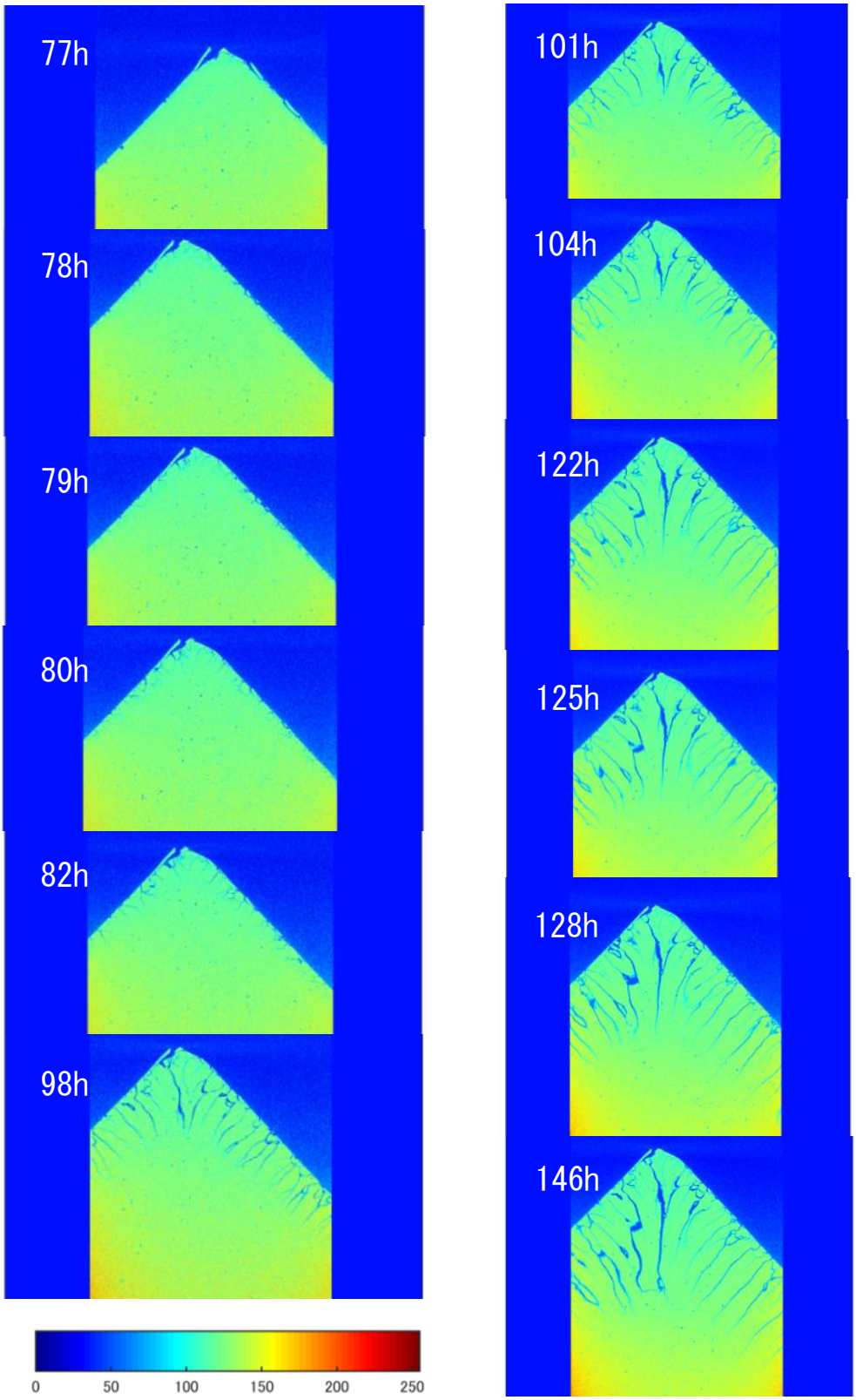

Figure 4.5: The time evolution of crack propagation at one cross section at the right angle. The Color range corresponds to 0-255 in grayscale. Cracks from two drying surfaces propagate perpendicular to each drying surface and propagated cracks below the corner of the right angle curve without intersecting. The area which cracks propagated becomes smaller brightness with time, which indicates lower water concentration.

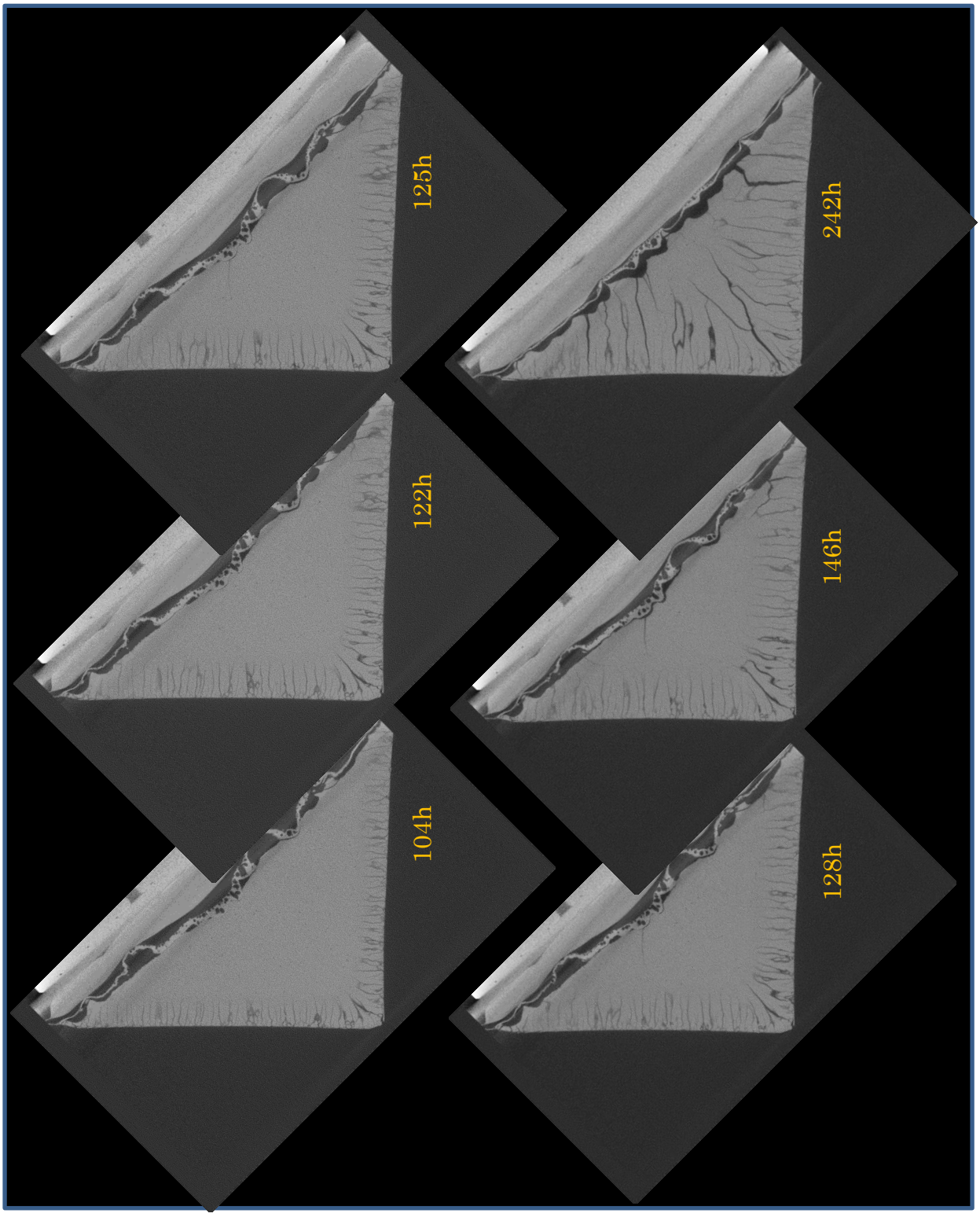

Figure 4.6: CT images in grayscale from 104 to 242 hours. The part of right angle is set at the bottom left in all images (all images are rotated 135 degrees from the direction in Figure 4.3). Except around the right angle part, cracks occur at the both drying surfaces each and develop perpendicular to the surfaces, while cracks around the right angle develop curved to the center of the mixture.

4.3 Straight line measurement on CT images

In this experiment cracks developed perpendicular to the two drying surfaces each and curved to the center of the mixture without traversing each other. Cracks can be separated into two parts in terms of configuration: straight part and curved part as shown in Figure 4.7.

I picked up some cross sections of CT images in 242 hours (completely dried) and measured the length of straight part by using Image J. The measurements were conducted to cracks developing from two surfaces (x direction and y direction each) and the results are shown later in Section 4.4.

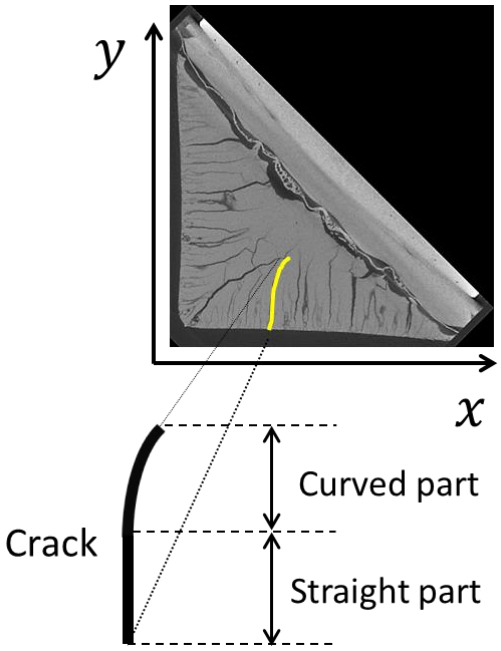

Figure 4.7: The method of measurement. Cracks propagated from two drying surfaces are consisted of straight and curved part. The measurements of straight part of CT images at 242 hours were conducted with Image J.

4.4 Discussion

4.4.1 Diffusion hypothesis in rectangle area

For comparing with the results of measurement as explained in Section 4.3, I introduce the formula of cooling process from two surfaces in rectangle（$x \geq 0$， $y \geq 0$）from Carslaw and Jaeger (1959) as follows.

The initial temperature of magma at T_0 ($x > 0$， $y > 0$, $t = 0$) and the country rock temperature is 0 $\left(x = 0,\ y = 0\right)$ at initial. The temperature T at depth x and y at time t is given by the solution ($x > 0$， $y > 0$)

$$T = T_0 Erf\left(\frac{x}{2\sqrt{Kt}}\right) Erf\left(\frac{y}{2\sqrt{Kt}}\right) \qquad (9)$$

where Erf x is the error function defined by

$$\text{Erf x} = \frac{2}{\sqrt{\pi}} \int_0^x e^{-u^2}\, du \qquad (10)$$

K is the diffusion constant.

According to the assumption from Jaeger (1961), if there is the isotherm $T = T_c$ at which the crack generates, I will consider some cases of T_c with time. The calculation of the above solution is shown as colored isotherms in Figure 4.8, which I picked up two cases of T_c representatively: (a) T_c=0.6T_0 and (b) T_c=0.9T_0. I also measured the length of straight part of isotherms in Figure 4.8 in both x and y direction.

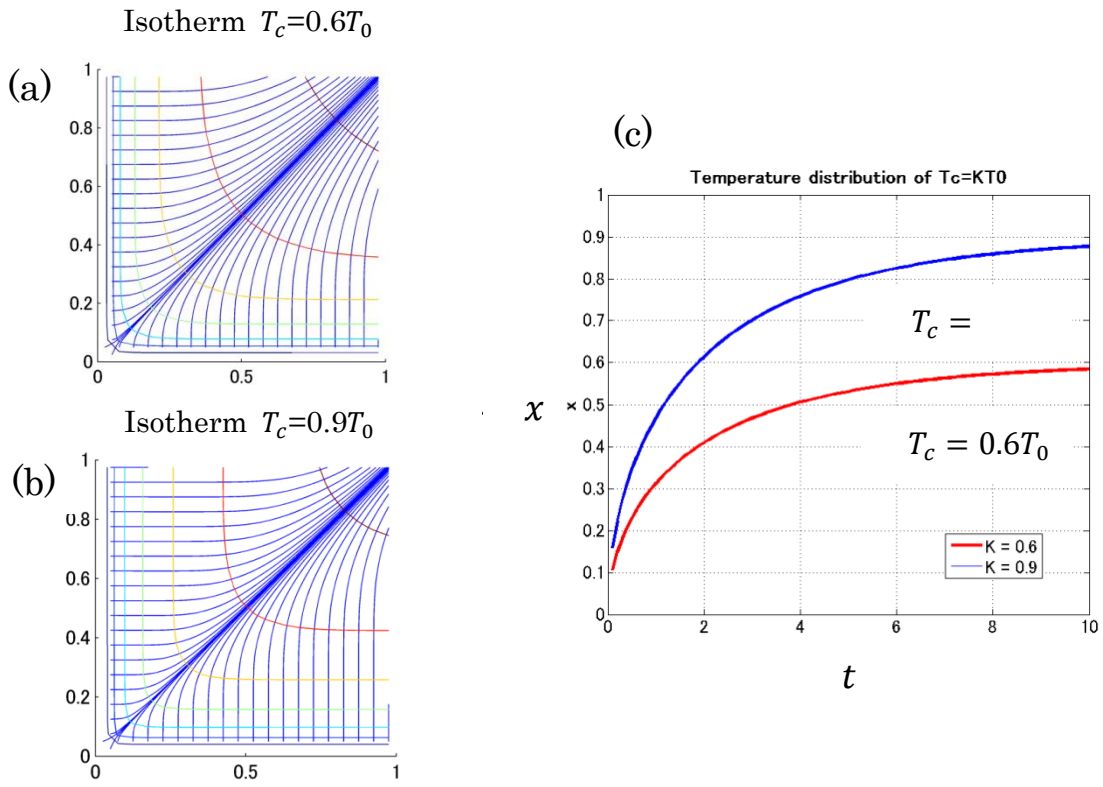

Figure 4.8: Temperature distribution in case of T_c=0.6T_0 and T_c=0.9T_0. T_0 is the initial temperature and T_c is the temperature which cracks will occur over fracture strength of material. x can be considered as a depth of the rock at a time. The calculation results show that larger T_c can reach deeper position of rock after a certain time.

4.4.2 Comparison between experiment and model

T_c is the temperature at which cracking occurs when the tensile stress of material overcomes fracture strength. Figure 4.8 (a) $T_c = 0.6\,T_0$ and (b) $T_c = 0.9\,T_0$ show isotherms with time as colored lines and blue lines develop perpendicular to the isotherm of T_c with time. The patterns of isotherm $T_c = 0.6T_0$ have more gradual curve than that of isotherm $T_c = 0.9T_0$. Figure 4.8 (c) is the magnitude relation between two isotherms with time. x can be considered as a depth of the rock at a time. When the value of the isotherm for cracking is larger at a time, the isotherm can be reached deeper part of the rock.

From the results of measurement of straight lines in Figure 4.9, experimental results are similar to the result in the case of $T_c = 0.6T_0$. It can be interpreted that the crack propagation in Experiment 2 advanced perpendicular to the isotherm $C_c = 0.6C_0$ (C_0 is the initial concentration of the mixture and C_c is the concentration which cracks generate), which the shape of iso-concentration C_c is described with more gradual curve after diffusion process proceeds in Figure 4.8.

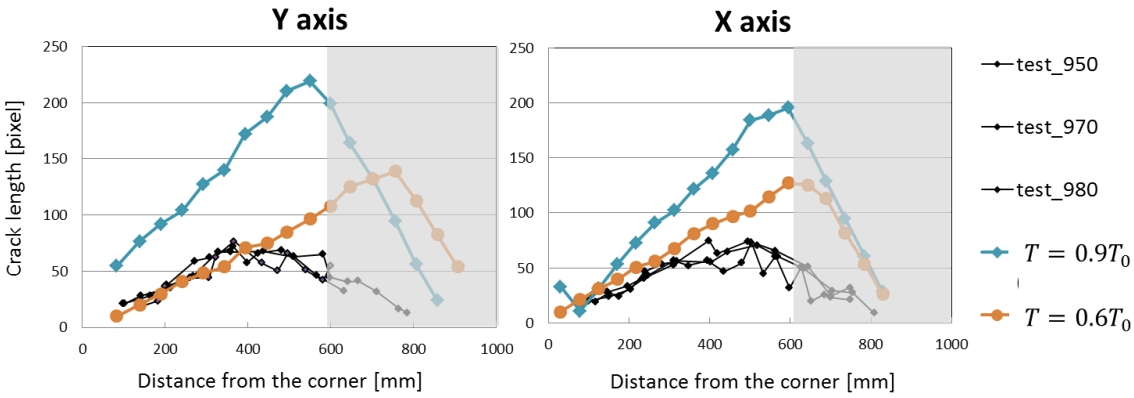

Figure 4.9: The comparison of straight crack length between Experiment 2 (black dots) and the simulation results in case of T_c=0.6T_0(orange dots) and T_c=0.9T_0(blue dots). Crack length is measured along both x axis and y axis at the distance from the right angle. Gray area is the area that experimental data has large error because of the limited area (triangle) of crack propagation. The results from the experiment is close to the result in case of T_c=0.6T_0.

4.5 Summary of Experiment 2

Experiment 2 is the experimental case that the mixture is dried from two directions at the right angle. Cracks which propagated perpendicular to the drying surface each develop straight and form curved structure into the center of the mixture without intersecting by diffusion process. In the case of drying process, the curved structure was formed when the iso-water concentration C_c, which cracks generate, 0.6 C_0, which is initial water concentration in the mixture.

Chapter 5

Experiment 3: Instantaneous increase of desiccation rate

This experiment attempts to confirm that the column width change happens in analogue experiments when the desiccation rate is instantaneously increased during drying process. Since some results of Experiment 3 have already mentioned in my master thesis in 2012, therefore I summarize the experimental setup and results, then address state new analysis done this thesis. Because the idea of this experiment for reproducing the threefold structure (Upper Colonnade – Entablature －Lower Colonnade) in which has relatively smaller width of columns at the center, the starch and water mixture dried from both surfaces from the top and the bottom.

5.1 Experimental setup

The mixture of 160g potato starch and 160g distilled water is poured into an acrylic cylindrical container and set 10 cm under a 60 W lamp initially (Fig. 5.1). A membrane is attached on the bottom of the container to drain extra water and to dry the mixture from the bottom as well as the top. The distance between the lamp and the surface of the mixture is changed to 1.5 cm when cracks develop a depth of about 3 cm from the surface. All instruments are put into within a desiccator except

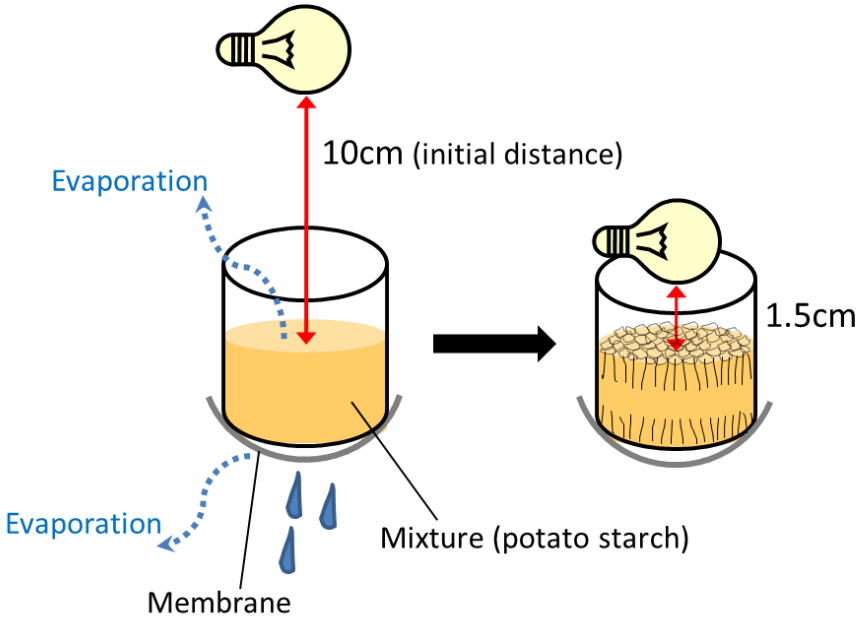

Figure 5.1: Experimental setup of Experiment 3. The mixture is put into an acrylic cylindrical container which bottom with a membrane to evaporate from the bottom. Extra water is removed through the membrane at initial state. Crack propagation can be seen through the container. The distance between the lamp and the surface of mixture is set 10 cm initially. When crack front reaches about 3 cm at depth, the distance is changed from 10cm to 1.5 cm.

a PC. Temperature and humidity are recorded the same way as Experiment 1 and 2.

5.2 Weight and desiccation rate changes

The weight and the desiccation rate change shows in Figure 5.2. The weight shows monotonically decrease and black arrow indicates the time, t_0 = 29.8 hours when first cracks appear on the top surface of the mixture. At t_1 = 117 hours indicated by dashed line, I changed the distance between the lamp and the upper surface of mixture from 10 to 1.5 cm. The desiccation rate rapidly decreases just after first cracks occur, and instantaneously increase when the distance between the lamp and the upper surface of mixture was changed.

Figure 5.3 show log-log plot of desiccation rate change, $\frac{dM}{dt}$, as function of time. In Figure 5.3 (a), data are taken from the first stage from t_0 = 29.8 to before t_1 = 117 hours. In Figure 5.3 (b), data are taken from the second stage from t_1 = 117 hours to the end of record. The slope of graph in first stage indicates about -0.5081, while that in second stage indicates about -0.3319.

Because the slop in the first stage in Figure 5.3 (a) indicates about -0.5, it can be considered that diffusion process controls the drying process during this period.

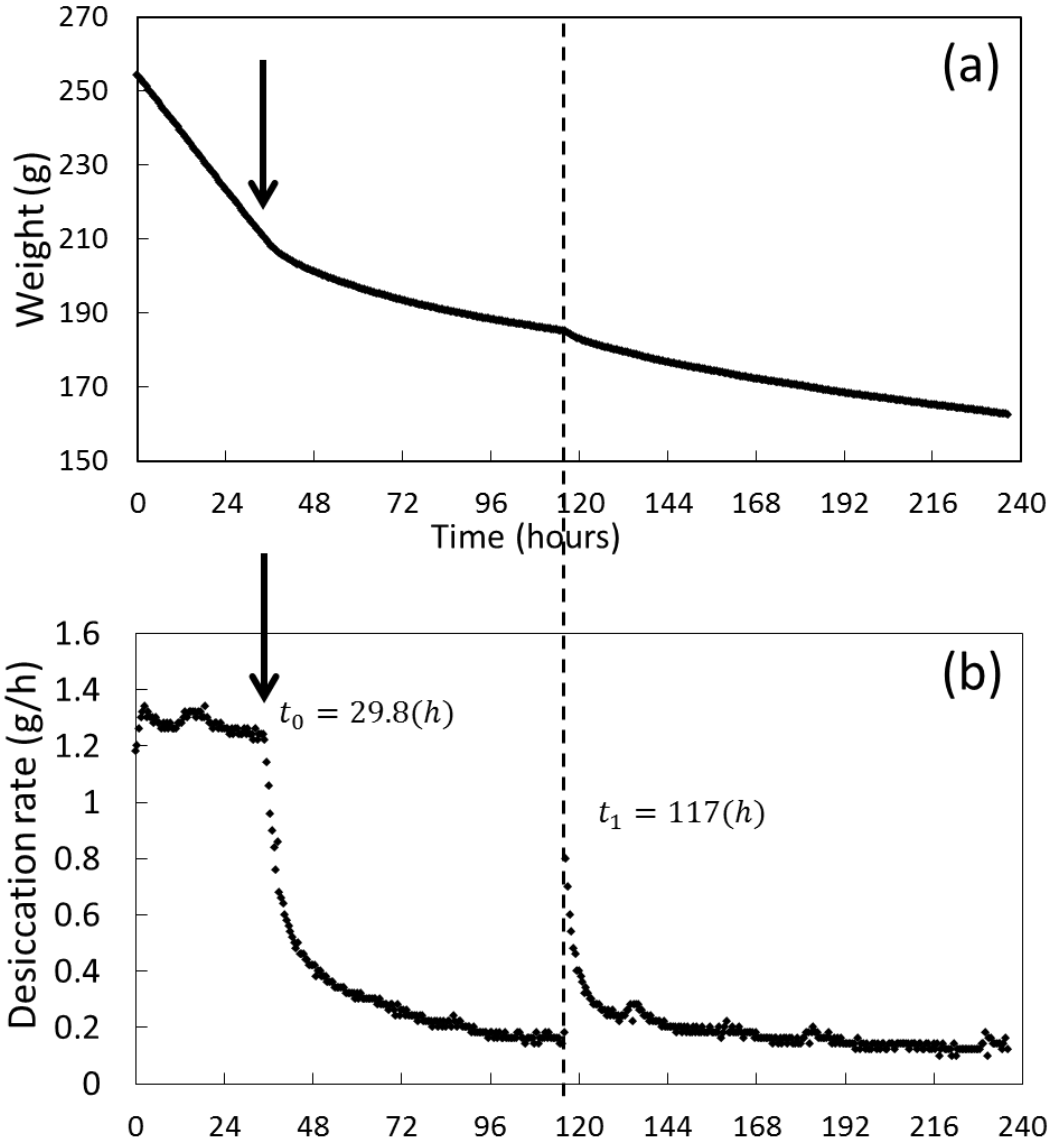

Figure 5.2: Weight and desiccation rate change of Experiment 3. (a) Weight change is automatically recorded by electric balance every 5 mins. It decreases monotonically and the slope changes at t_0= 29.8 hours shown as black arrow when first cracks appear on the upper surface of mixture. At t_1=117 hours shown by dashed line, the slope changes rapidly for a short time. (b) Desiccation rate change is calculated by differential weight change per 5 mins. It is constant around 1.3 g/h until first cracks appear on the upper surface of mixture, but after first cracking desiccation rate drops rapidly and becomes about 0.2 g/h down at the end of first stage. At t_1=117 hours, the desiccation rate instantaneously increases and then drops to 0.2 g/h again.

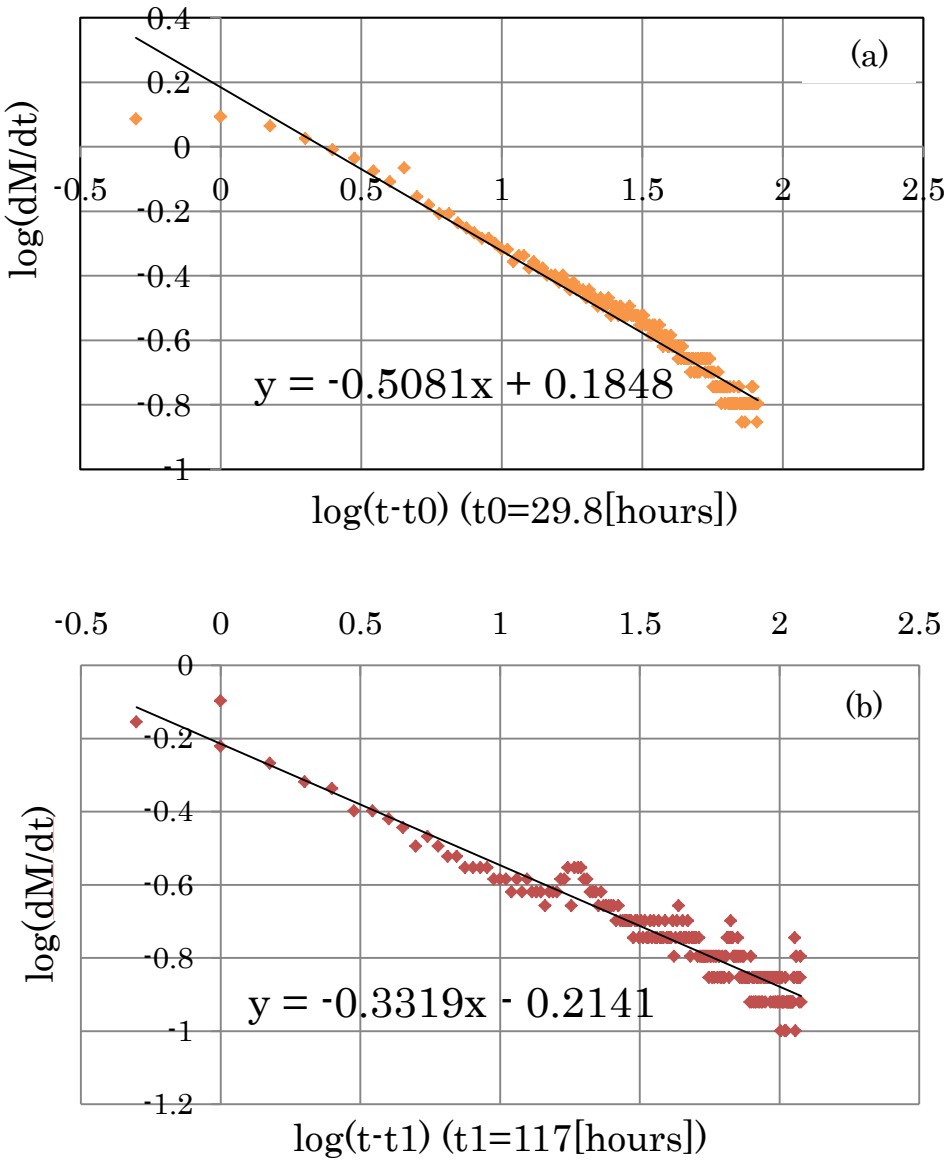

Figure 5.3: Desiccation change with log-log plot in the first stage, (a) and the second stage, (b). (a) The plots indicate along the slope about - 0.5. t_0 is 29.8 hours when first cracks appear on the upper surface of mixture. (b) The plots indicate along the slope about - 0.3. t_1 is 117 hours when the desiccation rate instantaneously increases.

5.3 Analysis of X-ray CT images

I took X-ray CT images of Experiment 3 just one time after the drying process completely finished. I have already conducted CT observation and analysis on my master thesis in 2012, however, I got the data of measurements by the same CT images using Image J (instead of Matlab), which focused on the number of columns and the average area of columns (instead of the total crack length in each CT image). In addition, I suggest how the nucleation part can be recognized at the side view of columns in this section.

5.3.1 The change of the number of columns and their areas

Figure 5.4 shows one of vertical slice images including the side view of columns. I used 390 CT images for the analysis. Figure 5.4 (b) and (c) show the number of columns and average cross sectional area of columns each with depth, which equals to slice numbers of 390 CT images. Red dashed line corresponds to the depth of crack front when the desiccation rate was suddenly increased because of being confirmed by direct observation through the acrylic cylindrical container. The number of columns rapidly decreases until the desiccation rate changes and then increases just after the desiccation rate was increased shown as red arrow. After the

temporary increase, the number of columns gradually decreases to the depth (around slice number 225) and then gradually increases because of the columns developed from the bottom of specimen. After slice number 300, the number of columns rapidly increases to slice number 350 and then decreases rapidly to the end of slices.

The average cross sectional area of columns in Figure 5.4 (c) shows a gradual increase until the depth of red dashed line. After the depth of red dashed line the area decreases shown as blue arrow and then increases rapidly until slice number 225. After slice number 225 the area decreases to the end of slices.

5.3.2 Column nucleation after instantaneous desiccation rate increase

Figure 5.5 shows the parts of spatially continuous 5 CT images (slice number 100, 110, 112, 113, 116) which correspond to the depth of increasing desiccation rate. It is found that the morphology also simultaneously changes from constant to abrupt increase of number of columns at the depth of red dashed line from the side view of the sample. In a series of cross sectional view with depth, columns which color is yellow generate at the triple or quadruple points consisted of the existing columns which color is red. The number of new columns increases with depth and the cross sectional area of existing

columns decreases. This morphological change can be seen throughout this depth.

Figure 5.6 (a) shows nucleation points at the side view of a CT image. Red circles indicate the column nucleation points in lateral direction. The shape at nucleation points can be recognized as a branch consisted of existing columns and new column as shown in Figure 5.6 (b).

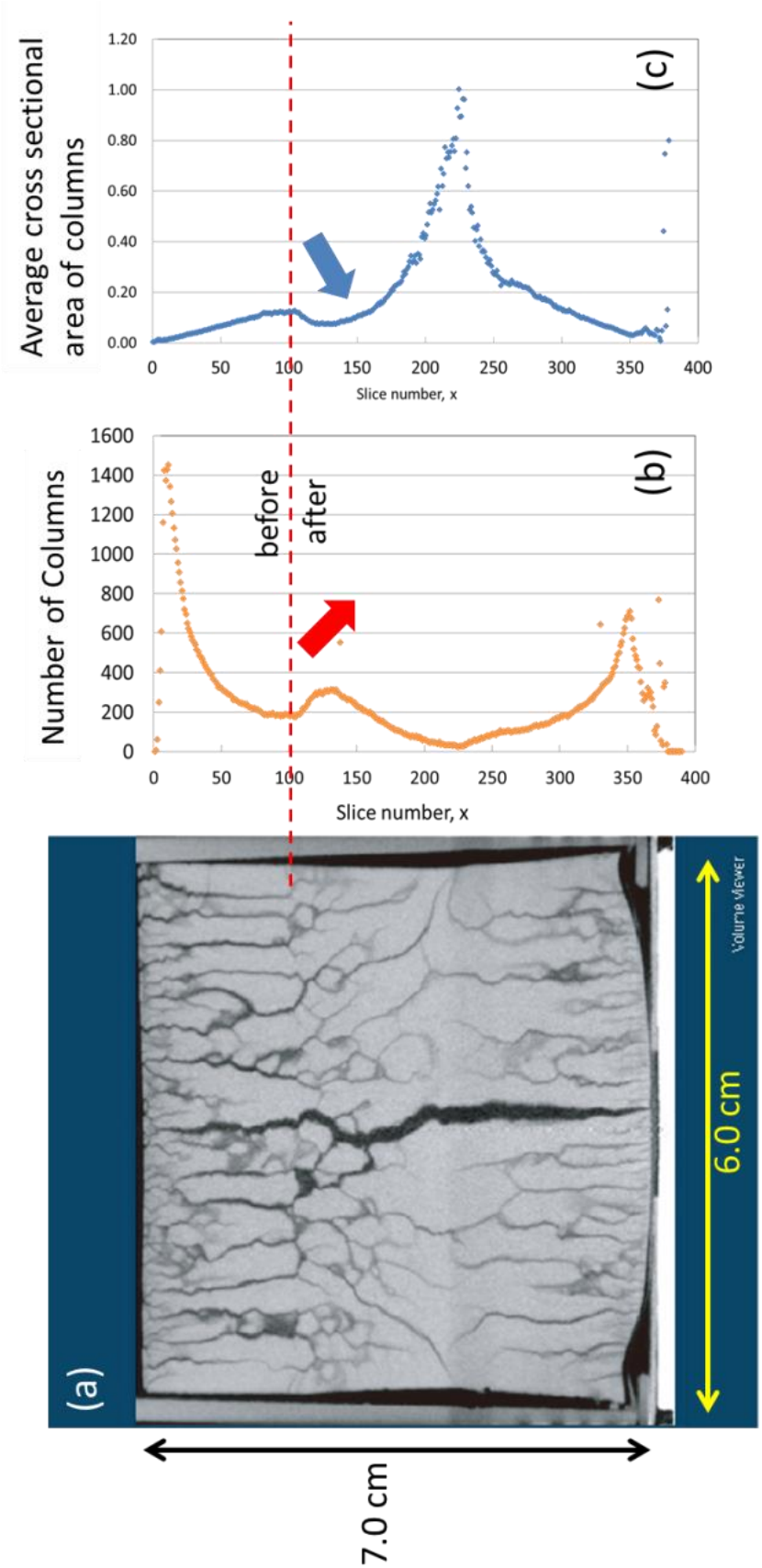

Figure 5.4: Number of columns and average cross sectional area of columns.

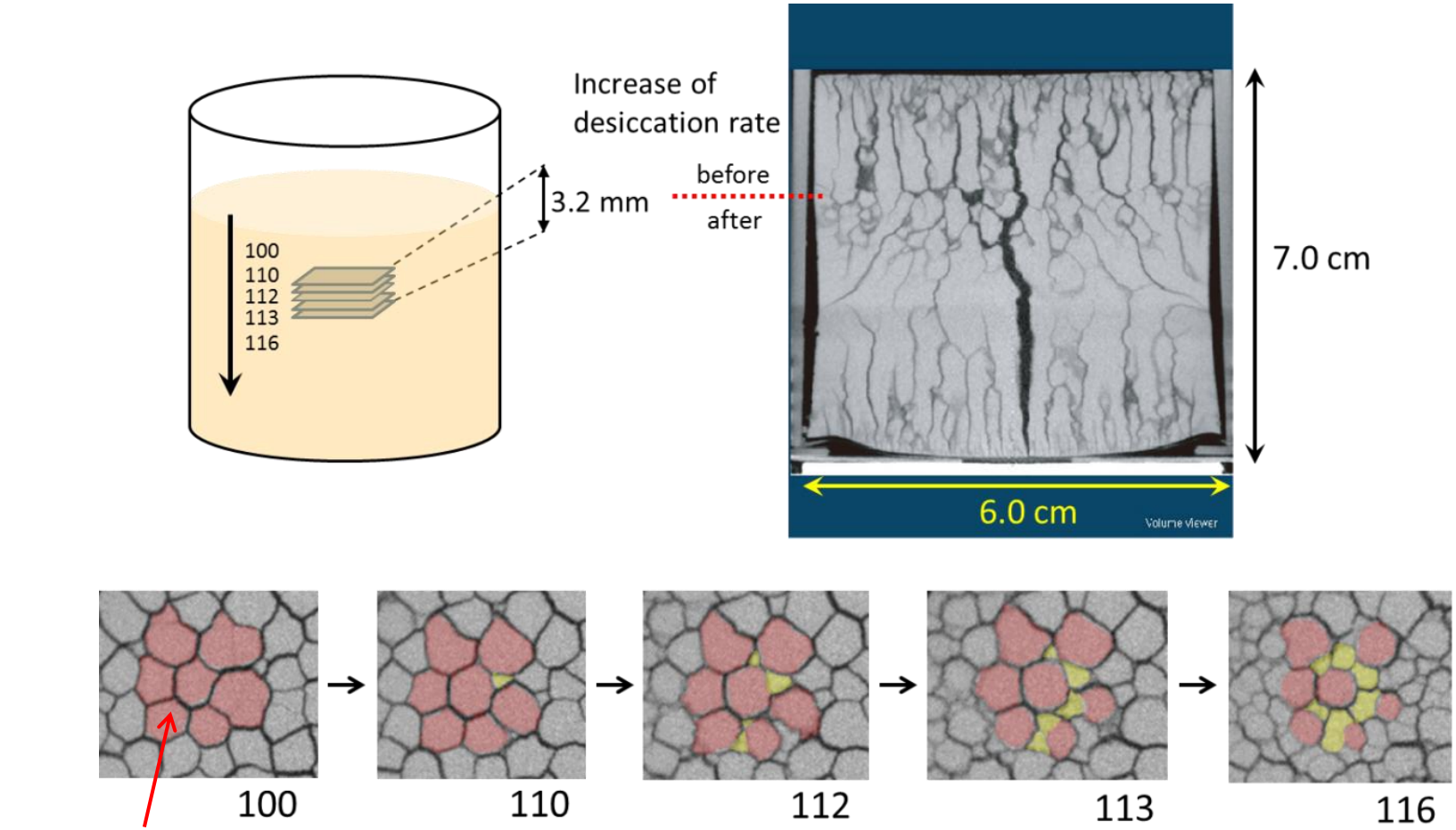

Figure 5.5: The columns nucleation at triple or quadruple points of existing columns.

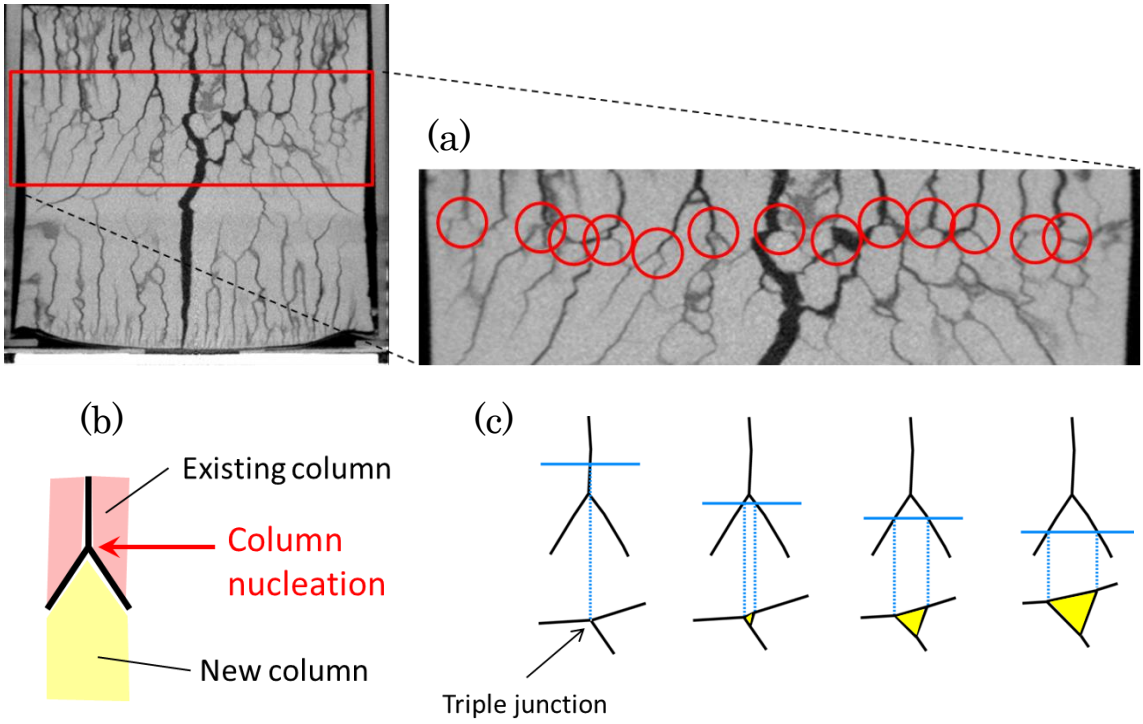

Figure 5.6: Nucleation points at the side view of a CT image. (a) Red circles indicate the column nucleation points. They get into line in lateral direction. (b) Schematic diagram of the point of column nucleation. (c) Schematic diagram of the growth of columns and its cross sectional view.

5.4 Summary of Experiment 3

Experiment 3 was conducted to observe the morphological change when instantaneous increase of the desiccation rate was given to the drying mixture. Abrupt increase of the desiccation rate causes column nucleation at triple or quadruple points of existing columns. The branched shape, which is column nucleation from the side view, may have the possibility to recognize columns nucleation of columnar joints of rock.

Chapter 6

Implications for morphological transition from Colonnade to Entablature

I'll suggest a scenario of morphological transition from Colonnade to Entablature by showing an example of the outcrop at Shakushiiwa in Oita prefecture, Japan, on the basis of the suggestions from Chapter 3 to Chapter 5.

6.1 Description of columnar joints at Shakushiiwa in Oita prefecture, Japan

The outcrop named Shakushiiwa is located along the Okudakegawa river at Bungo-Ono shi, in Oita prefecture in Japan (Fig. 6.1). The steep cliff consists of welded tuff which is originated from Aso-4 pyroclastic flow 90,000 years ago. The welded tuff layer can be seen over about 70 m height and about 500 m in a lateral extent with well-developed columnar joints as shown in Figure 6.2. The outcrop shows threefold structure of columnar joints within one flow unit as shown in Figure 6.3. Upper Colonnade develops from the top of the flow into 10－15 m in depth. Uppermost part is relatively rough and massive structure which is not like columns, but a few meters down of it, about 1 m width columns develop down to the level of Entablature. Lower Colonnade developing from the bottom of the flow unit has homogeneously about a half smaller size of columns than Upper Colonnade. It continues to develop upward the flow with nearly constant width of columns and encounters Entablature part. The configuration of Entablature part consists of

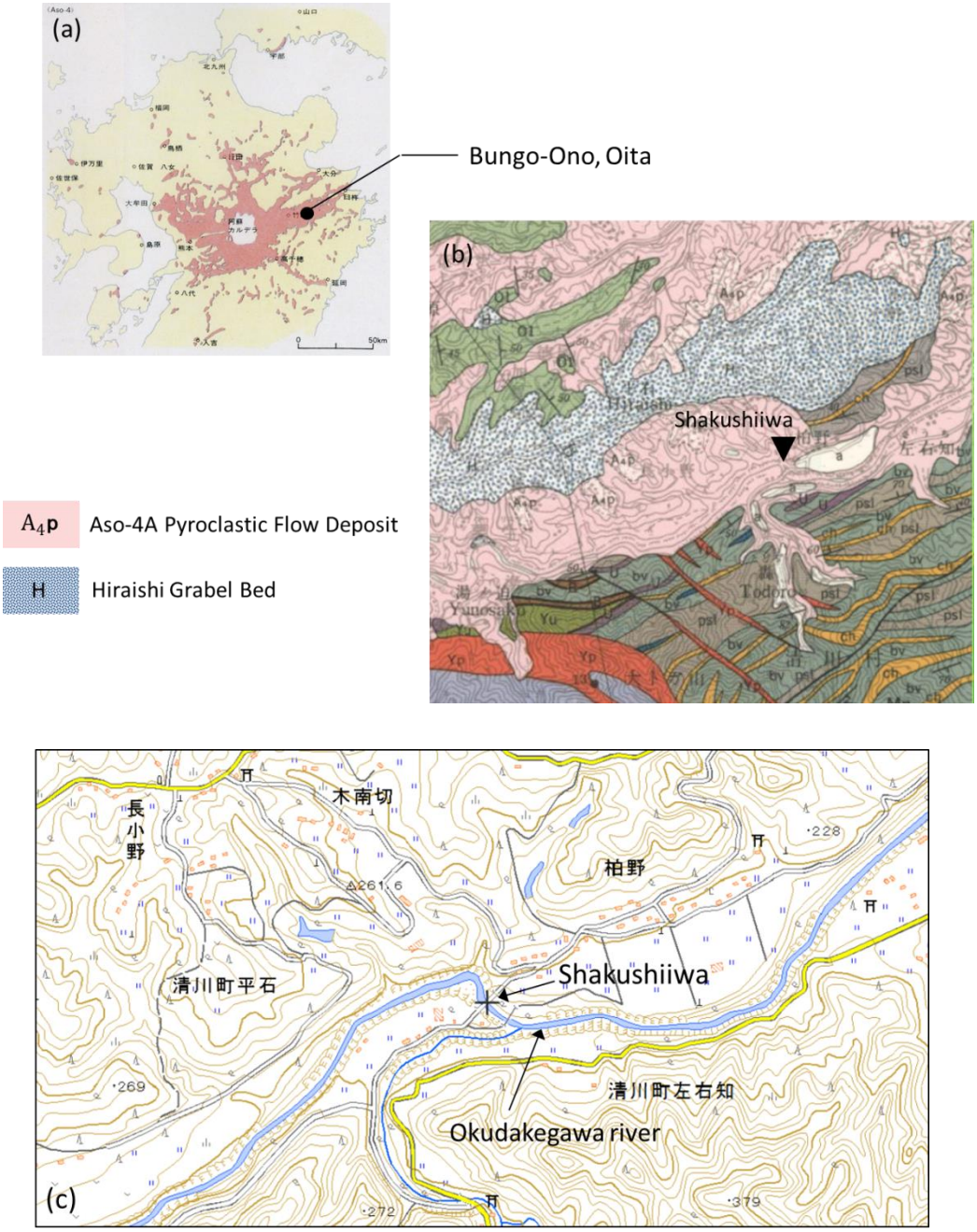

Figure 6.1: Geological map of Shakushiiwa, Bungo-Ono shi, Oita prefecture in Japan. (a) The area of Bungo-Ono shi covered Aso-4 pyroclastic flow deposit about 90,000 years ago [modified from Ono et al., 1984]. (b) Shakushiiwa is consisted of Aso-4 pyroclastic flow deposit [GeomapNavi from Geological Survey of Japan]. (c) The cliff of Shakusiiwa is located along Okudakegawa river [GSI Maps from Geospatial Information Authority of Japan]

domains radially-propagated from the bottom of Upper Colonnade side. The columns in Entablature part are much smaller than that in Lower Colonnade. The side surfaces of columns are rougher than those of both Colonnades. Entablature part is depicted in Figure 6.4. As shown by red dashed line in Figure 6.4 (a), Entablature part is composed of multiple domains of radial structures horizontally. One of the radial structures is shown in Figure 6.4 (b) and Figure 6.4 (c) is the schematic sketch of cracks of (b). The crack, which is indicated by a thicker line, develops from a crack of the Upper Colonnade and penetrates into the upper part of Entablature. From the conclusion by Experiment 2, if crack propagation advances perpendicular to the isotherm T_c at a time, the pattern of isotherms T_c can be drawn as red dotted curves in Figure 6.4 (c). Such isotherms seem to enclose the thicker crack developing from Upper Colonnade to upper part of Entablature possibly played a role of cooling surface.

Figure 6.2: The whole outcrop of Shakushiiwa consisted of Aso-4 welded tuff along the Okudakegawa river, in Oita. Well-developed columnar joints can be seen 70 m in height and 500 m wide here. 10－15 m long Upper Colonnade and 50 m high Lower Colonnade develop from top and bottom of one flow unit each. Radial shape Entablature is also recognized between Upper and Lower Colonnade with 10－20 m long.

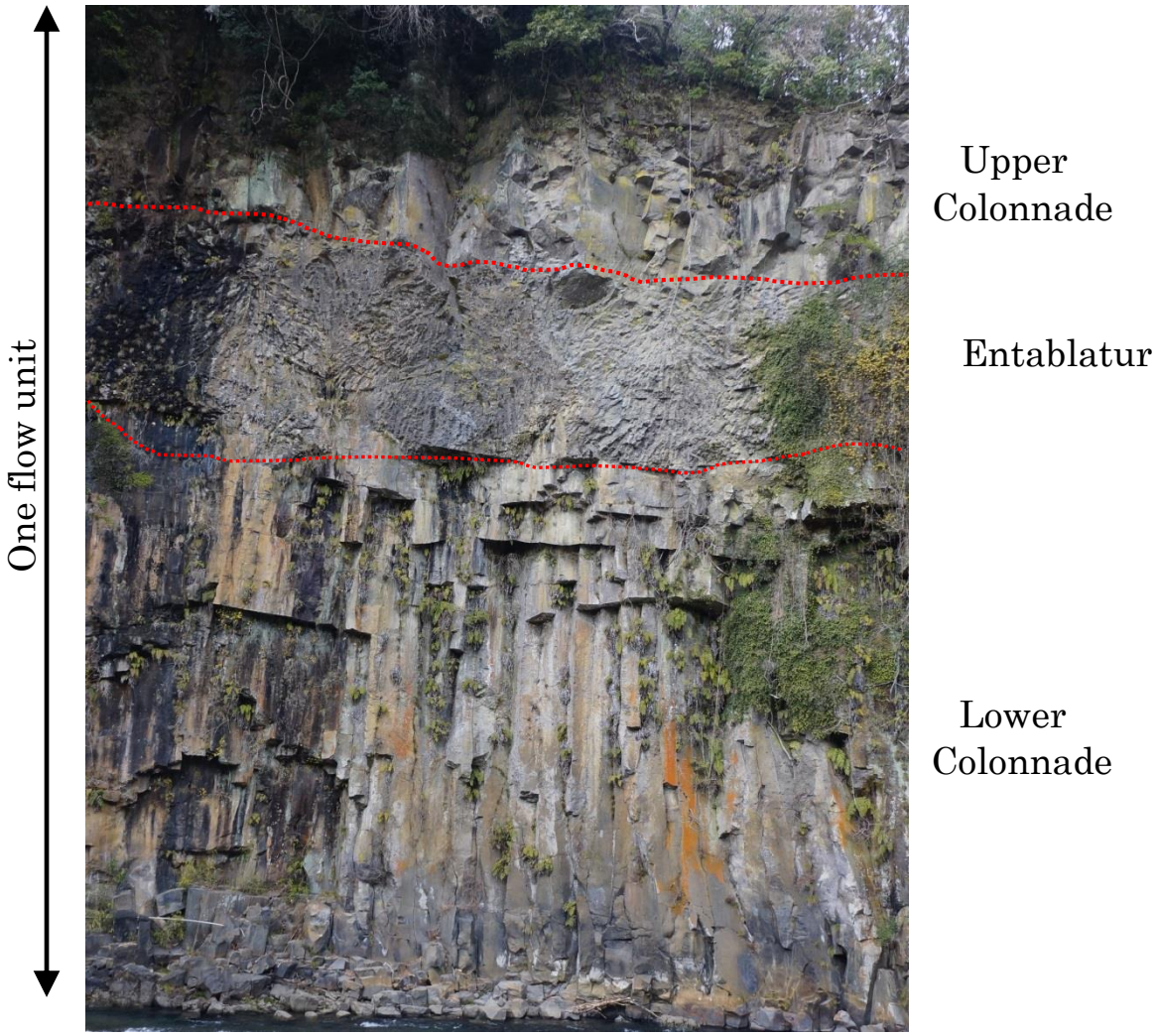

Figure 6.3: Morphological transition of Shakushiiwa. The outcrop is consisted of threehold structure of columnar joints within one flow unit: Upper Colonnade, (middle) Entablature and Lower Colonnade. The boundaries between Colonnade and Entablature are indicated by red dotted line.

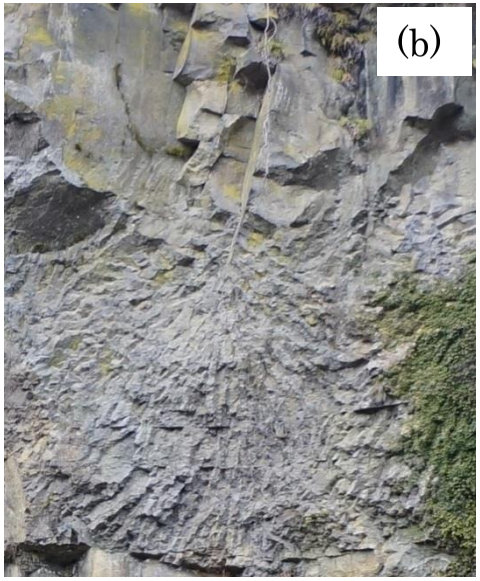

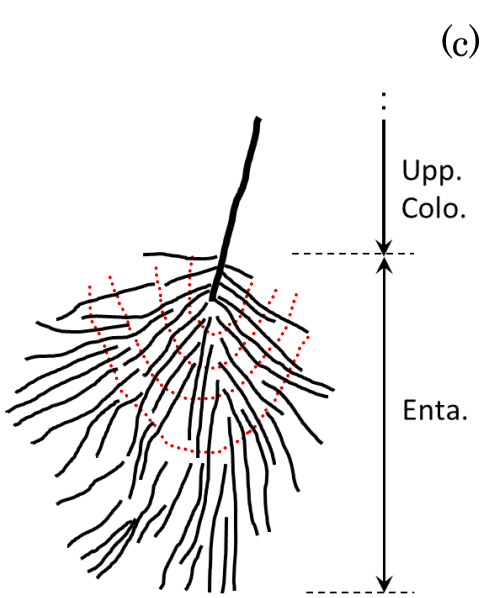

Figure 6.4: Entablature part of Shakushiiwa. (a) Radial structures closely line to horizontal direction. Individual radial structure is circled by red dashed line. (b) The radial structure, which is second right of (a) indicated with black arrow. (c) The sketch of cracks of (b). The thick crack developing from Upper Colonnade part penetrates upper Entablature part slightly. Red dotted lines are expected isotherms of T_c in case that crack propagations advance perpendicular to the isotherms.

6.2 Introduction of heat transport, Q_2

To suggest new cooling surfaces along the cracks developing from Upper Colonnade, I will introduce the effect of heat transport through cracks as Q_2. Figure 6.5 describes the schematic description of cooling process in rock where cracks propagate downward with time. Suppose that the rock at $t = t_1$ is cooled from the upper surface by heat transport Q_1. Q_1 accounts for the thermal diffusion through the rock in vertical direction. At $t = t_2$, cracks develop downward from the upper surface and the temperature at the tip of cracks must be $T_c = T(t^*, x^*)$ at which cracks are formed. The isotherms around the tips of cracks would become convex downward because of heat transfer, Q_2 through the crack, which is horizontal conduction from the inside of the rock toward cracks. As crack propagations downward advance with time when tips of cracks reach a depth at $t = t_3$, I assume that they becomes a new effective cooling surfaces (C.S.) as represented by heat transfer through existing cracks Q_2. Because the original cooling surface was set horizontally, after the heat transfer Q_2 becomes effective as a new cooling process, cooling processes from two directions must be taken into account according to the result of Experiment 2. As the result in Figure 4.8 (c), the magnitude of T_c determines the location or the distance between the cooling surface and position at

T_c of isotherm in rock after the same elapsed time. Therefore such a difference in T_c can also affect the geometry of isotherm as described in Figure 6.6. Assuming that cracks develop perpendicular to each isotherm, cracks are described in Figure 6.7. As a result, crack propagation in the case of smaller T_c isotherm advances steeper angle against a horizontal direction. Comparison between Entablature structure in Figure 6.4 (b) and crack directions in Figure 6.7, small T_c for crack formation is reasonable. This is suggested from the result of Experiment 2 that crack propagation by cooling from two directions with right angle is perpendicular to the smaller T_c value after enough diffusion process.

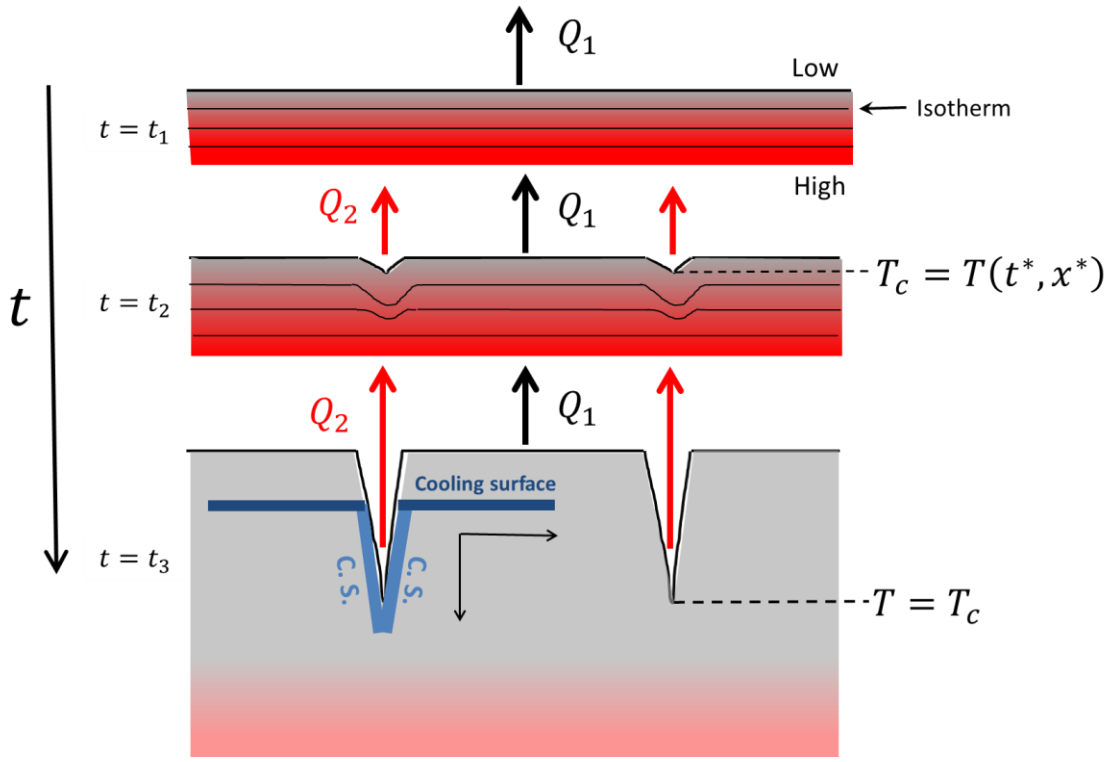

Figure 6.5: Schematic description of cooling process and crack development from one cooling surface. Time evolution of developing cracks and heat transfer change are shown downward. Red color shows higher temperature, while gray shows lower temperature. The isotherm shape around the tip of cracks changes convex downward as cracks advance because the horizontal conductive heat transfer Q_2 proceeds after cracks generate at $T_c = T(t^*, x^*)$. At $t = t_3$, cracks themselves become new effective cooling surface (C.S.) and the cooling process from two direction would begin afterward.

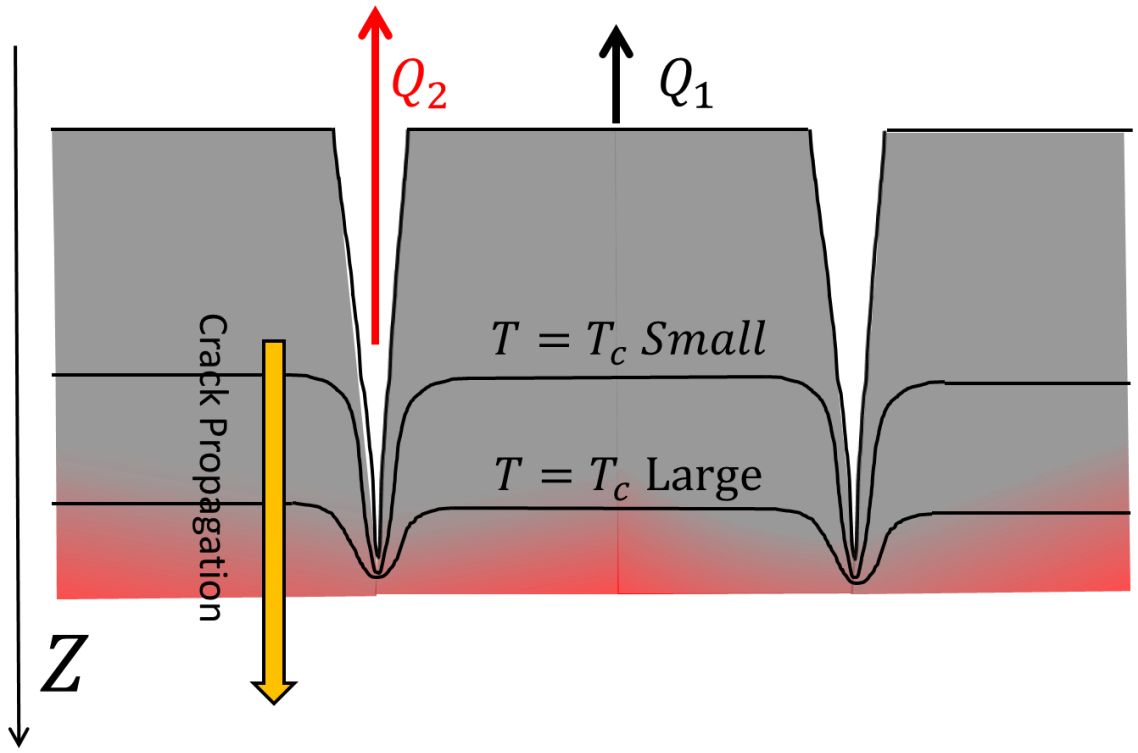

Figure 6.6: The difference of crack direction depending on the isotherm shape. As the effect of Q_2 gradually dominates, the shape of the isotherm around the tip of cracks becomes convex downward. The magnitude of T_c determines the location or the distance between the cooling surface and position at T_c of isotherm in rock after the same elapsed time as shown in Figure 4.8 (c), which indicates the larger T_c reach deeper in the rock.

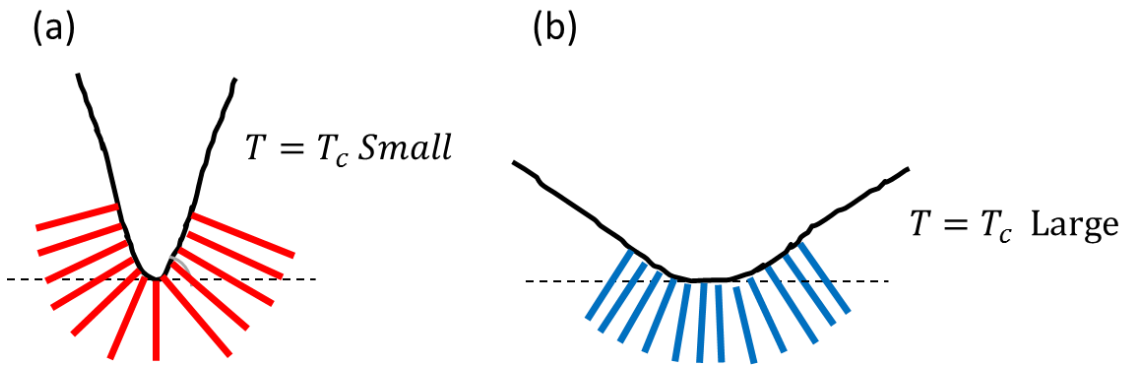

Figure 6.7: The difference of isotherm shapes depending on the magnitude of T_c. Cracks develop perpendicular to each isotherm. (a) Columns with sharp angle to the horizon can be developed to the isotherm with the larger curvature (T is the smaller T_c). (b) Columns with obtuse angle to the horizon can be developed to the isotherm with the smaller curvature (T is the larger T_c).

6.3 Interpretation of the formation of Shakushiiwa

Figure 6.8 describes the schematic diagram to explain the formation of columnar joints at Shakushiiwa. Upper and Lower Colonnades are formed from each cooling surface according to diffusion process. In Upper Colonnade part, some of cracks stop and the size of columns become coarser. When advancing cracks reach a depth L = L_{Q_2}, heat transfer Q_2 through existing cracks near the crack tips becomes effective because of new cooling surfaces, and the shape of isotherms T_c around crack tips is changed from a flat to a convex. Diffusion process advances enough to form steeper curved shape of isotherm T_c and additionally abrupt increase of heat transfer Q_2, which causes abrupt cooling at upper part of Entablature, generates column nucleation as shown in Figure 6.9. At the point (a) in Figure 6.9 that Entablature is started to form, column nucleation happens one after another during a short time as shown in order as (b). Geometric change in cross-section of columns with depth is shown in (c). Cracks at the nucleation points develop perpendicular to the steeper curved shape of isotherm T_c and columns with smaller width than that in Upper Colonnade are formed. Therefore, individual radial structures are formed in Entablature part. Abrupt increase of heat transfer Q_2 can be considered the effective thermal convection within cracks, which circulates between hotter inside

and cooler outside of the rock. Lower Colonnade is formed more slowly than the time Upper Colonnade and Entablature are formed.

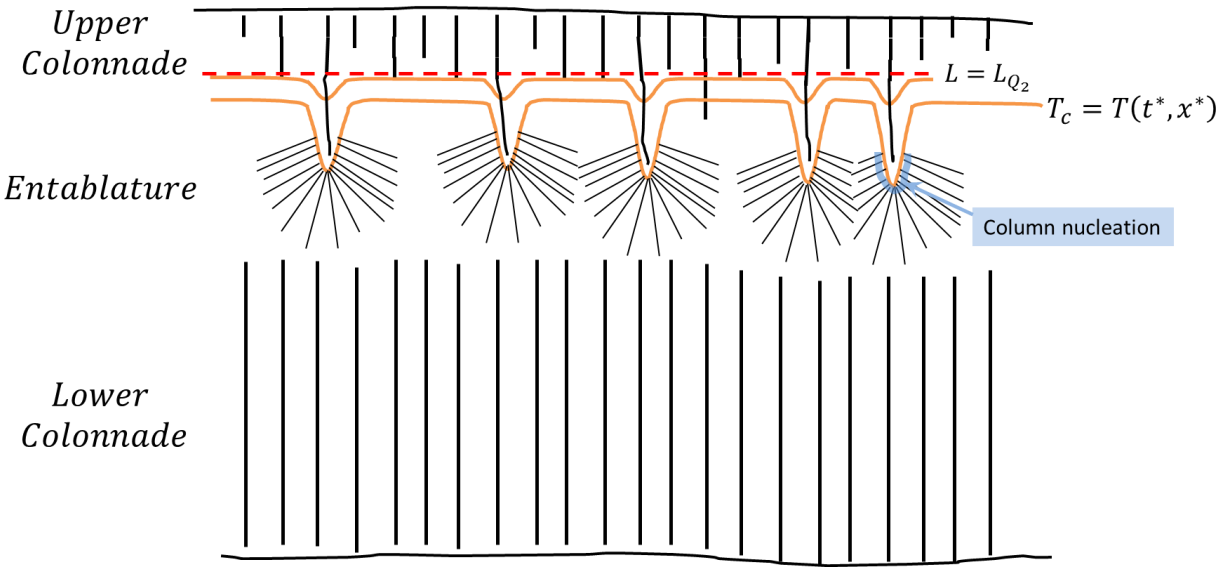

Figure 6.8: Schematic description of the formation of Shakushiiwa. Red dotted line shows the depth that heat transfer Q_2 proceeds to make the isotherm shape to be convex downward effectively.

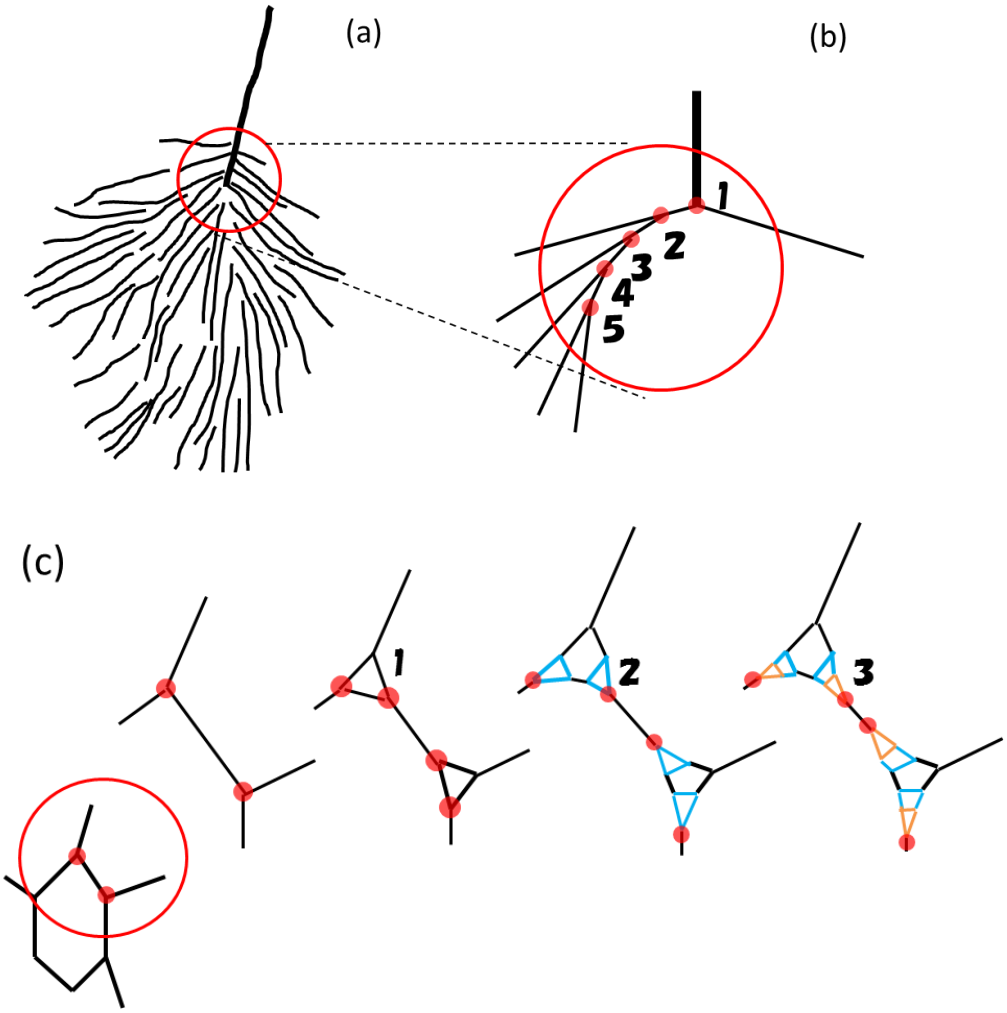

Figure 6.9: Geometric description for forming small size of columns by column nucleation. (a) The same sketch of cracks with Figure 6.4 (c). (b) The origination of horizontal columns which is magnified from the red circle part in (a). The numbers from 1 to 5 are the order of column nucleation with time. Red dots indicate the points of column nucleation. Column nucleation happens one after another by forming branched shape (cf. Figure 5.6 (b)). (c) The ideal cross section change of successive column nucleation with time. Red dots indicate the points of column nucleation. The numbers correspond to the position with the numbers in (b). Column nucleation occurs at triple points of existing column and next column nucleation happen at the triple points 1 formed by existing columns and new columns, which were formed shortly before. Column nucleation 2 and 3 occur in the same way as 1 and form smaller columns than columns of Upper Colonnade part.

Chapter 7

General conclusion

I suggest following possibilities to explain the morphological transition from Colonnade to Entablature based on the interpretations from the results of three experiments in this thesis: (1) Development of crack front can be explained by diffusion process (Chapter 3). (2) When the rock is cooled by two surfaces with the right angle, curved structure is formed after thermal diffusion process advances (Chapter 4). (3) The increase of cooling rate makes column nucleation to occur and the width of columns after successive column nucleation can be smaller as observed at radial structures of Entablature (Chapter 5). The abrupt increase of cooling rate, which is recognized from the change of column width from Colonnade (larger width) to Entablature (smaller width), is interpreted as the effective enhanced cooling process by heat transfer Q_2 through cracks, which can be heat convection within the cracks.

References

Aydin, A., DeGraff, J.M., 1988. Evoluton of Polygonal Fractutre Patterns in Lava Flows. Science. 239, 471-476.

Budkewitsch, P., Robin, P.-Y., 1994. Modelling the evolution of columnar joints. J. Volcanol. Geotherm. Res. 59, 219–239.

Carslaw, H.S. and Jaeger, J.C., 1959. Conduction of Heat in Solids. Oxford University Press, Oxford, 510 pp.

DeGraff, J.M., Aydin, A., 1987. Surface morphology of columnar joints and its significance to mechanics and direction of joint growth. Geol. Soc. Am. Bull. 99, 605–617.

DeGraff, J.M., Long, P.E., Aydin, A., 1989. Use of joint-growth directions and rock textures to infer thermal regimes during solidification of basaltic lava flows. J. Volcanol. Geotherm. Res. 38, 309–324.

Forbes, A.E.S., Blake, S., Tuffen, H., 2014. Entablature: fracture types and mechanisms. Bull Volcanol 76, 820.

Goehring, L., 2008. On the scaling and ordering of columnar joints. Ph-D Thesis. University of Toronto.

Goehring, L., Lin, Z., Morris, S.W., 2006. An Experimental Investigation of the Scaling of Columnar Joints. Phys. Rev. E 74, 036115.

Goehring, L., Mahadevan, L., Morris, S.W., 2009. Nonequilibrium scale selection mechanism for columnar jointing. PNAS 106, 387–392.

Goehring, L., Morris, S.W., 2008. Scaling of columnar joints in basalt. J. Geophys. Res. 113, doi:10.1029/2007JB005018

Hamada, A., 2012. Analogue experiments of columnar jointing: Focus on entablature. Master Thesis, Kyushu University.

Iddings, J.P., 1886. The columnar structure in the igneous rock on Orange Mountain, New Jersey. Am. J. Sci. s3-31, 321–331. doi:10.2475/ajs.s3-31.185.321

James, A.V.G., 1920. Factors Producing Columnar Structure in Lavas and Its Occurrence near Melbourne, Australia. J. Geol. 28, 458–469.

Jaeger, J.C., 1961. The cooling of irregularly shaped igneous bodies. Am. J. Sci. 259, 721–734.

Jaeger, J.C., 1959. Temperatures outside a cooing intrusive sheet. Am. J. Sci. 257, 44–54.

Long, P.E., Wood, B.J., 1986. Structures, textures, and cooling histories of Columbia River basalt flows. Geol. Soc. Am. Bull. 97, 1144-1155.

Lovering, T.S., 1935. Theory of heat conduction applied to geological problems. Geol. Soc. Am. Bull. 46, 69–94.

Mathews, W.H., 1951. The Table, a flat-topped volcano in southern British Columbia. Am. J. Sci. 249, 830–841. doi:10.2475/ajs.249.11.830

Mizuguchi, M., Nishimoto, A., Kitsunezaki, S., Yamazaki, Y., Aoki, I., 2005. Directional crack propagation of granular water systems. Phys. Rev. E 71.

Müller, G., 1998a. Experimental simulation of basalt columns. J. Volcanol. Geotherm. Res. 86, 93–96.

Müller, G., 1998b. Starch columns: Analog model for basalt columns. J. Geophys. Res. 103, 15,239–15,253.

Müller, G., 2001. Experimental simulation of joint morphology. J. Struct. Geol. 23, 45–49.

Ryan, M.P., Sammis, C.G., 1978. Cyclic fracture mechanisms in cooling basalt. Geol. Soc. Am. Bull. 89, 1295–1308.

Schmincke, H. U., 2004. Volcanism. Springer.

Sosman, R.B., 1916. Types of prismatic structure in igneous rocks. J. Geol. 24, 215–234.

Spry, A., 1962. The origin of colunar jointing, particularly in basalt flows. J. Geol. Soc. Aust. 5, 191-216.

Tomkeieff, S.I., 1940. The basalt lavas of the Giant's Causeway district of Northern Ireland. Bull Volcanol. 6, 89-146.

Toramaru, A., Matsumoto, T., 2004. Columnar joint morphology and cooling rate: A starch-water mixture experiment. J. Geophys. Res. 109, B02205.

Weaire, D., O'Carroll, C., 1983. A new model for the Giant's Causeway. Nature 302, 240-241.

水口毅, 西本明宏, 狐崎創, 山崎義弘, 青木伊知男, 2005. 乾燥亀裂における含水量分布. 数理解析研究所講究録 1413, 45–52.

狩野謙一, 村田明広, 1998. 構造地質学. 朝倉書店.

中野司, 中島善人,中村光一,池田進, 2000. X線CTによる岩石内部構造の観察・解析法. 地質雑, 106, 363–378.

Appendix 1: Temperature and humidity during experiments

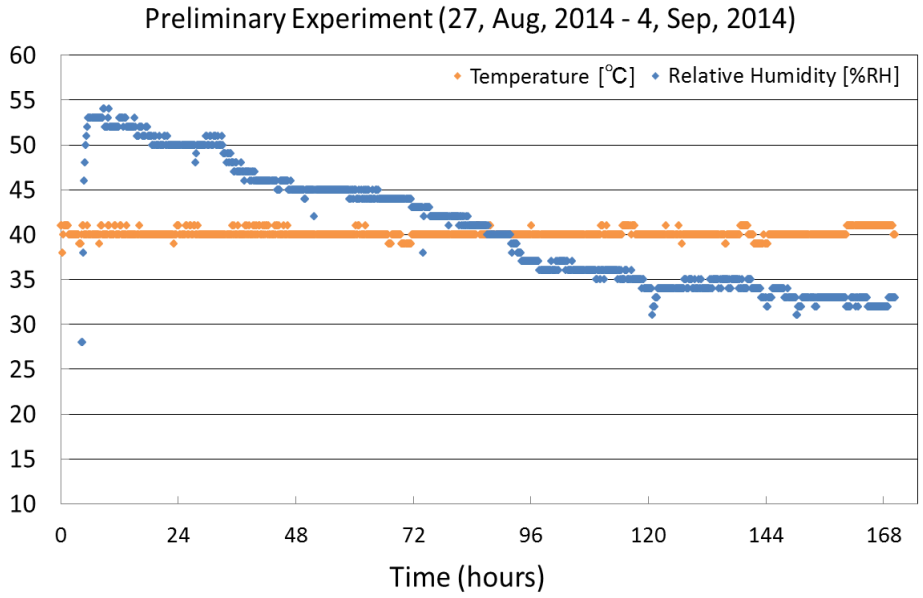

Appendix 1-A: Temperature and humidity in the desiccator during preliminary experiment in Experiment 1. The data was recorded for a week.

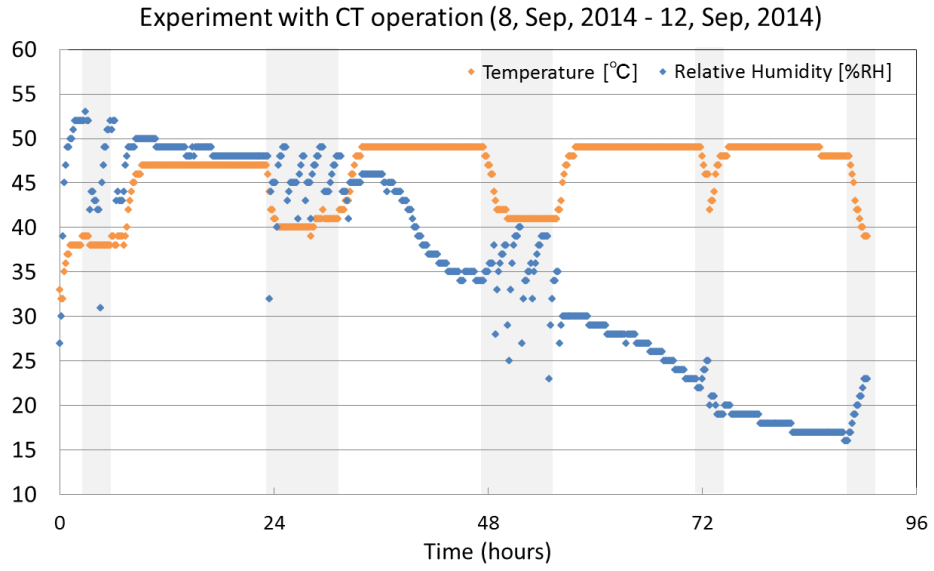

Appendix 1-B: Temperature and humidity in the desiccator during the experiment with CT operation in Experiment 1. The data was recorded for 4 days. Gray bars indicates the time for taking CT images.

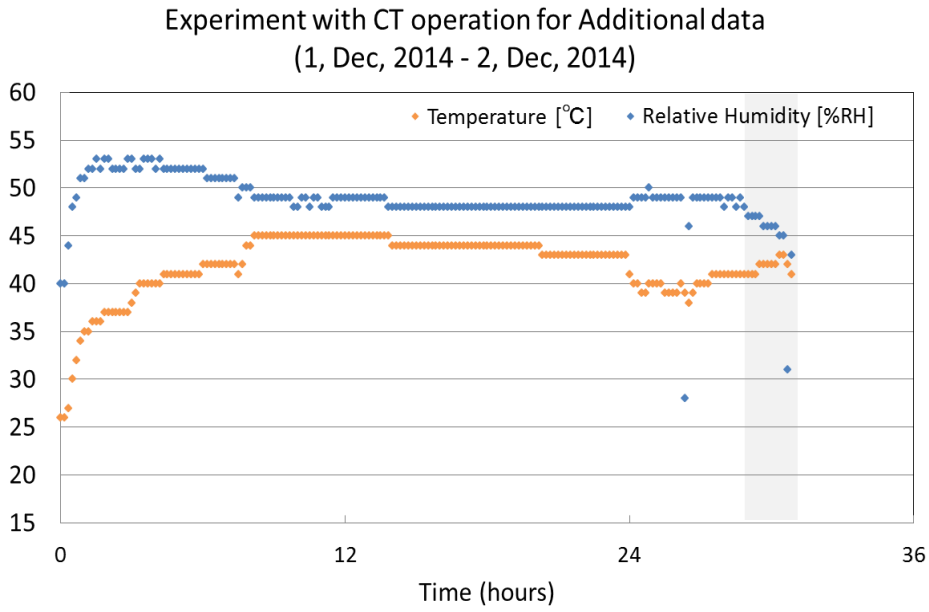

Appendix 1-C: Temperature and humidity in the desiccator during the experiment with CT operation for getting additional data of Experiment 1. The data was recorded for 3 days. Gray bars indicates the time for taking CT images.

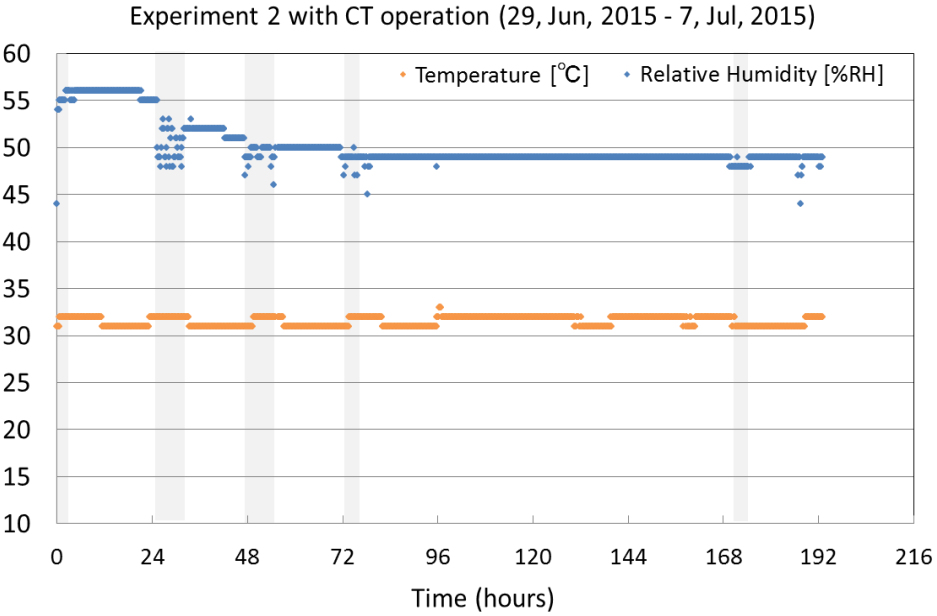

Appendix 1-D: Temperature and humidity in the desiccator during the experiment with CT operation in Experiment 2. The data was recorded for 8 days. Gray bars indicates the time for taking CT images.

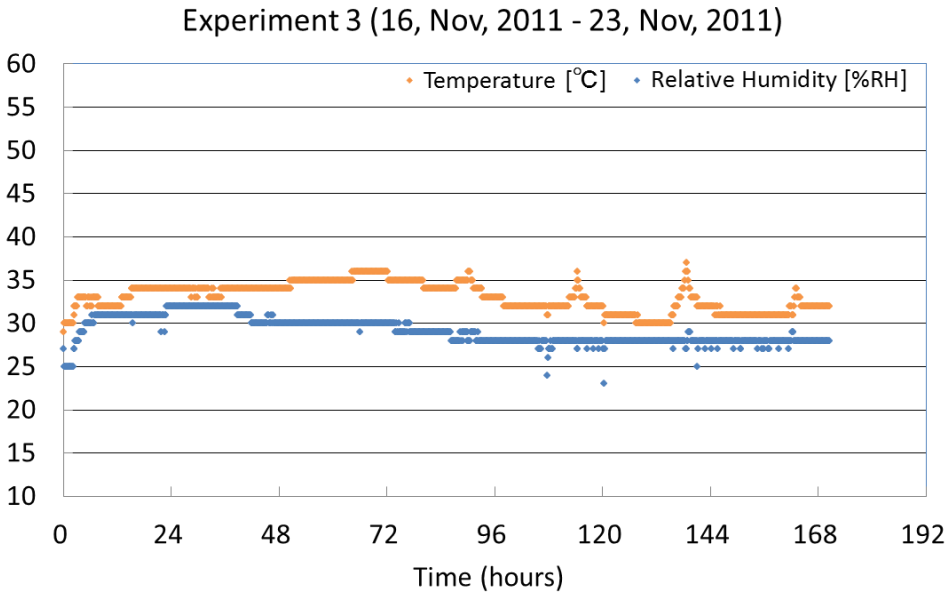

Appendix 1-E: Temperature and humidity in the desiccator during Experiment 3. The data was recorded for a week. CT images were taken after the specimen completely dried.

Appendix 2: Additional experiment of Experiment 1 for CT scanning just after cracking on the drying surface

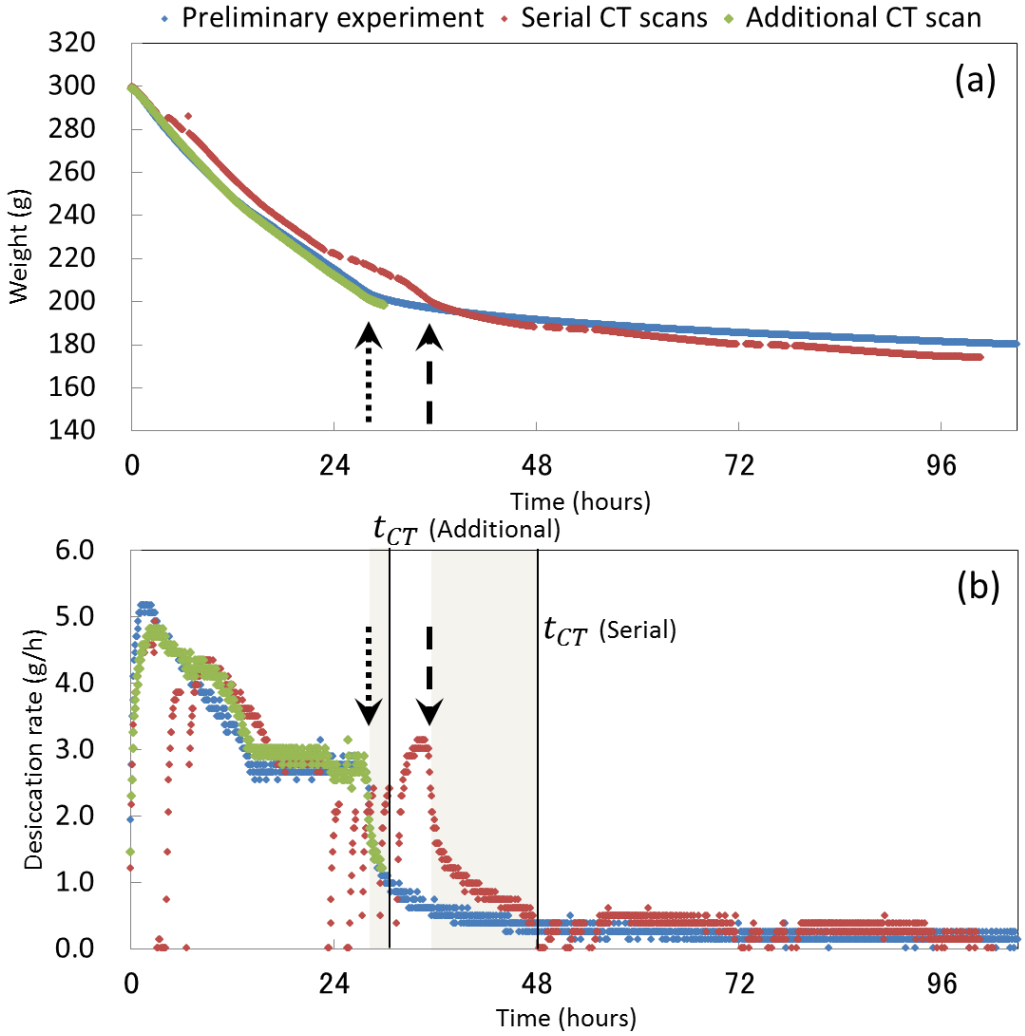

Appendix 2-A: Weight and desiccation rate change of three experiments in Experiment 1. The figure of preliminary experiment and the experiment with serial CT scans are the same as Figure 3.2. The experiment for additional CT scan just after cracks generated is shown as green dots. The data was recorded for 4 days. Dashed and dotted arrows correspond to the time when first cracks were formed on the surface of specimen. (a) Weight changes in three experiments. (b) Desiccation rate changes in three experiments calculated by differentiation from the weight loss.

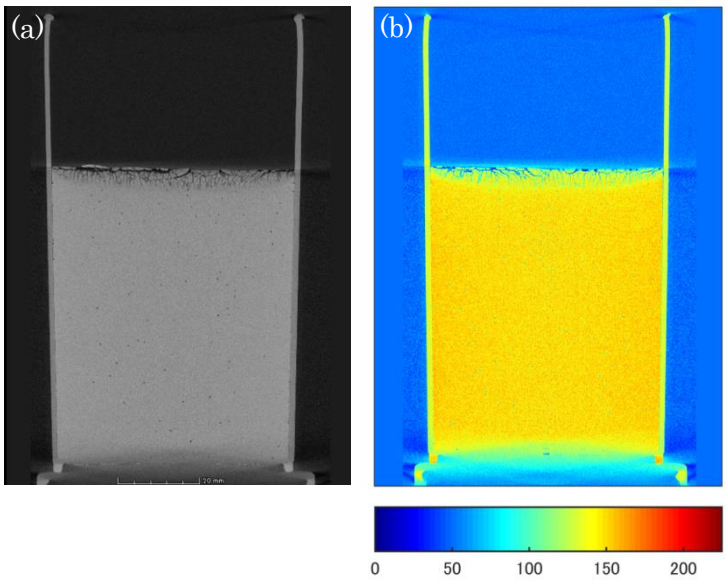

Appendix 2-B: CT images of additional experiments in Experiment 1. (a) The CT image in grayscale. Cracks can be seen at the surface of specimen. (b) The colored CT images depending on the brightness. The range is 0 – 255. As the crack length at the depth of this experiment as a red dot shown in Figure 3.10, This additional data corresponds to the time just after cracking, which couldn't be got during Experiment 1 with CT operations.

Appendix 3: Photographs by infrared camera at the surface of mixture

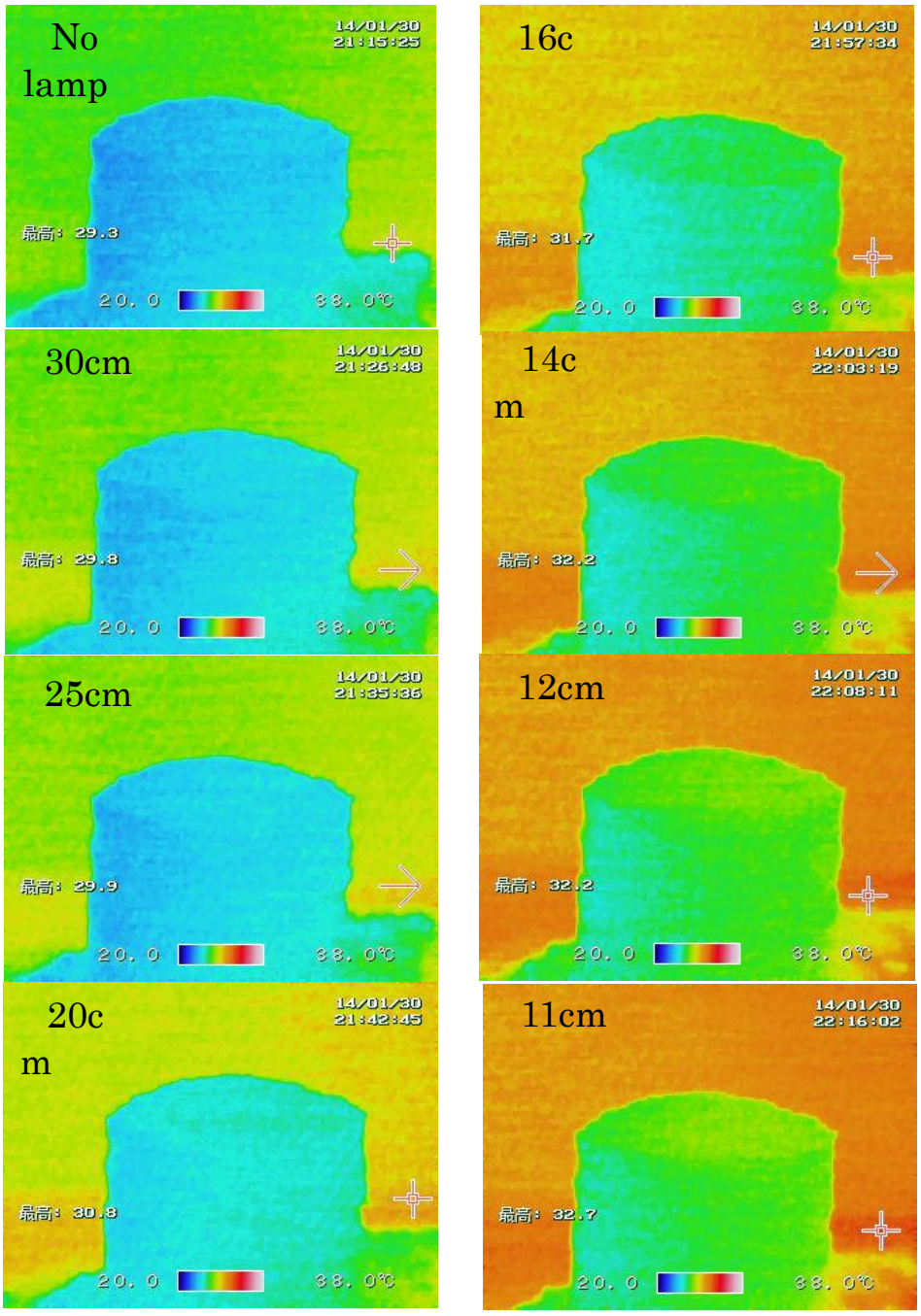

Appendix 3: Photographs by infrared camera at the surface of mixture depending of the distance between the lamp and the surface of mixture. The range of temperature is from 20.0 to 38.0 degrees C.

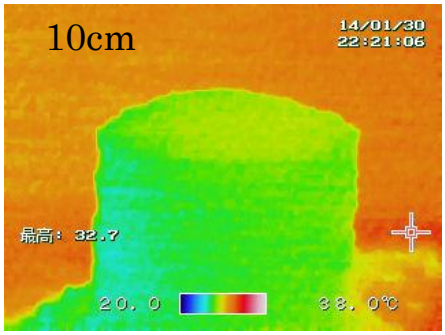
10cm
14/01/30
22:21:06
最高: 32.7
20.0
38.0℃

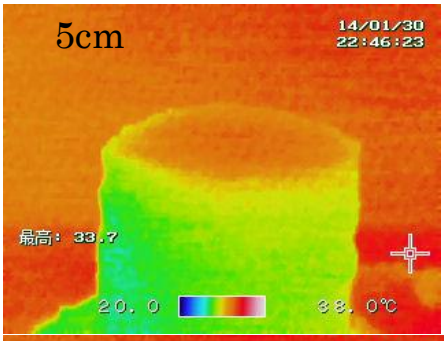
5cm
14/01/30
22:46:23
最高: 33.7
20.0
38.0℃

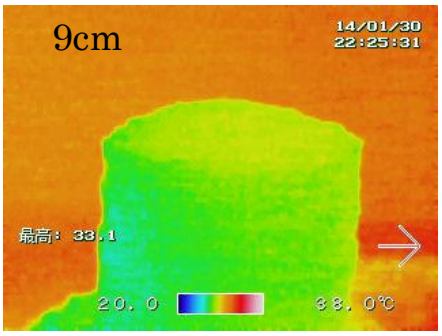
9cm
14/01/30
22:25:31
最高: 33.1
20.0
38.0℃

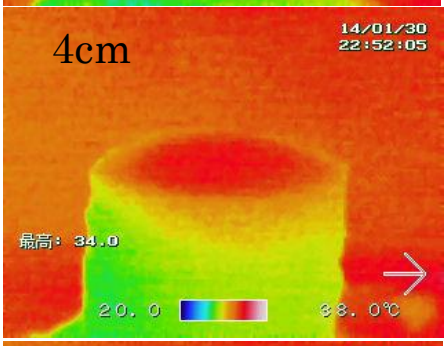
4cm
14/01/30
22:52:05
最高: 34.0
20.0
38.0℃

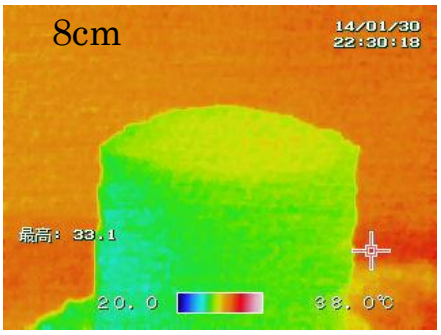
8cm
14/01/30
22:30:18
最高: 33.1
20.0
38.0℃

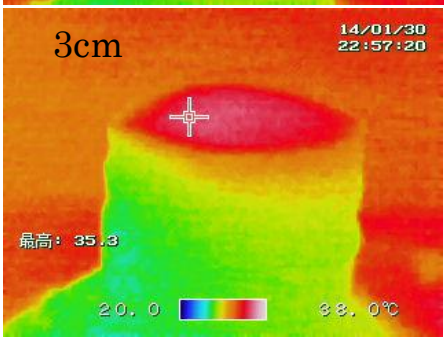
3cm
14/01/30
22:57:20
最高: 35.3
20.0
38.0℃

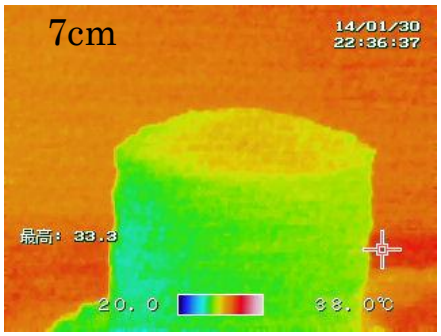
7cm
14/01/30
22:36:37
最高: 33.3
20.0
38.0℃

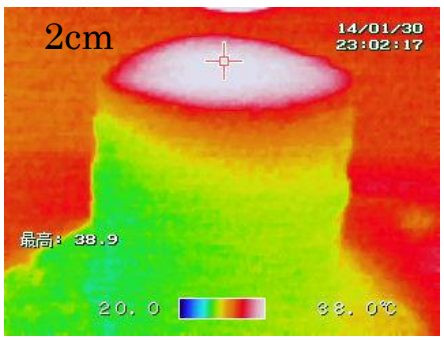
2cm
14/01/30
23:02:17
最高: 38.9
20.0
38.0℃

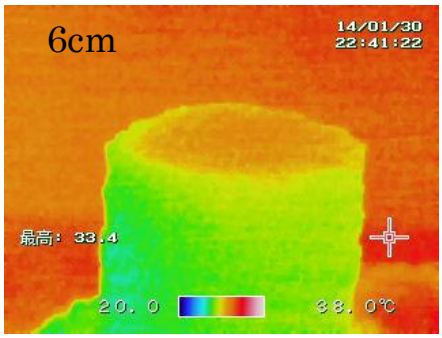
6cm
14/01/30
22:41:22
最高: 33.4
20.0
38.0℃

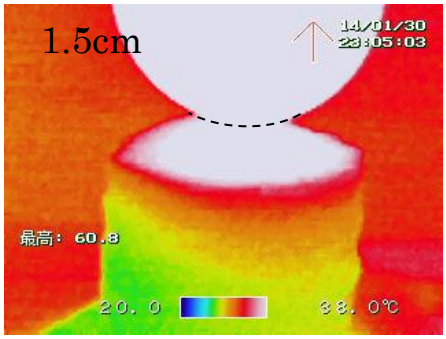
1.5cm
14/01/30
23:05:03
最高: 60.8
20.0
38.0℃

Appendix 4: Cooling rate and curvature of isotherms at T_c

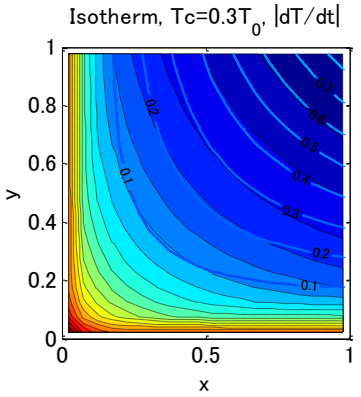

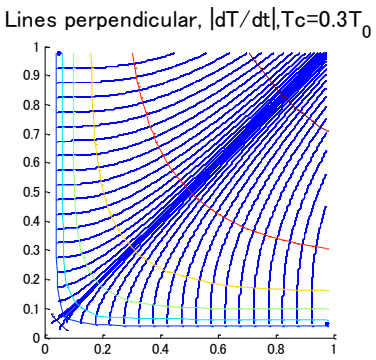

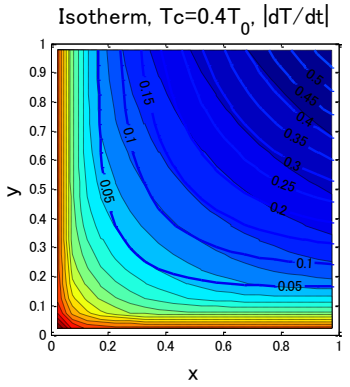

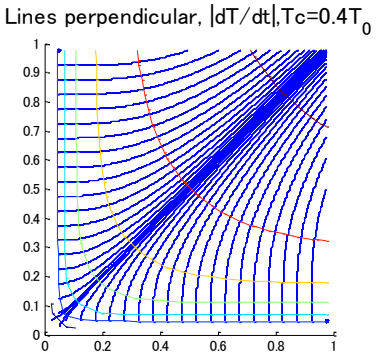

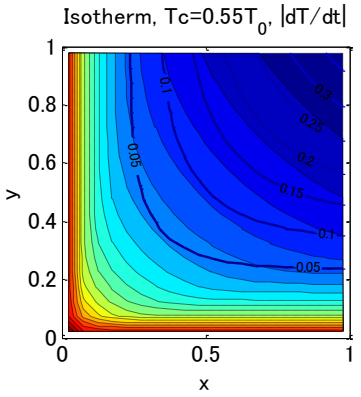

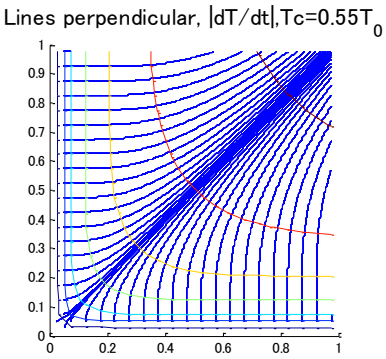

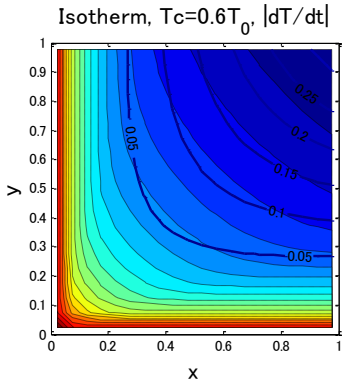

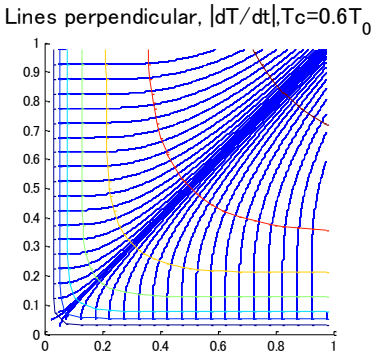

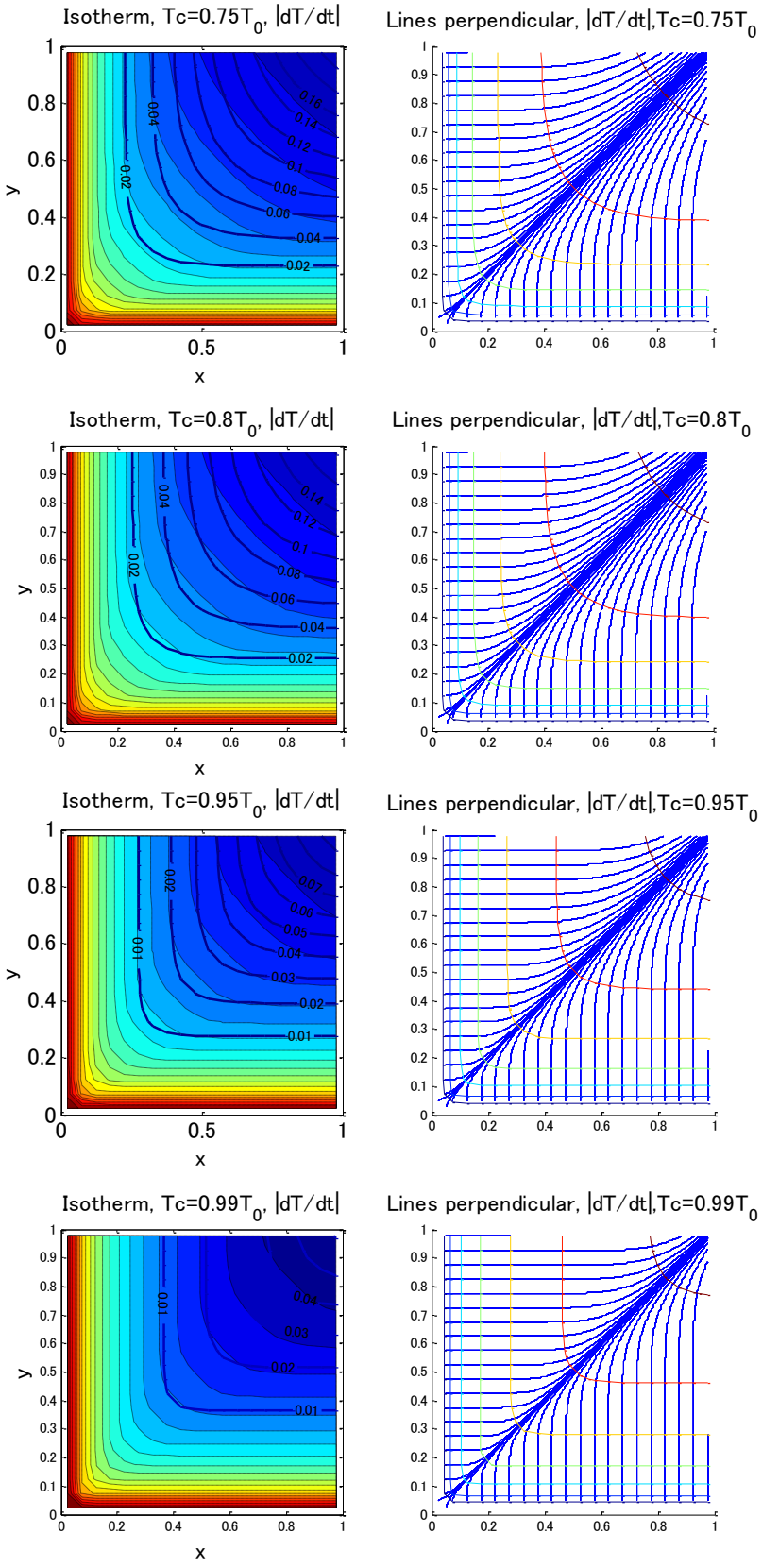

Appendix 4: Cooling rate and the curvatures of various values of isotherms at T_c.

Appendix 5: Other experiments for the future works

I put some interesting experimental results in morphology for some keys for the future works.

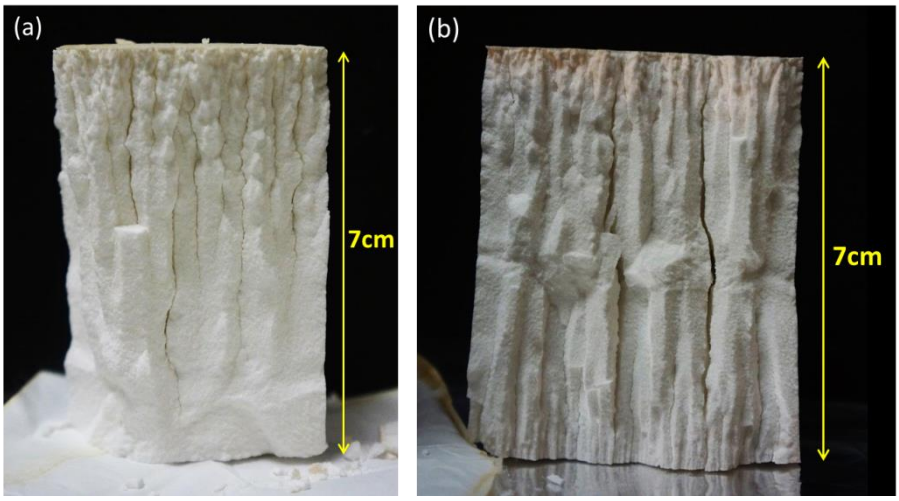

Appendix 5-A: Experimental results with the acrylic cylindrical container. (a) The specimen dried from the top. The smaller columns develop near the drying surface and become the larger width of columns at the depth. Morphological features of columns are relatively straight with wavy columns at the upper part. (b) The specimen dried from both the top and the bottom at the same time. The developed columns from both surfaces meet at the center of the specimen. Morphological features of columns are straight. The smaller columns near the bottom of the specimen have more clear shape than that near the top of the specimen.

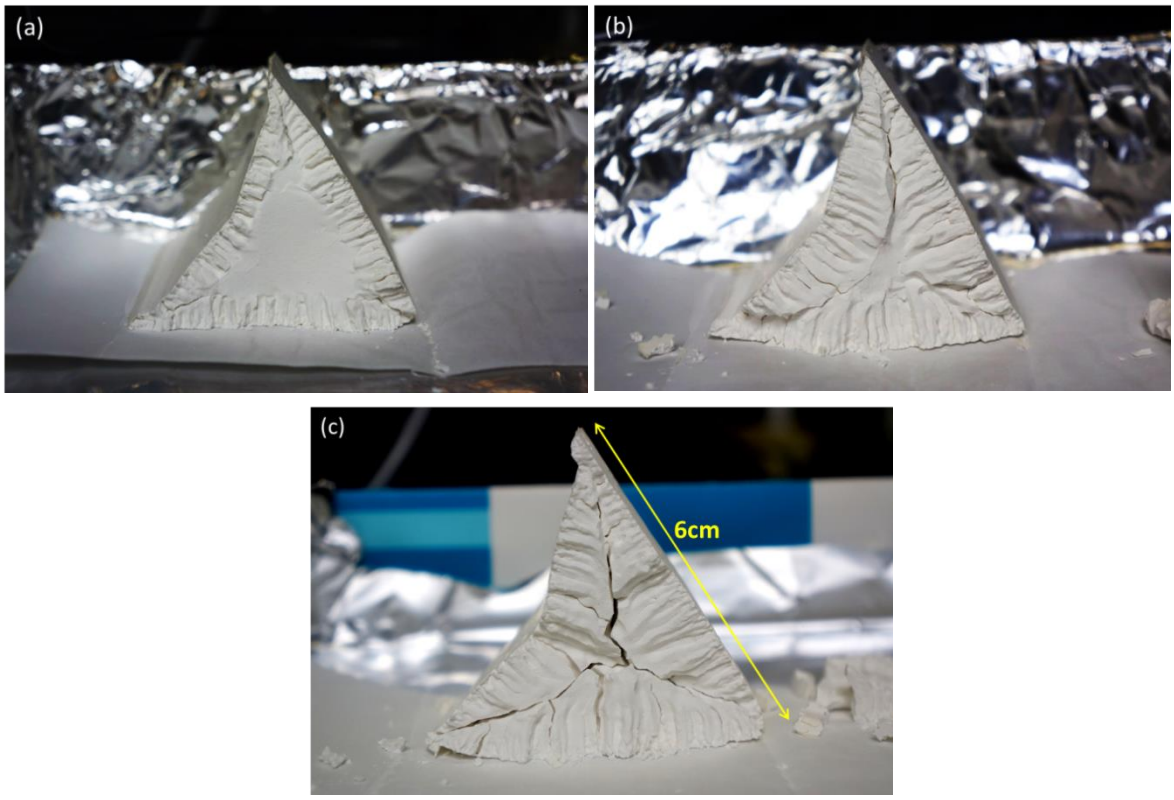

Appendix 5-B: Experimental results with stainless prism container with 60 degrees in all angles. Each specimen removed from the container at different weight to observe its internal structure in different experiments. (a) The specimen was removed to observe when it includes about 6 % of water. (b) The specimen was removed to observe when it includes less 1 % of water. (c) The specimen was removed to observe when it was completely dried.

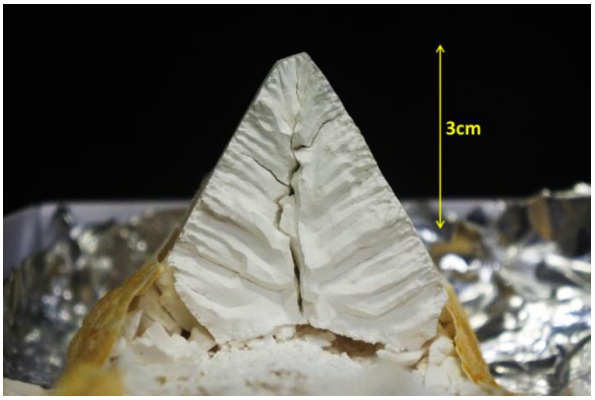

Appendix 5-C: Experimental results with stainless prism container with 60 degrees. Since the bottom side of the triangle was covered by resin, crack propagation developed from the other two surfaces, which is perpendicular to them.

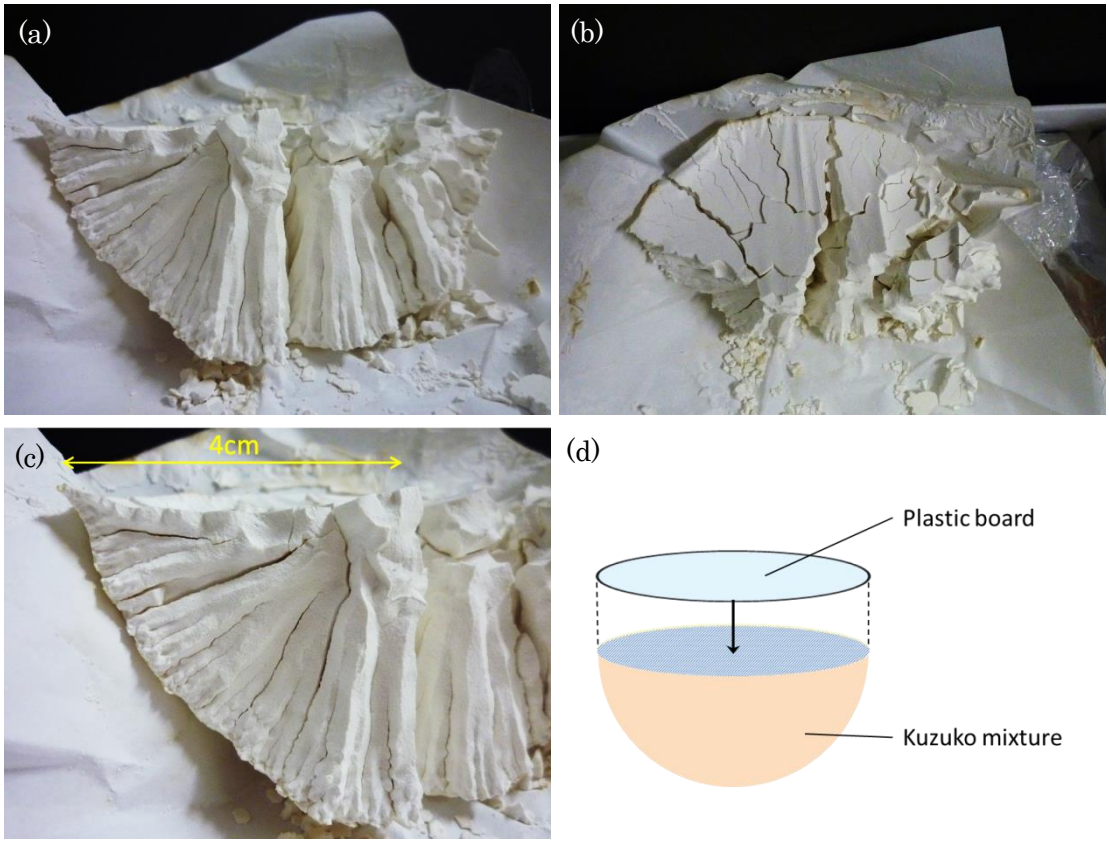

Appendix 5-D: Experimental results in the case of drying from round surface. Kuzuko mixture is put into semi-sphere container and the other flat surface is covered by plastic board. The drying process was conducted naturally. (a) The internal structure of completely dried specimen. Cracks developed perpendicular to the round drying surface and met at the center of the semi-sphere mixture. (b) The top of the specimen. (c) The magnified view of (a). The number of columns decreases at the depth from 2 or 3 to 1 larger column. (d) Schematic figure of experimental setup.

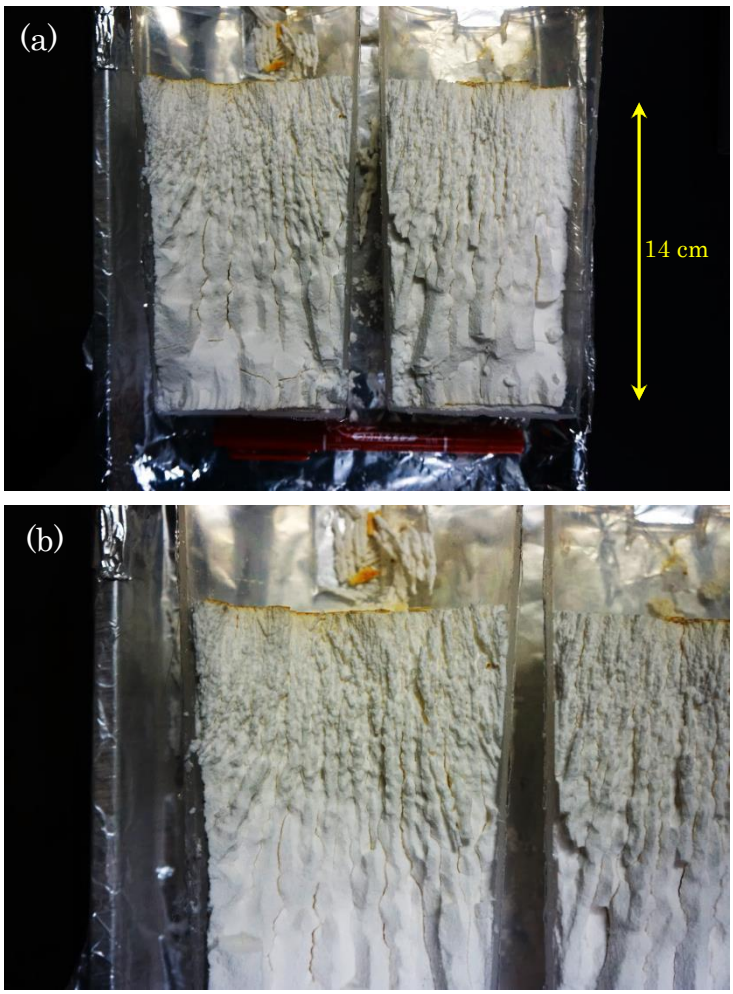

Appendix 5-E: Experimental results with long cylindrical container. The top of specimen was dried and it took about 60 days before removing from the container (it was still wet inside of the specimen). (a) The cross sectional view along the height of container. Small size of columns (2 – 3 mm in diameter) developed from the top of specimen and advanced into the depth with the increase of the size of columns (5 – 6 mm in diameter at 7 cm depth). (b) The magnified view of upper part of (a). The columns at upper part have irregular, wavy configuration.